Bioenergetic implications of the AMPKγ_3 R225W mutation in human muscle

Nina Hadzimustafic

A thesis submitted in partial fulfillment of the requirements for the
Master's degree in Biochemistry

Department of Biochemistry, Microbiology and Immunology
Faculty of Medicine
University of Ottawa

Abstract

AMPK is a master regulator of cellular energy homeostasis. The gain-of-function AMPKγ_3 R225W mutation in human skeletal muscle increases resistance to fatigue during exercise, mitochondrial content, and glycogen storage. We demonstrate that primary myotubes exhibit increased OCR, decreased ECAR, increased FAO, and increased activities of several mitochondrial complexes. To examine whether functional effects are attributable to mitochondrial content, we inhibited AMPK; differences between R225W and control were diminished. Glycogen phosphorylase inhibition demonstrated normal respiration independent of glycogen. We examined markers of quality/quantity control of mitochondria. In R225W muscle, fusion markers increased, biogenesis markers remained unchanged, mTOR pathway was inhibited, and there was greater capacity for autophagic flux and mitophagy. We thus determine that bioenergetic effects of R225W are in part due to active AMPK, but also due to capacity for more robust mitochondria. Overall, R225W provides a model for evaluating effects of AMPK, and new avenues toward treatment of metabolic disease.

Acknowledgements

First and foremost, I would like to thank my supervisor, Dr. Mary-Ellen Harper for her constant, unwavering guidance and support over the past 2 years. You truly allowed me to grow as, and become, a scientist, and to develop my interests in the metabolism field. Without your support in my studies, I undoubtedly would have not been able to succeed throughout my Honours and Master's programs. I am ever grateful to have had such a welcoming, thoughtful, intelligent, and overall incredible supervisor.

To Dr. Chantal Pileggi, thank you for being the best teacher I could have asked for over the past two years. From teaching me to run the simplest experiments and answering my questions about data in the middle of the night, to reading every single draft report and thesis over the past two years, I could not have done it without you! The time that you have put into supporting me in both my academics and personally is invaluable and I am beyond thankful for the friendship you've offered me.

To Dr. Ruth McPherson and Dr. Morgan Fullerton, thank you for offering me ideas for new and exciting experiments as my TAC members, and for creating a space that I felt comfortable discussing the shortcomings of my work and helping me develop direction for my project. I would also like to especially thank Dr. Ruth McPherson alongside Dr. Robert Dent for their clinical experience and for conducting the *vastus lateralis* biopsies.

To my fellow lab members over the years: Gaganvir Parmar, Claire Fong-McMaster, Breana Hooks, Luke Kennedy, Baher Migally, Ziyad El-Hankouri, Michaela Norgren, Keili Shepherd, Ashvent Malik, Nidhi Kuksal, Michel Kanaan, Jian Xuan, Dr. Alessandra Gentile, Dr. Rajaa Sebaa, Dr. Neoma Boardman, Dr. Denis Blondin, Dr. Jens Frey Halling, and Dr. David Patten; you have all uniquely contributed to shaping me into a scientist and to my experience in the

Harper Lab. Special mentions go out to Gaganvir who started on the same day as me and has patiently taught and helped me so much, and is someone I am lucky to have as a friend; to Claire for listening to my every-day silly problems even when they take an hour to explain; to Breana for her support, kindness and friendship; to Baher for his warm friendship (and warm car for drives to RGN!); to Alessandra for getting cappuccinos (with mocha powder!) with me every day and teaching me Italian; and to Dave for entertaining me in several discussions from disagreeing on calculations to chatting in line at the weekly BBQ. You all made my day-to-day experience more enjoyable!

Lastly, to thank my family and friends: my sisters Alma and Ema, parents Rozalija and Sulejman, and Andrew, Cassidy, Emily, Sophie, Rahna, and Maya, for their love and for supporting me in every aspect of this program and my life.

Table of Contents

Abstract ..... *ii*

Acknowledgements ..... *iii*

Table of Contents ..... *v*

List of Figures ..... *vii*

List of Tables ..... *viii*

List of Abbreviations ..... *ix*

Introduction *1*

Laws of Thermodynamics and Biological Fuel Currency 1

Mitochondria: Structure and Function 2

Mitochondrial Respiration 3

Carbohydrate Digestion 3

Glycolysis 3

Fatty Acid Oxidation 7

Electron Transport Chain 10

ROS Production 11

Metabolic Disease 12

Type 1 Diabetes Mellitus (T1DM) 13

Type 2 Diabetes Mellitus (T2DM) 14

Skeletal Muscle Insulin Resistance 14

Energy Regulation and AMPK 15

Regulatory Subunits 16

AMPK Signalling 18

AMPK, Glucose Uptake and Glycogen Synthesis 19

AMPK and Fatty Acid Catabolism and Synthesis 19

AMPK and Mitochondrial Fusion/Fission 20

AMPK and Mitochondrial Biogenesis 21

AMPK and mTOR Signalling 22

AMPK, Autophagy and Mitophagy 23

R225W Phenotype 24

Methods *29*

Subjects/Participants 29

Vastus lateralis biopsy 29

Cell culture 30

Oxygen consumption of primary myotubes 30
Oxygen consumption of AMPK-inhibited myotubes 31
Oxygen Consumption of myotubes with glycogen phosphorylase inhibitor 31
Fatty acid oxidation mitochondrial stress test in primary myotubes 32
Metabolic enzyme activities 32
Maximal activities of mitochondrial respiratory complexes 33
High resolution respirometry of permeabilized myotubes 34
Permeabilization of biopsied fibres 35
Assays to measure oxygen consumption, FAO and ROS production 35
Western Blots 37
Statistics 38
Results *39*
Anthropometric and biochemistry data of follow-up biopsies 39
Oxygen consumption and ATP production are increased in R225W myotubes 40
Acute AMPK inhibition leads to loss of difference in bioenergetic capacity, and increased glycogen content does not affect respiration 43
R225W myotubes exhibit increased fatty acid oxidation 46
Activities of mitochondrial ETC complex proteins are increased in primary myotubes from R225W individuals 49
Respiration rates are lower in biopsied skeletal muscle of R225W individuals than in muscle of matched controls 52
Mitofusin protein levels are elevated in muscle from R225W individuals 53
Markers of mitochondrial biogenesis in biopsied muscle are similar in R225W and control individuals 54
mTOR pathway is inhibited in R225W muscle homogenate 55
The R225W mutation is associated with increased markers of autophagic flux capacity and mitophagy 58
Discussion *61*
Conclusion *72*
Bibliography *74*
Contributions of Collaborators *83*
Curriculum Vitae *84*

List of Figures

Figure 1. Molecular structure of adenosine triphosphate (ATP).....1
Figure 2. Summary of glycolysis. 5
Figure 3. Summary of TCA cycle. 7
Figure 4. Carnitine shuttle system from cytosol to mitochondrial matrix. 8
Figure 5. Summary of fatty acid oxidation. 9
Figure 6. Oxidative phosphorylation in mitochondrial inner membrane. 11
Figure 7. AMP-bound AMPK in active form. 17
Figure 8. Summary of AMPK pathways. 19
Figure 9. Families of two probands with the R225W mutation. 25
Figure 10. Leak respiration and bioenergetic capacity are increased in individuals with the R225W AMPK mutation.....42
Figure 11. OCR and ECAR of R225W myotubes in presence of glycogen phosphorylase and compound C inhibitors. 45
Figure 12. Increased FAO and increased CPT1 activity in myotubes from R225W individuals. 48
Figure 13. Increased activities of ETC proteins in myotubes of R225W affected individuals than in myotubes of matched controls. 51
Figure 14. CS activity is decreased in R225W muscle homogenate, OXPHOS, FAO, and ROS production in biopsied muscle preparations did not change. 53
Figure 15. Fusion proteins MFN-1 and MFN-2 are increased in biopsied muscle of R225W individuals compared to controls. 54
Figure 16. Levels of marker proteins of mitochondrial biogenesis are similar in biopsied muscle of R225W and control individuals. 55
Figure 17. p70S6K, p-4E-BP1, and p-S6RP are decreased, and p-p70S6k is increased in biopsied muscle from R225W individuals as compared to controls. 57
Figure 18. Protein levels of p62 are decreased in biopsied R225W compared to control muscle. 59
Figure 19. Increased level of LC3BII after chloroquine treatment in R225W compared to control myotubes. 60

List of Tables

Table 1. Characteristics of R225W and age-matched control subjects who underwent follow-up muscle biopsies in September 2018. 39

List of Abbreviations

^{o}C	degree Celcius
2PG	2-phosphoglycerate
3PG	3-phosphoglycerate
4E-BP1	eukaryotic Initiation Factor 4E binding protein 1
ACC	acetyl-CoA carboxylase
ADP	adenosine diphosphate
AICAR	5-aminoimidazole-4-carboxamide-1-b-D-ribofuranoside
AKAP1	A kinase anchoring protein 1
AMP	adenosine monophosphate
AMPK	adenosine monophosphate kinase
ANT	adenine nucleotide transporter
ATP	adenosine triphosphate
BCA	bicinchoninic acid
BMI	body-mass index
BNIP3	BCL2/adenovirus E1B 19 kDa protein-interacting protein 3
BPG	1,3-bisphosphoglycerate
BSA	bovine serum albumin
CACT	carnitine translocase
cal	calorie
CAMKK2	calcium/calmodulin-dependent kinase 2
CBS	cystathionine-β-synthase
CI	complex I
CII	complex II
CIII	complex III
CIV	complex IV
CO_2	carbon dioxide
CoA	coenzyme A
CoQ	coenzyme Q, ubiquinone
CPT1	carnitine palmitoyltransferase 1
CPT2	carnitine palmitoyltransferase 2
CS	citrate synthase
CV	complex V
DHAP	dihydroxyacetone phosphate
DNMT1	DNA (cytosine-5)-methyltransferase 1
DRP1	dynamin-related protein 1
DTT	dithiothreitol
ECAR	extracellular acidification rate
ETC	electron transport chain

Eto	etomoxir
F6P	fructose-6-phosphate
FA	fatty acid
FAD^+	flavin adenine dinucleotide (oxidized state)
$FADH_2$	flavin adenine dinucleotide (reduced state)
FAF	fatty acid-free
FAO	fatty acid oxidation
FBP	fructose-1,6-bisphosphate
FCCP	carbonyl cyanide p-(trifluoromethoxy) phenyl-hydrazone
FFA	free fatty acids
Fis1	fission protein 1
g	gram
G6P	glucose-6-phosphate
GAP	glyceraldehyde-3-phosphate
GAPDH	glyceraldehyde-3-phosphate dehydrogenase
GLUT4	glucose transporter type 4
Gly	glycolysis
GP	glycogen phosphorylase
GS	glycogen synthase
GSH	glutathione, γ-glutamylcysteinylglycine
GSSG	glutathione disulphide
GTP	guanosine triphosphate
GWAS	genome wide association studies
H_2O_2	hydrogen peroxide
HAT1	histone acetyltransferase 1
HFD	high-fat diet
HRP	horseradish peroxidase
IMTG	intramuscular triglyceride
IR	insulin resistance
J	Joule
kb	kilobase
kcal	kilocalorie
LC3	microtubule-associated protein 1A/1B light chain 3
LKB1	liver kinase B1
MFN-1	mitofusin-1
MFN-2	mitofusin-2
mLST8	mammalian lethal with Sec13 protein 8
MnSOD	manganese superoxide dismutase
mtDNA	mitochondrial DNA
mTOR	mammalian target of rapamycin

mTORC1	mammalian target of rapamycin complex 1
mTORC2	mammalian target of rapamycin complex 2
NAD^+	nicotinamide adenine dinucleotide (oxidized form)
NADH	nicotinamide adenine dinucleotide (reduced form)
nDNA	nuclear DNA
NRF-1	nuclear respiratory factor 1
NRF-2	nuclear respiratory factor 2
O_2	oxygen
O_2^-	superoxide
OCR	oxygen consumption rate
OH^-	hydroxyl radical
OPA-1	optic atrophy protein 1
OXPHOS	oxidative phosphorylation
p-	phosphorylated
PAS	periodic acid Schiff stain
PBS	phosphate-buffered saline
PDK1	phosphoinositide-dependent kinase 1
PEP	phosphoenolpyruvate
PFK	phosphofructokinase
PFKFB3	6-phosphofructo-2-kinase/fructose-2 bisphosphatase-3
PGC1α	peroxisome proliferator-activated receptor-gamma coactivator 1α
PI3K	phosphoinositide 3-kinase
PINK1	PTEN-induced kinase
PKA	protein kinase A
PTM	posttranslational modification
Raptor	regulatory protein associated with mTOR
RBBP7	retinoblastoma-binding protein 7
Rictor	rapamycin insensitive companion of mTOR
RN^-	Rendement Napole phenotype
ROS	reactive oxygen species
RT	room temperature
S6K1	p70S6 kinase
S6RP	S6 ribosomal protein
T1DM	type I diabetes mellitus
T2DM	type II diabetes mellitus
TBS-T	Tris buffered saline containing 0.1% Tween 20
TCA	tricarboxylic acid
TEM	transmission electron microscopy
TFAM	mitochondrial transcription factor A
TBK1	TANK binding kinase 1

TOM20	translocase of outer membrane 20
TPI	triose phosphate isomerase
ULK1	Unc51-like autophagy activating kinase 1
UOHI	University of Ottawa Heart Institute

Introduction

Laws of Thermodynamics and Biological Fuel Currency

"Energy can be neither created nor destroyed, only transferred or converted from one form to another" (Clausius, 1850). The first law of thermodynamics, which although originally coined in 1850, remains the guiding principle at the foundation of all energy-related research. Solar energy can be harnessed by photosynthetic autotrophs, capable of undergoing the fundamental reaction:

$$6\ H_2O + 6\ CO_2 + \text{Energy} \rightarrow C_6H_{12}O_6 + 6O_2$$

Heterotrophs, such as *Homo sapiens* (humans), rely on the ability of other living organisms that are capable of performing this photosynthetic reaction by consuming autotrophs or other heterotrophs. They then extract this energy largely through a process called cellular respiration, converting the energy into a usable form called adenosine triphosphate (ATP) (figure 1). ATP harnesses this energy in its 2 high-energy phosphoanhydride bonds (between the α and β phosphates, and β and γ phosphates) and releases this energy when these bonds are hydrolyzed (Bonora et al., 2012).

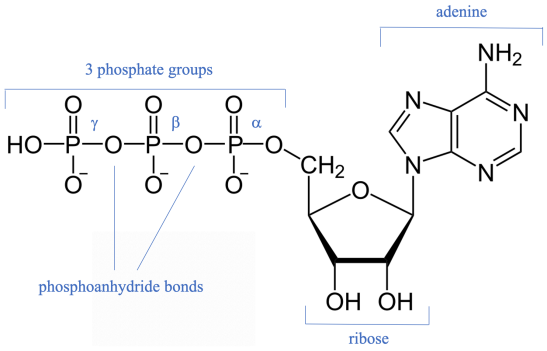

Figure 1. Molecular structure of adenosine triphosphate (ATP).

Each ATP molecule is comprised of an adenine group, with its N9 group covalently bonded to a ribose at C1, which in turn is bonded to 3 phosphate groups at C5. Energy is stored in the phosphoanhydride bonds between the α and β phosphates, and the β and γ phosphates.

The basic unit of energy is Joule (J), but in biological processes and everyday life, energy is often referred to in terms of calories (cal). 1 calorie is equivalent to the energy needed to raise one gram (g) of water by one degree Celsius (°C) which corresponds to 4.184 J. Heterotrophs extract energy by consuming carbohydrates, lipids, proteins, and alcohol (Merrill, 1973). Carbohydrates and proteins contain approximately 4 kcal/g, alcohol contains 7 kcal/g and fat contains 9 kcal/g (Merrill, 1973).

Mitochondria: Structure and Function

Mitochondria are primarily recognized for being the main site of ATP production in the cell through the process of oxidative phosphorylation (OXPHOS). Mitochondria also play essential roles in processes including cell death signalling, calcium homeostasis, and heme synthesis (Duchen, 2000). Evolutionarily, mitochondria arose from the engulfment of a bacterium by a eukaryotic cell, and remained in eukaryotes as a form of mutual symbiosis (Friedman and Nunnari, 2014). Mitochondria are circumscribed by a double membrane – one membrane is from the original bacterial cell membrane, and the other as a result of the endocytosis (Friedman and Nunnari, 2014). Mitochondria contain a roughly 16 kilobase (kb) circular genome in human cells which encode proteins essential to mitochondrial structure and function (Friedman and Nunnari, 2014). The inner mitochondrial membrane is arranged in cisternal invaginations called cristae which house the 5 OXPHOS complexes (Friedman and Nunnari, 2014). The space contained by the inner membrane is known as the mitochondrial matrix which is the site of β-oxidation and most steps of the tricarboxylic acid (TCA) cycle, and the space between the inner and outer membrane is the intermembrane space, critical for processes related to the electron transport chain (ETC) and proton motive force (Friedman and Nunnari, 2014).

Mitochondrial Respiration

Carbohydrate Digestion

Carbohydrate digestion begins with salivary α-amylase which breaks the α1-4 glycosidic linkages to release glucose and maltose, basic monosaccharide and disaccharide units of hexose carbohydrates (Smith and Morton, 2010). Salivary amylase is inactivated by the low pH of gastric acid when the bolus of food arrives in the stomach (Smith and Morton, 2010). Pancreatic juice is secreted into the duodenum (first part of small intestine), containing a second α-amylase which continues the digestion of the carbohydrate (Smith and Morton, 2010). Glucose is reabsorbed in the small intestine via active transport with the Na^+/glucose cotransporter into the epithelial cells, then enters the blood stream, where it is transported to tissues that require it for ATP production (Chen et al., 2016). When glucose concentrations in the blood increase postprandially, the pancreas releases insulin into the blood (Del Prato et al., 2002). Insulin-sensitive tissues such as skeletal muscle, adipose tissue, and liver increase their glucose uptake in response to this insulin increase (Honka et al., 2018). Increased insulin activates the phosphoinositol 3-kinase/AKT pathway which causes the glucose transporter type 4 (GLUT4) to translocate to the plasma membrane, leading to an increase in cellular glucose uptake (Honka et al., 2018).

Glycolysis

Glycolysis is a 10-step pathway in the cytoplasm that converts a glucose monomer into two pyruvate molecules. Glycolysis begins when the α-D-glucose is irreversibly phosphorylated to form glucose-6-phosphate (G6P) by hexokinase at the expense of one ATP molecule (Lunt and Vander Heiden, 2011). G6P is then isomerized into fructose-6-phosphate (F6P) by G6P isomerase. F6P is then irreversibly phosphorylated at carbon 1 by phosphofructokinase 1

(PFK) to generate fructose-1,6-bisphosphate (FBP) at the expense of one ATP (Lunt and Vander Heiden, 2011). FBP is then cleaved by aldolase to form glyceraldehyde-3-phosphate (GAP) and dihydroxyacetone phosphate (DHAP) (Lunt and Vander Heiden, 2011). DHAP is isomerized by triose phosphate isomerase (TPI) to from another molecule of GAP (Lunt and Vander Heiden, 2011). The GAP molecules are oxidized and phosphorylated by GAP dehydrogenase (GAPDH) to form 1,3-bisphosphoglycerate (BPG); nicotinamide adenine dinucleotide (NAD^+) acts as the electron acceptor (Lunt and Vander Heiden, 2011). The BPG molecules each donate a phosphoryl group to adenosine diphosphate (ADP) to form 2 molecules of ATP, resulting in the formation of 2 molecules of 3-phosphoglycerate (3PG) (Lunt and Vander Heiden, 2011). Then, the 3PG molecules are isomerized to form 2-phosphoglycerate (2PG) by phosphoglycerate mutase (Lunt and Vander Heiden, 2011). Enolase dehydrates 2PG to form 2 phosphoenolpyruvate (PEP) molecules (Lunt and Vander Heiden, 2011). Lastly, a phosphoryl group is irreversibly transferred from PEP to an adenine diphosphate (ADP) to form 2 ATP molecules and 2 molecules of pyruvate (Lunt and Vander Heiden, 2011). The process of glycolysis has a net generation of 2 ATP and 2 NADH (figure 2) (Lunt and Vander Heiden, 2011).

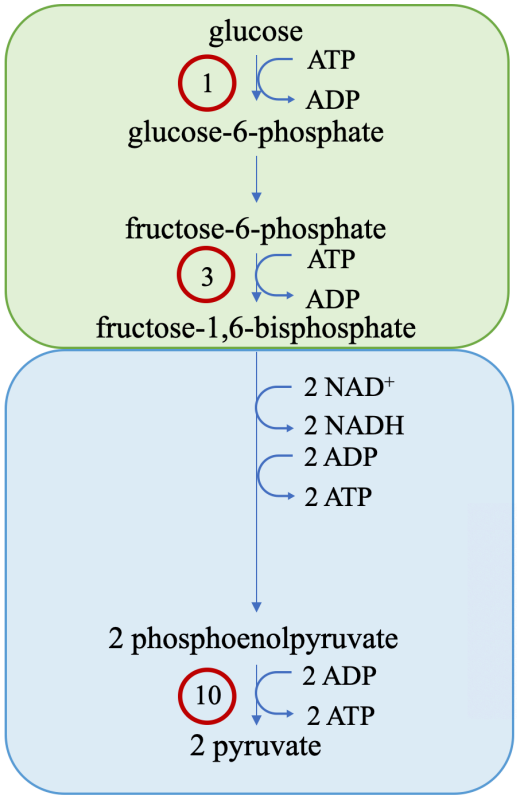

Figure 2. Summary of glycolysis.

Glycolysis has two stages: investment (green) and payoff (blue) with a total of 10 steps. The net production from glycolysis includes 2 NADH and 2 ATP for 1 glucose molecule. Steps 1, 3, and 10 are highlighted for their use or production of ATP and are the only 3 steps that are irreversible in the glycolysis process.

The pyruvate molecules can then undergo one of two fates: aerobic or anaerobic respiration (Lunt and Vander Heiden, 2011; Ghosh, 2004). Anaerobic respiration occurs in hypoxic conditions resulting in the formation of 2 lactate molecules and 2 ATP molecules (or 2 ethanol molecules in yeast fermentation) from the two molecules of pyruvate (Engelking, 2015; Huang and Tang, 2007). Aerobic respiration generates considerably more ATP and is the preferable ATP production method in mammals (Lunt and Vander Heiden, 2011). In aerobic respiration, pyruvate gets shuttled into the mitochondria, and is converted to acetyl-CoA by pyruvate dehydrogenase in an irreversible manner, resulting in the formation of 2 NADH (Lunt and

Vander Heiden, 2011). The acetyl-CoA molecules can subsequently go into the TCA cycle, better known as the Krebs cycle (Lunt and Vander Heiden, 2011).

Krebs Cycle

Acetyl-CoA enters the TCA cycle and combines with oxaloacetate in a reaction catalyzed by citrate synthase (CS) to form citrate (Martínez-Reyes and Chandel, 2020). Citrate (figure 3, step 1) is then dehydrated by aconitase to form *cis*-aconitate, then rehydrated to form isocitrate (Martínez-Reyes and Chandel, 2020). Isocitrate (figure 3, step 2) undergoes oxidative decarboxylation by isocitrate dehydrogenase to form α-ketoglutarate (figure 3, step 3), simultaneously producing one NADH (Martínez-Reyes and Chandel, 2020). Then, there is a second oxidative decarboxylation by the α-ketoglutarate dehydrogenase complex to form succinyl-CoA (figure 3, step 4) and another NADH (Martínez-Reyes and Chandel, 2020). Succinyl-CoA is then used in a substrate level phosphorylation step to produce one guanosine triphosphate (GTP) and succinate (figure 3, step 5) via succinyl-CoA synthetase (Martínez-Reyes and Chandel, 2020). Then succinate dehydrogenase produces fumarate (figure 3, step 6) in a dehydrogenation reaction, which produces one flavin adenine dinucleotide ($FADH_2$) (Martínez-Reyes and Chandel, 2020). Fumarase hydrates the fumarate to form malate (figure 3, step 7) (Martínez-Reyes and Chandel, 2020). Lastly, to complete the cycle, malate dehydrogenase reforms oxaloacetate (figure 3, step 8), which is then ready to enter a new cycle with another acetyl-CoA molecule (Martínez-Reyes and Chandel, 2020). The overall cycle from one glucose molecule which yields 2 acetyl-CoA molecules results in the production of 2 GTP, 6 NADH, 2 $FADH_2$, and 4 CO_2 (from each decarboxylation) (Martínez-Reyes and Chandel, 2020).

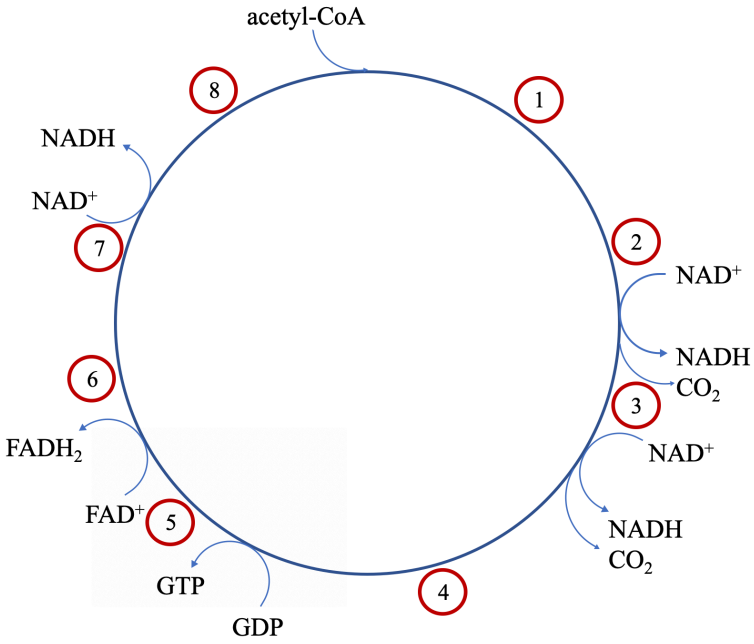

Figure 3. Summary of TCA cycle.

Acetyl-CoA proceeds into the TCA cycle which takes place in the mitochondrial matrix. The main purpose of the cycle is to produce reduced NADH and $FADH_2$ which can provide electrons to the electron transport chain in the mitochondrial inner membrane. Each TCA cycle produces 3 NADH, 1 $FADH_2$, and 1 GTP molecule. Each number corresponds to a metabolite present in the TCA cycle (Martínez-Reyes and Chandel, 2020).

Fatty Acid Oxidation

Free fatty acids (FAs) exist freely in the cellular environment in varying hydrocarbon chain lengths (Cholewski et al., 2018). The nomenclature of saturated (no double bonds) FAs depends on the length of its hydrocarbon chain (Davidson and Cantrill, 1985). Unsaturated (include 1 or more double bonds) FAs are also named for the length of their hydrocarbon chain, but include *cis* and *trans* designations for special orientation around the double bond alongside the number for the carbon at which the double bond is located (Davidson and Cantrill, 1985). Depending on the length of the FA, it may be metabolized in a different location within the cell. Most FAs are oxidized inside the mitochondria to produce the electron carriers NADH and $FADH_2$ to send electrons to the ETC (Houten et al., 2016). Fatty acid oxidation (FAO) or

β-oxidation is a critical source of electrons in limited-glucose or glucose starvation states (Houten et al., 2016). In order to undergo β-oxidation, FAs must first enter the mitochondria (Houten et al., 2016). Small-chain FAs can readily diffuse across the mitochondrial membranes, whilst medium-, long-, and very long-chain FAs are unable to do so (Schönfeld and Wojtczak, 2016). Very long-chain FAs are metabolized through non-mitochondrial β-oxidation at peroxisomes (Reddy and Hashimoto, 2001). Medium- and long-chain FAs are imported into the mitochondria using the carnitine cycle (Houten et al., 2016). The carnitine shuttle system requires L-carnitine, carnitine palmitoyltransferases 1 and 2 (CPT1 and CPT2), and carnitine translocase (CACT) (Houten et al., 2016). CPT1 is located on the outer mitochondrial membrane and is responsible for catalyzing the transesterification of the acyl-CoA to acylcarnitine (Houten et al., 2016). Then, the CACT transports the acylcarnitines across the inner mitochondrial membrane, where CPT2 converts the acylcarnitine back to an acyl-CoA (Houten et al., 2016). The main rate-controlling step of β-oxidation is the CPT1 reaction catalysis, and it is controlled by ATP levels in the cell (Shriver and Manchester, 2011).

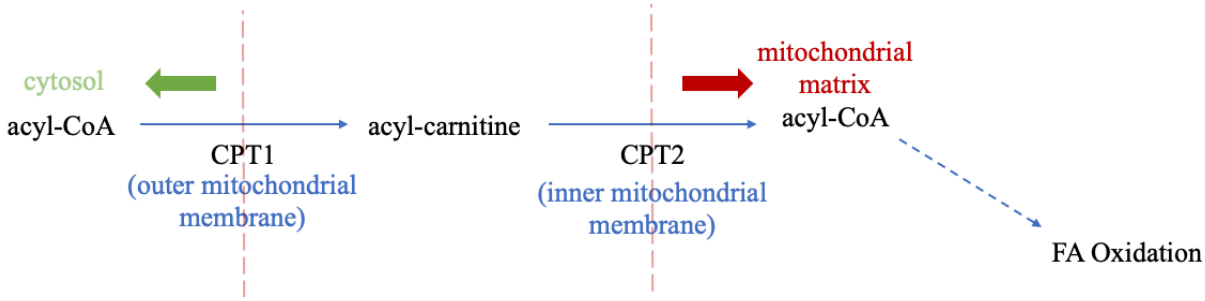

Figure 4. Carnitine shuttle system from cytosol to mitochondrial matrix.

CPT1 and CPT2 work to do opposite reactions, with the intermediate between the two enzymes being acyl-carnitine, which is capable of crossing the inner mitochondrial membrane with the help of CACT. Once the acyl-CoA is in the mitochondrial matrix, it can undergo fatty acid oxidation.

CPT1 is also up-regulated in the presence of adenosine monophosphate activated kinase (AMPK) because AMPK is capable of suppressing the lipogenic pathway in WAT leading to a reduction of malonyl-CoA, a CPT1 repressor (Srivastava et al., 2012). Malonyl-CoA is involved in the feedback loop inhibition of β-oxidation, and this allosteric inhibition has been thought to be linked to the development of insulin resistance (Ruderman et al., 1999).

Once the FA is in the mitochondria, FAO proceeds with a cycle of 4 steps: dehydrogenation by acyl-CoA dehydrogenase which forms 1 $FADH_2$ (figure 5, step 1), hydration by enoyl-CoA hydratase (figure 5, step 2), dehydrogenation by 3-hydroxyacyl-CoA dehydrogenase which forms 1 NADH (figure 5, step 3), and cleavage by thiolase to yield 1 acetyl-CoA, and a fatty acid that is now 2 carbons shorter than before the first cycle (figure 5, step 4) (Houten et al., 2016). The acetyl-CoA formed can proceed to the citric acid cycle, and the NADH and $FADH_2$ can transfer their electrons to the ETC (Houten et al., 2016).

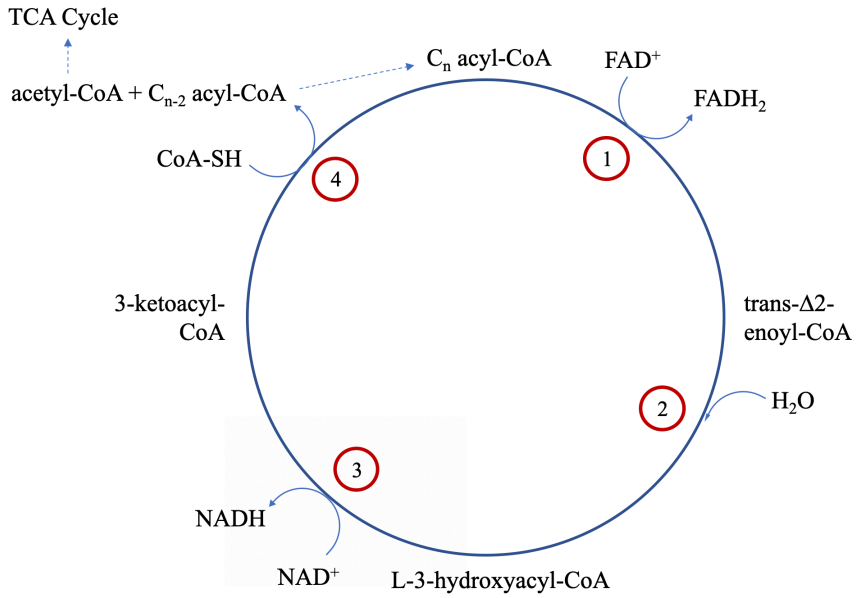

Figure 5. Summary of fatty acid oxidation.

Fatty acid oxidation proceeds in 4 steps: dehydrogenation, hydration, another dehydrogenation, and lastly thiolytic cleavage. Each number corresponds to a step. The cycle continues with the C_{n-2} acyl-CoA, cutting 2 carbons off to form acetyl-CoA until the entire chain has been metabolized.

Electron Transport Chain

Electrons enter the ETC at complex I (NADH dehydrogenase) or complex II (succinate dehydrogenase) via electron carriers, either NADH or $FADH_2$ (Zhao et al., 2019) and at complex III from FAO where electrons are transferred via electron transport flavoprotein (ETF) (Wang et al., 2010). CI is the largest multi-subunit enzyme in the chain and its primary function is transferring electrons from NADH to ubiquinone (Zhao et al., 2019). CII, succinate dehydrogenase, is a 4-subunit complex and a component of both the TCA cycle and the ETC; receiving electrons from $FADH_2$ (Zhao et al., 2019). Although the other mitochondrial complexes are encoded by both mitochondrial DNA (mtDNA) and nuclear DNA (nDNA), CII is the only complex encoded entirely by nDNA, which speaks to the evolutionary origins of the ETC (Marusich et al., 1997). Electrons are shuttled from CI and CII to coenzyme Q (CoQ, ubiquinone), complex III (cytochrome C reductase), cytochrome C, and then complex IV (cytochrome C oxidase). Cytochrome C is a mobile electron carrier which is loosely held in place by electrostatic interactions on the outer-side of the inner mitochondrial membrane; allowing the transfer of electrons from CIII to CIV (Zhao et al., 2019). Cytochrome C transfers 4 electrons to oxygen (O_2) which bind and result in the reduction of O_2 to H_2O (Zhao et al., 2019). 8 protons in total are removed at CIV from the matrix, 4 are pumped into the intermembrane space, and 4 are used to form H_2O (Zhao et al., 2019). Protons are pumped out from the mitochondrial matrix as the electrons pass complexes I, III, and IV, which generates an electrochemical gradient ultimately capable of driving ATP production at complex V (F_1F_0 ATP synthase) (figure 6) (Zhao et al., 2019). This proton gradient is also known as the proton motive force; the driving force for ATP synthesis (Zhao et al., 2019; Divakaruni et al., 2014).

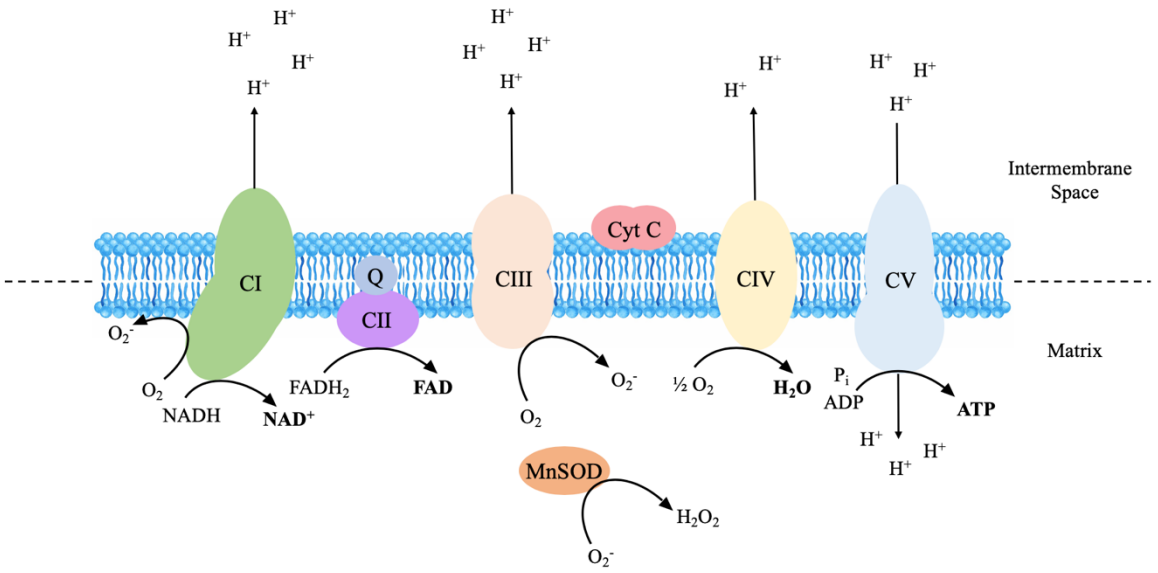

Figure 6. Oxidative phosphorylation in mitochondrial inner membrane.

A series of complexes where electrons donated by NADH and $FADH_2$ are transferred from CI and CII to the rest of the complexes, and from FAO through ETF at CIII; until finally at CIV, oxygen is reduced to water. Complexes I, III, and IV pump protons into the intermembrane space, and these protons flow down their concentration gradient at CV, or ATP synthase, producing ATP. Superoxide is produced largely at CI and CIII, and manganese superoxide dismutase (MnSOD) coverts superoxide to hydrogen peroxide.

The understanding about the organization and control of the 5 complexes is evolving, and the current thought is that the ETC organization has a plasticity. Complexes I, III, and IV are able to associate into specific supercomplexes, and this stabilizes the complexes and decreases reactive oxygen species (ROS) production (Dudkina et al., 2010). Deficiencies in the formation of mitochondrial supercomplexes have been observed in skeletal muscle from individuals with type II diabetes mellitus (T2DM) (Antoun et al., 2015).

ROS Production

ROS is an important by-product of the ETC. There are various forms of ROS including the superoxide anion (O_2^-), hydrogen peroxide (H_2O_2), and hydroxyl radicals (OH^-) (Schieber and Chandel, 2014). ROS have been shown to be damaging to macromolecules, and have traditionally been thought of as toxic by-products of metabolism, but can also be important in

cell signalling reactions (Li and Zhou, 2011; Mittler, 2017). It was initially thought that cell death was a direct outcome of increased ROS, but it is now better understood that ROS also act as signalling molecules, and that it is not necessarily just a cell succumbing to oxidative stress (Mittler, 2017). ROS appears to have been an early evolutionary mechanism to allow organisms to adapt to environmental oxidative state and changes in nutrient availability (Schieber and Chandel, 2014). Within cells, mitochondria are a major source of ROS. Specifically, O_2 is reduced to H_2O at complex IV once it receives 4 electrons, however partial reduction of O_2 leads to the production of ROS (Li and Zhou, 2011). In mitochondria, ROS are primarily produced at complex I, and III in the form of O_2^- (Li and Zhou, 2011). Molecules that contain unpaired electrons and are able to exist freely are referred to as free radicals (Schieber and Chandel, 2014). O_2^- has only one unpaired electron and thus is more reactive than O_2 because it will readily accept electrons in its less stable form (Schieber and Chandel, 2014). For this reason, O_2^- is converted to hydrogen peroxide by MnSOD because this reduced form is more stable (Li and Zhou, 2011; Schieber and Chandel, 2014). MnSOD is an enzyme in mitochondria which helps mitigate the ROS production by the partial reduction of O_2 and has been implicated in a variety of diseases related to excessive oxidative stress (Li and Zhou, 2011). Apoptosis is just one example of an essential role of basal ROS in the cellular microenvironment; others include differentiation by activating proliferative pathways, maintaining levels of ROS within an appropriate range for proper development, maintaining appropriate immune responses, and more (Mittler, 2017).

Metabolic Disease

In many societies internationally, there is a rapidly increasing prevalence in metabolic diseases such as obesity, T2DM, and cardiovascular disease. Development of metabolic disease is often

attributed to a chronic energy imbalance (Kerr et al., 2007). In 2018, the Canadian Diabetes Association reported 11 million people living with diabetes or are pre-diabetic, which is characterized by hyperglycemia resulting from insufficient insulin secretion (Diabetes Canada). Approximately 90% of the 11 million Canadians have T2DM, which often develops in adulthood (Diabetes Canada). Skeletal muscle accounts for up to 80% of postprandial insulin-stimulated glucose uptake, and therefore plays a critical role in the development of insulin resistance and T2DM (DeFronzo and Tripathy, 2009). Dysregulated skeletal muscle cellular bioenergetics that lead to alterations in metabolic flux and energetic efficiency are implicated as an underlying cause of obesity and T2DM (Misra and Chakrabarti, 2007). Current approaches for management of insulin resistance and T2DM prior to becoming insulin-dependent include lifestyle modifications such as exercise and pharmacological interventions such as metformin, which stimulate glucose uptake in skeletal muscle, by initiating the translocation of GLUT4 to the plasma membrane (Polianskyte-Prause et al., 2019).

Type 1 Diabetes Mellitus (T1DM)

T1DM is considered a chronic, autoimmune disease, most often presenting in childhood or adolescence (Katsarou et al., 2017). In T1DM, insufficient insulin is produced by the β-cells of the pancreas because these cells are destroyed by T-cells (Katsarou et al., 2017). As a result of insufficient insulin, the body is unable to properly regulate blood glucose (Katsarou et al., 2017). Presently, there is no cure for this disease, and it is treated by lifelong insulin injections/pump infusions (Katsarou et al., 2017).

Type 2 Diabetes Mellitus (T2DM)

T2DM can be developed at any point during life and is often linked to obesity (DeFronzo et al., 2015). Where T1DM is typically associated with genetic factors, T2DM is more associated with environmental factors, however genetic factors are also significant (DeFronzo et al., 2015). Risk genes have been identified such as *CAPN10* and *TCF7L2* and several others through genome wide association studies (GWAS) (Ali, 2013). Studies have shown that heritability of T2DM ranges from 20%-80% T2DM is characterized by insulin insensitivity as a result of hyperinsulinemia, with heritability substantially increasing if one or both biological parents has/have T2DM (DeFronzo et al., 2015). Insulin is no longer able to have an effect on peripheral tissues, its ability to cause glucose uptake from the blood is diminished (DeFronzo et al., 2015). As T2DM progresses, pancreatic β-cells are no longer able to produce enough insulin to regulate blood glucose, and hyperglycemia develops (DeFronzo et al., 2015).

Skeletal Muscle Insulin Resistance

Insulin resistance (IR) is a hallmark feature of T2DM and is believed to appear as a symptom long before β-cells begin to fail producing sufficient insulin and hyperglycemia becomes evident (DeFronzo and Tripathy, 2009). IR is characterized by a decreased response of skeletal muscle to insulin signalling and a failure to suppress gluconeogenesis in the liver (DeFronzo and Tripathy, 2009; Hatting et al., 2018). In normal glucose control conditions, when insulin signalling is active (e.g. post-prandially), up to 80% of glucose uptake occurs in skeletal muscle (DeFronzo and Tripathy, 2009). Studies have shown that glucose uptake by muscle in individuals with T2DM may be reduced up to 50% in hyperinsulinemic conditions (DeFronzo and Tripathy, 2009). Furthermore, insulin regulates production of glucose in the liver under normal conditions, but when an individual develops insulin resistance, hepatic glucose

production increases (Hatting et al., 2018). Mitochondrial dysfunction has been heavily correlated with IR although the mechanisms have yet to be clearly elucidated (Sergi et al., 2019; Gonzalez-Franquesa and Patti, 2017). Studies of individuals with IR and T2DM have consistently shown a wide variety of differential mitochondrial dynamics including biogenesis, mitophagy, fission and fusion (Sergi et al., 2019; Gonzalez-Franquesa and Patti, 2017). Individuals with T2DM have also characteristically shown a decreased CI activity which aligns with mitochondrial dysfunction (Sergi et al., 2019).

Energy Regulation and AMPK

AMPK is a serine/threonine kinase and is the master regulator of cellular metabolism in eukaryotes (Sanz, 2008). Due to its ability to sense energy levels, it has been the focus of much research related to treatment of various metabolic diseases, particularly T2DM. In humans, there are 2 isoforms of the α- and β-subunits (α_1, α_2 and β_1, β_2), and 3 isoforms of the γ-subunit (γ_1, γ_2, and γ_3) – this suggests the possibility of 12 different combinations of subunits (Jeon, 2016). The α-subunits are encoded by *PRKAA1* and *PRKAA2,* the β-subunits are encoded by *PRKAB1 and PRKAB2,* and the γ-subunits are encoded by *PRKAG1*, *PRKAG2*, and *PRKAG3* genes respectively (Herzig and Shaw, 2018). In human *vastus lateralis* muscle, only 3 combinations exist: $\alpha_1/\beta_2/\gamma_1$, $\alpha_2/\beta_2/\gamma_1$, and $\alpha_2/\beta_2/\gamma_3$ (Crawford et al., 2010; Mahlapuu et al., 2004). The γ_3 isoform of the subunit has been shown to be highly specific to skeletal muscle, whilst the γ_1 and γ_2 isoforms have broader distribution in tissues (Mahlapuu et al., 2004). The γ_3 subunit is upregulated in human skeletal muscle upon differentiation of human primary myoblasts to multinucleated myotubes (Jeon, 2016; Costford et al., 2007). The isoform combination $\alpha_2/\beta_2/\gamma_3$ is also predominantly activated during exercise in human skeletal muscle (Birk and Wojtaszewski; Herzig and Shaw, 2018). AMPK is controlled by the naturally

fluctuating levels of adenosine monophosphate (AMP) and ATP in the cellular environment (Herzig and Shaw, 2018). The role of AMPK is to upregulate the production of ATP by initiating energy generating pathways and inhibiting energy consuming processes upon sensing that the AMP:ATP ratio is increased (Herzig and Shaw, 2018). It is critical for the cell to minimize futile metabolic cycles to avoid exhausting its remaining resources when ATP levels are low (Herzig and Shaw, 2018). The α-subunit of AMPK contains the kinase domain and the critical residue Thr172 which must be phosphorylated by an upstream kinase to be activated (Herzig and Shaw, 2018). Thr172 is found in the activation loop of the α-subunit and when phosphorylated stimulates a 100-fold increase in activity of AMPK (Willows et al., 2017). AMPK is most commonly phosphorylated at Thr172 by upstream kinases liver kinase B1 (LKB1) and calcium/calmodulin-dependent kinase 2 (CAMKK2) (Herzig and Shaw, 2018).

Regulatory Subunits

The β- and γ-subunits are regulatory: the β-subunit contains a carbohydrate-binding domain that allows association of AMPK with glycogen, and the γ-subunit contains the domain responsible for responding to AMP:ATP ratio changes (Herzig and Shaw, 2018). The γ-subunit is able to bind to AMP with high affinity and with lesser affinity to ATP because it contains 4 tandem cystathionine-β-synthase (CBS) domains (Herzig and Shaw, 2018). The binding of AMP can increase the basal AMPK activity by 2- to 5- fold (Viollet et al., 2010). There are 3 proposed mechanisms by which AMP binding at the γ-subunit can stimulate AMPK activity (Herzig and Shaw, 2018). The first potential mechanism involves the binding of AMP to stimulate the phosphorylation of Thr172 by an upstream kinase by either directly activating the upstream kinase, or by acting as an allosteric activator that changes the conformation of

AMPK to be more receptive to phosphorylation at Thr172 (Herzig and Shaw, 2018). The second proposed mechanism of action is that the bound AMP prevents dephosphorylation of the Thr172 residue by physically protecting the phosphorylation site from phosphatases (Herzig and Shaw, 2018). The last proposed mechanism is that AMP binding is necessary to allosterically activate AMPK that is already phosphorylated at Thr172 (Herzig and Shaw, 2018). The binding of AMP occurs in a cooperative manner in which the binding of one AMP greatly increases the binding affinity of AMPK for further AMP molecules (Gu et al., 2017). ATP is also capable of binding to the CBS domains in order to allow AMPK to respond to rising levels of ATP, which allows AMPK to become inactivated (Herzig and Shaw, 2018). The ability to bind both AMP, (ADP) and ATP competitively is in large part the reason why AMPK is considered a master regulator of cellular energy levels. It is critical in maintaining cellular energy homeostasis (Herzig and Shaw, 2018).

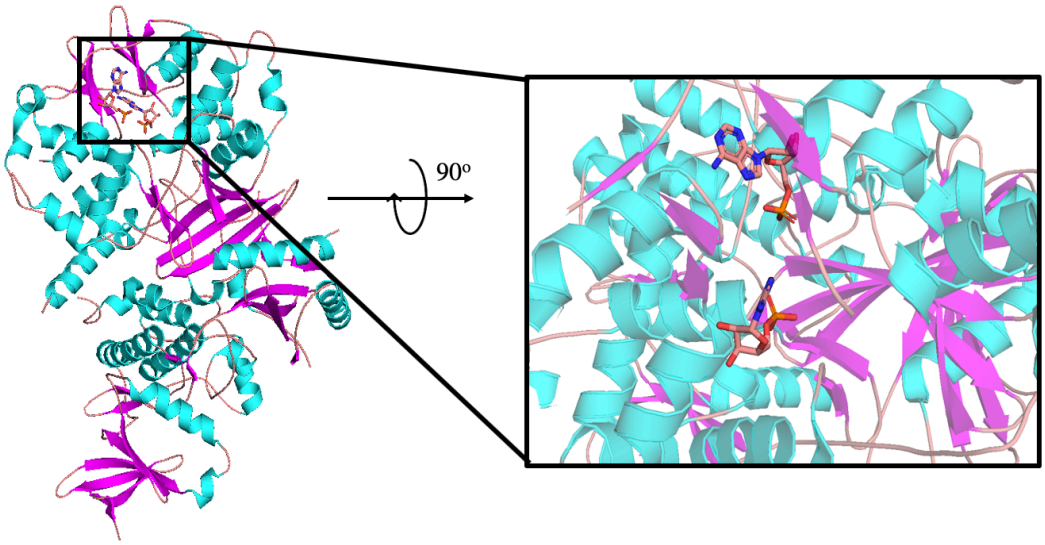

Figure 7. AMP-bound AMPK in active form.

A full view of active AMPK and a zoomed-in top view of the AMP-binding site with two AMP molecules present. Structure was produced from PDB ID: 4CFH in MacPyMOL by Schödinger ©.

AMPK Signalling

Active AMPK is able to phosphorylate and have an effect on several different targets related to energy homeostasis. AMPK can have an impact on every macromolecule synthesis, breakdown, and storage (Herzig and Shaw, 2018). Firstly, AMPK has an activating effect on glucose uptake in order to bring in glucose from which ATP can be generated, and an inhibitory effect on glycogen synthesis in order to pause the storage of glucose when there is a need for its oxidation (Hunter et al., 2011). Furthermore, in an effort to restore fuel levels, AMPK can activate fatty acid catabolism, and inactivate fatty acid synthesis processes to lead to production of more ATP (Hardie and Pan, 2002; Houten et al., 2016). It is also able to halt cholesterol synthesis processes by directly phosphorylating the rate-limiting step enzyme HMG-CoA reductase (Zhang et al., 2015). AMPK has been known to have an influence on processes involved in mitochondrial synthesis and turnover to maintain health of the mitochondrial reticulum (Thornton, 2017; Herzig and Shaw, 2018). Specifically, AMPK can induce mitochondrial biogenesis, regulate mitochondrial ultrastructure, and activate autophagy/mitophagy through the mammalian target of rapamycin (mTOR) (Saxton and Sabatini, 2017), and Unc51-like Autophagy Activating Kinase 1 (ULK1) (Hardie, 2011; De Palma et al., 2014).

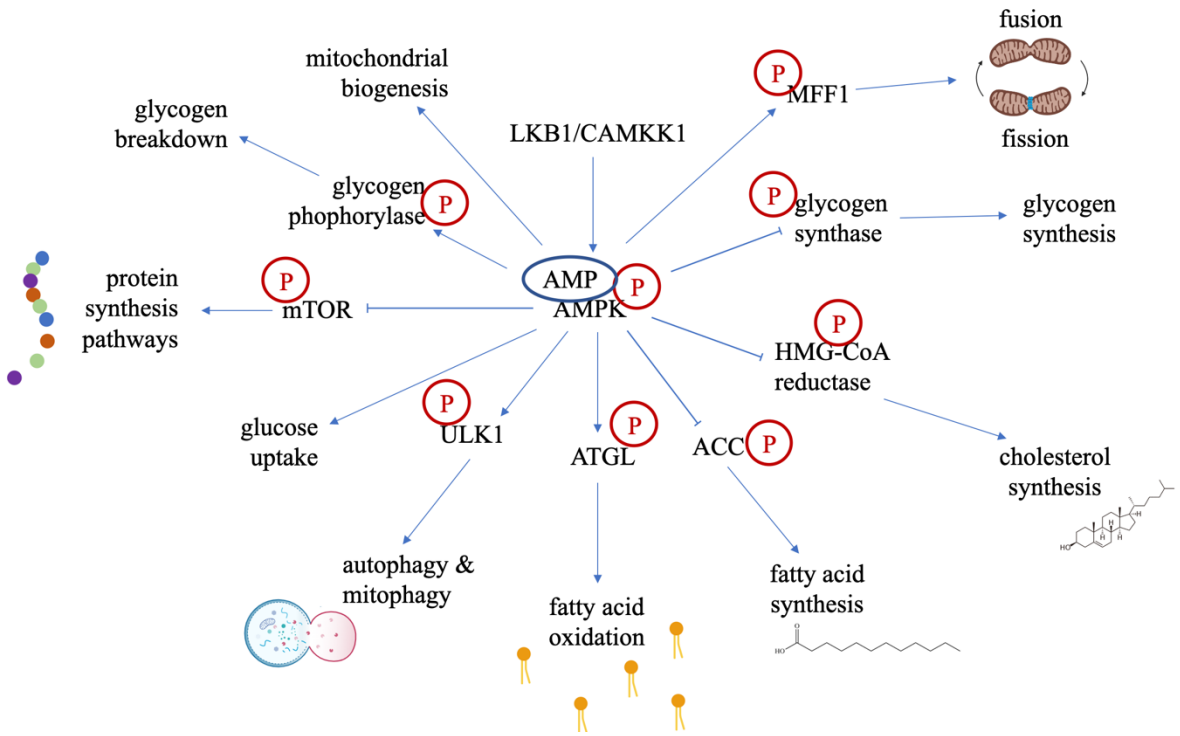

Figure 8. Summary of AMPK pathways.

Activated AMPK has many targets. It phosphorylates various proteins in order to activate downstream pathways. P is indicative of a phosphorylation event.

AMPK, Glucose Uptake and Glycogen Synthesis

AMPK promotes glucose transport into cells for glycolysis in times of energy deficit by activating GLUT4 translocation to the cellular membrane, whilst simultaneously inhibiting glycogen synthase, which is necessary for glycogenesis (Hunter et al., 2011). G6P, a glycolysis intermediate, is able to overcome the glycogen synthase inhibition by AMPK as it opposes the action by activating glycogen synthase (Hunter et al., 2011). Glycogen can also be broken down by glycogen phosphorylase in a process called glycogenolysis, which is activated by AMPK when phosphorylated (Jeon, 2016).

AMPK and Fatty Acid Catabolism and Synthesis

As noted previously, FAO is activated in energy-deficient cell environments, when ATP levels begin to drop. When AMPK is active, it is capable of phosphorylating and inactivating acetyl-

CoA carboxylase (ACC), which is responsible for the irreversible carboxylation of acetyl-CoA to produce malonyl-CoA (Hardie and Pan, 2002). AMPK directly phosphorylates ACC1 at Ser79 and ACC2 at Ser212 (Galic et al., 2018). In the absence of malonyl-CoA, a CPT1 inhibitor, FAs are capable of entering the mitochondria, and proceeding into FAO which produces acetyl-CoA and electron carriers (Hardie and Pan, 2002; Houten et al., 2016). Since FAO leads to the restoration of ATP levels, it is natural that AMPK would inhibit the opposite process, FA synthesis (Houten et al., 2016). Furthermore, AMPK is able to inhibit cholesterol synthesis by phosphorylating HMG-CoA reductase which is the rate-limiting enzyme and primary site of control in this process (Zhang et al., 2015). When there is an excess of acetyl-CoA and it does not need to be used to form ATP, it can be deposited in the form of cholesterol (Zhang et al., 2015). This occurs when AMPK is inactive; it is the main phosphorylating enzyme for HMG-CoA reductase (Zhang et al., 2015).

AMPK and Mitochondrial Fusion/Fission

Mitochondria are extremely dynamic organelles and are constantly undergoing fusion and fission cycles in order to preserve integrity and quality of mitochondria (Thornton, 2017). A long-term loss of the this dynamic cycle can be deleterious to an organism (Thornton, 2017). Fusion is governed by 3 key proteins: mitofusin-1 (MFN-1) and -2 (MFN-2), and optic atrophy protein 1 (OPA-1) (Westermann, 2010). Both MFN-1 and MFN-2 are in contact with each other in the cell and play an important role in fusion through mitochondrial membrane tethering (Li et al., 2019). Distinctive mechanistic differences between the two mitofusins have not been fully elucidated; however in yeast MFN-1 has a much higher GTP turnover than MFN-2, while mutations in MFN-2 are associated with many more human diseases (Li et al., 2019). Key fission proteins include dynamin-related protein 1 (DRP1) and mitochondrial

fission protein 1 (Fis1) (Westermann, 2010; Thornton, 2017). Fusion is thought to allow interchange of mitochondrial content within the cell in order to defuse accumulating mtDNA mutations and to increase ATP production by maintaining integrity of the mitochondrial complexes (Thornton, 2017). Fission is viewed as a precursor to mitophagy, as well as in preparation for apoptosis (Thornton, 2017). Importantly, AMPK has been suggested to promote fusion and to directly phosphorylate DRP1 in order to inhibit fission, but these mechanisms have yet to be fully elucidated (Thornton, 2017). It has been suggested that AMPK targets A kinase anchoring protein 1 (AKAP1) which can then recruit protein kinase A (PKA) to the mitochondrial membrane (Zhang et al., 2017; Merrill and Strack, 2014). PKA is able to phosphorylate and subsequently inhibit DRP1 at Ser637 (Merrill and Strack, 2014). DRP1 can be dephosphorylated by calcium-dependent phosphatase; however it is unknown whether this plays a role in DRP1-dependent fission (Merrill and Strack, 2014).

AMPK and Mitochondrial Biogenesis

Mitochondrial biogenesis is the process of growing and dividing pre-existing mitochondria in order to increase the overall mitochondrial mass in the cell (Herzig and Shaw, 2018). Both exercise and the AMPK-activating drug 5-aminoimidazole-4-carboxamide-1-β-D-ribofuranoside (AICAR) are able to lead to chronic AMPK activation and results in increase in mitochondrial biogenesis (Herzig and Shaw, 2018). Peroxisome proliferator-activated receptor-gamma coactivator 1α (PGC1α) is a master regulator of mitochondrial biogenesis and has 2 phosphorylation sites for AMPK: Thr155 and Ser538 (Herzig and Shaw, 2018). Active PGC1α directly affects biogenesis by acting as a transcriptional factor, promoting the expression of nuclear respiratory factors 1 (NRF-1) and 2 (NRF-2) (Reznick and Shulman,

2006). NRF-1 and NRF-2 are important in transcribing several mitochondrial enzymes and for replicating mtDNA in preparation for biogenesis (Reznick and Shulman, 2006).

AMPK and mTOR Signalling

The mTOR pathway plays a key role in coordinating and regulating cell growth and metabolism, respectively (Saxton and Sabatini, 2017). mTOR is a serine/threonine protein kinase, like AMPK, that forms the catalytic subunit of mTOR complex 1 (mTORC1) and 2 (mTORC2) (Saxton and Sabatini, 2017). mTORC1 contains 3 core units: mTOR, the regulatory protein associated with mTOR (Raptor), and mammalian lethal with Sec13 protein 8 (mLST8) (Saxton and Sabatini, 2017). Raptor is responsible for recruiting the substrate whilst mLST8 helps stabilize the kinase activation loop (Saxton and Sabatini, 2017). mTORC2 has similar core units, but instead of Raptor it contains the rapamycin insensitive companion of mTOR (Rictor) (Saxton and Sabatini, 2017). Rictor has analogous function to Raptor (Saxton and Sabatini, 2017). Protein synthesis is greatly implicated in the mTOR signalling pathway. mTORC1 acts by phosphorylating p70S6 kinase (S6K1) and eukaryotic Initiation Factor (eIF) 4E Binding Protein 1 (4E-BP1) (Saxton and Sabatini, 2017). S6K1 is phosphorylated at Thr389, a hydrophobic region of the kinase which allows it to be activated by phosphoinositide-dependent kinase 1 (PDK1) (Saxton and Sabatini, 2017; Peterson et al., 1999). Phosphorylation of S6K1 at Ser371 has also been shown to be essential in order to allow Thr389 to be phosphorylated, and thus is essential to the activity of S6K1 (Peterson et al., 1999). When active, S6K1 proceeds to phosphorylate several downstream targets in order to upregulate mRNA translation (Saxton and Sabatini, 2017). 4E-BP1 is phosphorylated at several sites by mTORC1; when unphosphorylated, it acts as an inhibitor of eIF4E, blocking mRNA translation and proliferation – it is considered to have tumour suppressing activity

(Musa et al., 2016). However, when it is phosphorylated, its inhibitory activity is prevented, thus promoting the opposite: mRNA translation and proliferation (Musa et al., 2016; Saxton and Sabatini, 2017). S6 ribosomal protein (S6RP) is also a target of active S6K1 phosphorylation and acts to control translation of proteins at the ribosome (Li et al., 2014). mTOR is a target of AMPK phosphorylation, and when phosphorylated, mTOR action is inhibited (Saxton and Sabatini, 2017).

AMPK, Autophagy and Mitophagy

Autophagy is a highly conserved, critical cellular process that allows the body to clean damaged cells and prevent stress caused by these cells (Khandia et al., 2019). Dysregulation of autophagy is associated with several human diseases such as cancer and degenerative diseases (Khandia et al., 2019). Autophagy is a lysosomal-degradation pathway that acts primarily as a quality control mechanism; however, it can also be used as a protein-recycling mechanism under conditions of cell starvation (Zachari and Ganley, 2017). AMPK has been shown to have an activating effect on ULK1, a key autophagy-related protein, by phosphorylation (Hardie, 2011). ULK1 is a serine/threonine protein kinase, which is a direct target of AMPK, and is capable of initiating autophagy pathways (Hardie, 2011).

p62 is an autophagy substrate used to deliver ubiquitinated proteins to proteasomes for degradation (Liu et al., 2016). p62 accumulates when autophagy is inhibited, and is depleted when autophagy is activated (Komatsu and Ichimura, 2010). The degradation of p62 is mediated by microtubule-associated protein 1A/1B light chain 3 (LC3) which plays an important role in autophagosome formation (Komatsu and Ichimura, 2010; Tanida et al., 2008). The interaction between p62 and LC3 causes p62 to be localized to the lysosome (Komatsu and Ichimura, 2010). LC3 levels are considered indicative of the quantity of

autophagosomes, and levels are often used as an indicator of autophagy, coupled with decreased p62 levels (Tanida et al., 2008). Chloroquine is a drug that is often used to block autophagy in *in vitro* experiments and then immunoblotting for LC3 and p62 is often used to demonstrate that protein levels are changing due to autophagy (Mauthe et al., 2018). Chloroquine blocks the degradation of target proteins by disrupting autophagosome-lysosome fusion (Mauthe et al., 2018), which allows for the study of autophagic flux.

Mitophagy is a subset function of autophagosomes and results in the degradation of damaged or excessive mitochondria (De Palma et al., 2014). PTEN-induced kinase (PINK1) distinguishes damaged mitochondria from healthy mitochondria and recruits Parkin to damaged mitochondria (Jin and Youle, 2012). Parkin ubiquitylates proteins located on the outer mitochondrial membrane to initiate mitophagy (Jin and Youle, 2012). Parkin is also capable of preventing mitochondrial fusion by degrading MFN-1 and MFN-2, both of which are critical components for mitochondrial fusion (Jin and Youle, 2012). AMPK is said to regulate mitophagy through activation of ULK1, similarly to autophagy, however the exact mechanism of action has not yet been elucidated (Herzig and Shaw, 2018).

R225W Phenotype

The Harper Laboratory and close collaborators have previously identified in humans a novel AMPK mutation, R225W, in *PRKAG3,* the gene coding for the γ_3 subunit (Crawford et al., 2010; Costford et al., 2007). This mutation was initially discovered as a part of a study on factors affecting leanness and ongoing studies in the Ottawa Hospital Weight Management Clinic. The mutation has only been identified in two distinct families to-date.

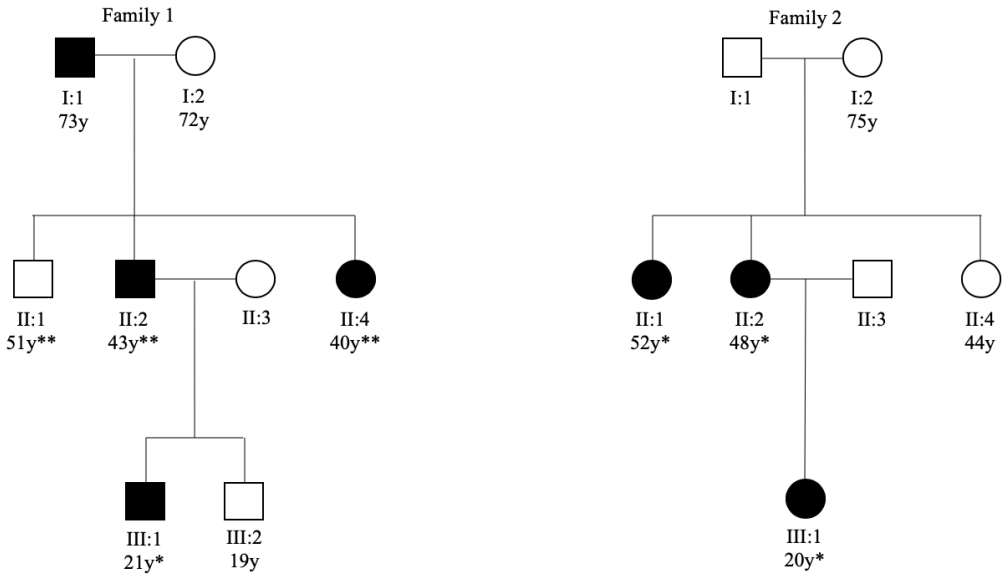

Figure 9. Families of two probands with the R225W mutation.

The * and ** denoted individuals had *vastus lateralis* skeletal muscle biopsies; the number of * indicates how many times they were biopsied over several years of research. Ages reported are from initial biopsies in 2007.

AMPKγ_3 R225W is a naturally existing, but rare, mutation in skeletal muscle. No other affected individuals have been identified internationally. However, the allele frequency is approximately 1 in 10,000, and has only been identified in individuals of European descent (rs138130157). R225W is believed to be a gain-of-function mutation in humans which leads to an overall increased resistance to fatigue (Crawford et al., 2010; Costford et al., 2007). This mutation in human cardiac muscle is analogously found as R302Q in the *PRKAG2* gene of the γ_2 subunit (Doevendans and Wellens, 2001). In cardiac muscle, this mutation is not advantageous and is one of the known mutations associated with Wolff-Parkinson-White Syndrome, a congenital heart defect that can cause periods of tachycardia (Doevendans and Wellens, 2001). An analogous *PRKAG3* gene mutation also exists in Hampshire pigs, R200Q, which has been linked to increased muscle glycogen storage (Costford et al., 2007; Doevendans and Wellens, 2001; Andersson, 2003). In skeletal muscle, their glycogen storage

is increased by 70%, with no changes in cardiac muscle or liver glycogen levels (Nilsson et al., 2006). This mutation in pigs has been identified as the Rendement Napole (RN^-) genotype, and these pigs are non-marketable because the high glycogen content results in high acidity and water content in the meat (Zhao et al., 2009; Du, 2004). In mice, the same phenotype is achieved with the R225Q mutation in the *Prkag3* gene (Nilsson et al., 2006). AMPK γ_3 knock-out (*Prkag3*$^{-/-}$) and transgenic R225Q (*TgPrkag3*^{225Q}) mice have been bred to exhibit the same phenotypes as the human R225W mutation (Nilsson et al., 2006).

The R225W mutation was initially identified through the Ottawa Hospital Weight Management Clinic through participants in a study on leanness by the University of Ottawa Heart Institute (UOHI) (Costford et al., 2007), leading to the discovery of these unique individuals who did not experience muscle fatigue. The cohort consisted of 761 individuals with obesity (mean BMI 39.9 kg/m^2) and 759 lean individuals (mean BMI 20.1 kg/m^2) (Costford et al., 2007). *Crawford et al.* assessed muscle fatigue resistance by electromyography during 60 second isometric contraction of the quadricep muscle and found that individuals with the R225W mutation were extremely resistant to fatigue when compared to their matched controls (Crawford et al., 2010). AMPK activity in cells was increased independently of changes in mRNA and protein expression of AMPKγ_3, suggesting that the impacts of this mutation specifically impacted activity and not its levels (Crawford et al., 2010; Costford et al., 2007). The mutation was thus shown to lead to AMPK being constitutively active (Crawford et al., 2010; Costford et al., 2007). Moreover, the R225W mutation in AMPKγ_3 has been shown to increase mitochondrial content. Specifically, *Costford et al.* found by bicinchoninic acid (BCA) assay that the increased AMPK activity in R225W individuals leads to a threefold increase in mitochondrial content (Costford et al., 2007). These findings

were consistent with mouse studies, showing that mitochondrial content was also increased in translational animals (Bergeron et al., 2001). *Costford et al.* used a Periodic Acid Schiff (PAS) stain to quantify skeletal muscle glycogen content, and it was found to be double, compared to matched controls (Costford et al., 2007). Furthermore, intramuscular triglyceride (IMTG) was found to be reduced in the R225W individuals as compared to matched controls; however, *Costford et al.* determined that when the R225W and control cells were treated with the AMPK activator AICAR, IMTG content decreased in the primary skeletal muscle cells from age-matched controls, but not in the cells isolated from R225W individuals (Crawford et al., 2010; Costford et al., 2007). Studies have demonstrated that treatment with AICAR, which stimulates activity of AMPK, similarly to the R225W mutation, is accompanied by a decrease in blood glucose concentration, likely due to increased glucose uptake (Musi and Goodyear, 2003). *Crawford et al.* observed this effect when conducting a glucose uptake assay by exposing cells to 2-deoxy[^{3}H]-glucose and 2-deoxy-glucose; the R225W cells were found to have an 80% higher basal glucose uptake than the matched control cells (Crawford et al., 2010). Glucose uptake was also determined with PET scans *in vivo,* and the volume of muscle actively taking up glucose in R225W affected individuals was significantly higher (Crawford et al., 2010). Furthermore, they investigated the oxidative capacity of R225W myotubes and determined that the oxygen consumption rate (OCR) was significantly greater at leak-dependent and maximal respiration (Crawford et al., 2010). The increased oxidative capacity was found accompanied by an increase in CS activity, a known biomarker for mitochondrial density in skeletal muscle (Crawford et al., 2010). To our knowledge, no other group internationally has found this mutation in humans and obtained primary skeletal muscle cells.

The overall goal of this study was to further characterize the R225W phenotype by delving deeper into the various pathways that AMPK is capable of affecting when constitutively active.

In this study, we assessed metabolic flexibility in primary human primary muscle cells by quantifying ATP production from glycolysis and OXPHOS. We hypothesized that oxidative capacity and metabolic flexibility of the muscle obtained from R225W individuals would be increased. Moreover, we expected the muscle fibres and primary myotubes from the R225W individuals would exhibit increased fatty acid oxidation, mitochondrial turnover and autophagic flux.

Methods

Subjects/Participants

Subject inclusion criteria for this study have previously been described by *Costford et al.* (Costford et al., 2007). Briefly, subjects were matched for gender, age, weight, body-mass index (BMI), and intensity of self-reported exercise each week. Experimental procedures were approved by the Research Ethics Board of the Ottawa Hospital and the UOHI. Written informed consent was obtained from all participants. Percentage body fat was determined by a bioelectrical impedance scale. Blood samples were collected after a 12-hr. fast, routine blood analyses were carried out in the Clinical Biochemistry Laboratory at the Ottawa Hospital.

Vastus lateralis biopsy

Four subjects with the R225W mutation and four control subjects were matched for gender, age, weight, BMI, and self-reported weekly physical activity. Participants refrained from physical activity for 3 days and fasted for 12 hr. prior to the biopsy. Percutaneous skeletal muscle biopsies of the *vastus lateralis* muscle were taken from the R225W individuals and their matched controls using a 5 mm Bergstrom needle (Opitek) under 1% lidocaine local anaesthetic as previously described by *Costford et al.* (Costford et al., 2007). *Vastus lateralis* muscle was immediately divided: one in ice-cold relaxing solution (BIOPS (5.77 mM Na_2ATP, 7 10 EGTA-CaEGTA buffer (60 mM K-lactobionate, 15 mM phosphocreatinine, 20 mM imidazole, 0.5 mM DTT, 50 mM MES, pH 7.1 at 0^{o}C)) for mitochondrial respiration analysis; and one in Ham's F10 medium used for tissue culture of primary myoblasts; remaining tissue was snap frozen in liquid nitrogen and stored at -80^{o}C for further analyses.

Cell culture

A 25 mg sample of tissue was cultured, and satellite cells were cultured in Ham's F10 medium with 1% antibiotic-antimycotic, 2.5 µ/mL gentamycin, 12.5% FBS, 826 nM dexamethasone, 8.3 ng/mL human epidermal growth factor, and 25 pmol of insulin. Satellite cells were isolated via immune sorting using a magnetic column and CD56 antibody coated magnetic microbeads. CD56 positive cells were differentiated into myotubes by incubation for 7-10 days in Dulbecco's modified Eagle's medium (DMEM) with 2% horse serum, 1% antibiotic-antimycotic, and 2.5 µg/mL gentamycin.

Oxygen consumption of primary myotubes

Cellular bioenergetics were assessed in primary myotubes using the Seahorse XFe96 (Agilent Technologies, Santa Clara, CA, USA). Briefly, 15,000 myoblasts were plated in each well on a 96-well Seahorse plate and differentiated into myotubes for 7-10 days. On the day of the assay, growth medium was changed to Seahorse medium (DMEM powder, 1 g/L D-glucose, 1 mM sodium pyruvate, 4 mM L-glutamine, pH 7.4) for 1 hr. prior to analysis. During the assay, basal respiration was measured first, followed by the measurement of leak respiration, which was induced by oligomycin (2 µg/mL). 2 µM of carbonyl cyanide p-(trifluoromethoxy) phenyl-hydrazone (FCCP) was then injected to induce maximal respiration. Subsequently, 5 µM antimycin-A and 10 µM rotenone were injected together to measure non-mitochondrial OCR. Lastly, 20 M monensin was injected to measure maximal extracellular acidification rate (ECAR). Oxygen consumption values were adjusted to the non-mitochondrial oxygen consumption following the addition of antimycin-A and rotenone. After the assay, the myotubes were washed twice with 100 µL of 1X phosphate-buffered saline (PBS), then placed in 40 µL of RIPA buffer (0.5M Tris-HCl, pH 7.4, 1.5M NaCl, 2.5% deoxycholic acid, 10%

NP-40, 10mM EDTA) containing 0.1% protease inhibitor cocktail (PIC)(Sigma Aldrich #P8340, 1:1000). A bicinchoninic acid (BCA) (Pierce BCA Protein Assay Kit; Thermo Fisher Scientific #23225, Rockford, IL, USA) assay was used to determine protein concentration in each well and Seahorse assay measurements were normalized to protein content (µg/mL). Bioenergetic capacity and fuel flexibility characteristics were investigated by graphing glycolytic and oxidative ATP production as previously described by *Mookerjee et al*. (Mookerjee et al., 2017). We used *Mookerjee et al*'s. openly available table for calculations with the following two assumptions: the buffering power of our media is estimated at 0.1 mpH/pmol H^+ in 7µL; and the maximal ECAR is a slight underestimation due to the presence of oligomycin during the assay, although the presence of rotenone and antimycin A should restrict this underestimation (Mookerjee et al., 2017).

Oxygen consumption of AMPK-inhibited myotubes

To assess the contribution of constitutively active AMPK to the observed increase in OCR of the R225W primary myotubes, cellular bioenergetics were assessed using the Seahorse XFe96 in the presence of Compound C. 24 hr. prior to the Seahorse assay, primary myotubes were incubated with 10 µM AMPK inhibitor Compound C (Sigma Aldrich #P5499).

Oxygen Consumption of myotubes with glycogen phosphorylase inhibitor

To assess whether the increased OCR in R225W primary myotubes was in part due to the glycogen storage, we treated the cells with a glycogen phosphorylase inhibitor, CP-316819 (Sigma Aldrich #PZ0189). 24 hr. prior to the Seahorse assay, primary myotubes were incubated with 10 mM of CP-316819 inhibitor. Cellular bioenergetics were assessed using the Seahorse XFe96.

Fatty acid oxidation mitochondrial stress test in primary myotubes

15,000 myoblasts/well were plated on XFe96 plates and differentiated for 7-10 days. 24 hr. prior to the Seahorse assay, cells were placed in a substrate-limited medium (DMEM powder, 0.5 mM glucose, 1mM L-glutamine, 0.5 mM carnitine, 1% FBS). The oligomycin (2 µg/mL), FCCP (2 µM) antimycin-A/rotenone (5 µM/10 µM), and monensin (20 µM) were prepared in fatty acid oxidation (FAO) assay medium (111 mM NaCl, 4.7 mM KCl, 1.25 mM $CaCl_2$, 2 mM $MgSO_4$, 1.2 mM NaH_2PO_4, 2.5 mM glucose, 0.5 mM carnitine, 5 mM HEPES, pH 7.4, 37^{o}C). The substrate-limited media was removed and replaced with FAO Assay medium and incubated in a non-CO_2 incubator at 37^{o}C for 30 min. 15 min. prior to the start of the assay, select wells were treated with 40 µM etomoxir to inhibit CPT1 and then incubated for 15 min. at 37^{o}C in a non-CO_2 incubator to allow for etomoxir to be taken up by the cells and to bind to CPT1. Prior to starting the assay, cells were treated with 0.17 mM palmitate:bovine serum albumin (BSA) or just 0.03 mM BSA (vehicle control). In brief, the conjugated palmitate:BSA was done using FA-free (FAF) BSA, which was added to 150 mM NaCl and stirred until dissolved at 37^{o}C. Then ½ of the BSA was diluted to 0.17 mM for stock at -20^{o}C. Sodium palmitate was added to the other ½ of BSA and stirred at 70^{o}C. Then pH was adjusted to 7.4 (Seahorse Bioscience). A BCA assay was performed to determine protein concentration in each well and Seahorse assay measurements were normalized to protein content (µg/mL).

Metabolic enzyme activities

Enzyme activities for CS and CPT1 were determined in differentiated myotubes. Pelleted cells were lysed in ice-cold RIPA buffer using a 28-gauge needle and syringe. Cellular debris was eliminated through centrifugation of the lysate at 14,000 g for 10 min. at 4^{o}C. The supernatant was collected and stored at -80^{o}C until further use. All assays were performed using the BioTek

Synergy 96-well microplate reading spectrophotometer at room temperature (RT). CS activity was determined by measuring absorbance at 412 nm in 50 mM Tris-HCl (pH 8.0) with 0.2 mM DTNB, 0.1 mM acetyl-coA and 0.25 mM oxaloacetate. CPT1 activity was determined by measuring absorbance at 412 nm in 50 mM Tris-HCl (pH 7.4) with 0.5 mM palmitoyl Co-A, 0.2 mM DTNB, 150 mM KCl, 1.88 nM BSA and 5 mM L-carnitine. Rate of absorbance change, and path length of each well was determined using BioGen 5.0 The enzyme activities were calculated using extinction factors 13.6 $mM^{-1}cm^{-1}$ for CS, and 6.22 $mM^{-1}cm^{-1}$ for CPT1.

Maximal activities of mitochondrial respiratory complexes

Mitochondrial complex activities were determined as described by *Spinazzi et al.* (Spinazzi et al., 2012). In brief: Complex I was measured as a decrease in NADH at 340nm in 50mM potassium phosphate buffer (pH 7.5) with 100 µM NADH, 60 µM coenzyme Q, 3 mg/mL FA free-BSA (FAF-BSA), 300 µM KCN. Complex II was measured as the reduction of dichlorophenolindopenol (DCPIP) at 600nm in 25mM potassium phosphate buffer (pH 7.5), 20mM succinate, 80 µM DCPIP, 50 µM decylubiquinone (DUB), 1 mg/mL FAF-BSA, and 300 µM KCN; Complex III was measured as the reduction of cytochrome C at 550nm in 0.025% tween-20 in 25mM potassium phosphate buffer (pH 7.5), 100 µM decylubiquinol, 75 µM cytochrome C, 500 µM KCN, and 100 µM EDTA; Complex IV was measured as the oxidation of cytochrome C at 550 nm in 50 mM potassium phosphate buffer (pH 7.0), and 50 µM of reduced cytochrome C. Complex I+III linked activity was measured as the reduction of cytochrome C at 550 nm in 50 mM potassium phosphate buffer (pH 7.5), 200 µM NADH, 50 µM cytochrome C, 1 mg/mL FAF-BSA, and 300 µM KCN. Complex II+III linked activity was measured as the reduction of cytochrome C at 550 nm in 0.5 M potassium phosphate buffer (pH 7.5), 10 mM succinate, 50 µM cytochrome C, and 300 µM KCN. Extinction coefficients

were used for data analysis (CI = 6.2, CII = 19.1, CIII, CIV, CI+CIII = 18.5, CII+CIII = 13.6 $mM^{-1}cm^{-1}$) and normalized to protein concentration and citrate synthase activity (Spinazzi et al., 2012).

High resolution respirometry of permeabilized myotubes

The oxygen consumption of myotubes isolated from affected and control individuals was determined using high resolution respirometry (OROBOROS Instruments, Innsbruck, Austria). Two assays were conducted at 37°C in MiR05 (0.5mM EGTA, 3mM $MgCl_2 \cdot H_2O$, 20mM taurine, 10mM K_2HPO_4, 20mM HEPES, 110mM sucrose, 1g/L BSA (pH 7.1, 37°C)). Myotubes were detached using 0.25% Trypsin-EDTA and resuspended in MiR05 buffer. Following addition of the cells to the chamber, myotubes were permeabilized with 4.05 µM digitonin, and the assay was started with the addition of 5mM malate and 10mM pyruvate to measure leak respiration in the presence of low endogenous ADP (CI leak), then 2.5mM ADP was added to measure CI-dependent phosphorylating oxidative phosphorylation (CI OXPHOS) Following that, 10mM succinate was added to measure combined CI and CII OXPHOS, and then phosphorylation was inhibited using 2.5 µM oligomycin which inhibits F_0F_1-ATPAse to measure proton leak (under conditions when mitochondria are energized). Finally, OXPHOS was uncoupled with 0.5 µM titrations of FCCP, and then 1 µM antimycin-A was added to inhibit electron flow at CIII.

To measure FA oxidation, 0.1mM malate was added to digitonin permeabilized myotubes to measure leak respiration (CI+FAO leak), and then 0.5mM L-carnitine and 20 µM palmitoyl-CoA was added to measure CI+FAO OXPHOS dependent on CPT1 activity. Following that, 5mM ADP was added to measure CI-dependent oxidative phosphorylation (CI OXPHOS), and then 10 µM palmitoyl-carnitine and 100 µM octanoyl carnitine were added to measure CPT1-

independent respiration using lipid-based substrates; then 10mM succinate was added to measure combined CI and CII OXPHOS, and then phosphorylation was inhibited with 2.5 μM oligomycin which inhibits F_0F_1-ATPAse to measure CI and CII leak. Finally, OXPHOS was uncoupled with 0.5 μM titrations of FCCP to assess uncoupled maximal respiration, and then 1 μM antimycin-A was added to inhibit electron flow at CIII. Data are normalized to protein content as determined by BCA assay.

Permeabilization of biopsied fibres

Within 1-2 hr. after each *vastus lateralis* biopsy, BIOPS-stored muscle fibres [BIOPS (5.77 mM Na_2ATP, 7 10 EGTA-CaEGTA buffer (0.1 μM free Ca2) 6.56mM $MgCl_2$-$6H_2O$, 20 mM Taurine, 60 mM K-lactobionate, 15 mM phosphocreatine, 20 mM imidazole, 0.5 mM DTT, 50 mM MES, pH 7.1 at 0°C] were teased into fibre bundles and placed into 1 mL of fresh ice-cold BIOPS solution, containing 50 μg/ml of freshly-prepared saponin, for 30 min. under gentle agitation. Fibres were then washed three times in ice-cold respiration media (MiRO5, 0.5 mM EGTA, 3 mM $MgCl_2$-$6H_2O$, 2 0mM Taurine, 10 mM K_2HPO_4, 20 mM HEPES, 110 mM sucrose, 1 g/L BSA, pH 7.1 at 37°C). Fibre bundles were quickly blotted on filter paper and weighed, and approximately 2 mg were used immediately in respiration assays.

Assays to measure oxygen consumption, FAO and ROS production

Oxygen consumption and H_2O_2 emission from permeabilized fibres were measured simultaneously using high-resolution respirometry, coupled with fluorimetry (OROBOROS Instruments, Innsbruck, Austria). Assays were conducted at 37^{o}C in MiR05, with medium oxygen concentration maintained between 300-500 nmol/mL. All assays were conducted in duplicate. For ETC and FAO determinations, a SUIT protocol was run as previously described (see Methods: “High resolution respirometry of permeabilized myotubes”, pg. 34). H_2O_2

emission was determined using 50 μM Amplex Ultra Red (Thermo Fisher Scientific A36006, Waltham, MA, USA) in the presence of 5U/mL superoxide dismutase (SOD) and horseradish peroxidase (HRP), with excitation of 525 nm and emission of 615 nm. To calibrate the fluorimeter, 0.1 μM of H_2O_2 was added to each chamber prior to each assay. The assay was started with the addition of 5 mM malate and 10 mM pyruvate to measure leak respiration (CI LEAK); next, 2.5 mM ADP was added to quantify CI OXPHOS. Following, 10mM succinate was added to measure combined CI, CII OXPHOS. Subsequently, phosphorylation was inhibited following the addition of 1μM carboxyatractyloside, which inhibits the adenine nucleotide transporter (ANT), and 2.5 μM of oligomycin which inhibits the F_0F_1-ATPase, thus leak respiration with complex I and II electron input was measured (CI, CII LEAK). To induce uncoupling of OXPHOS, and maximal rate of the ETS, repetitive 1μL titrations of 0.5 μM FCCP were carried out, ETS CI, CII. 1 μM antimycin A was added to inhibit the flow of electrons through CIII in the ETS.

Mass-specific oxygen and H_2O_2 flux were calculated as the time derivative of oxygen and H_2O_2 concentration respectively using DatLab 6 Software (Oroboros Instruments). Non-mitochondrial oxygen consumption was determined after addition of antimycin A and used to adjust oxygen flux rates in other respiratory states. Respiration states were defined according to *Gnaiger* (Makrecka-Kuka et al., 2015). Mitochondrial H_2O_2 emissions was determined at all steady-states (CI LEAK, CI OXPHOS, CI CII OXPHOS, CI, CII LEAK, and ETS). To account for variations in mitochondrial mass between separate biopsies, citrate synthase (CS) activity per mg muscle was determined (see Methods: “Metabolic enzyme activities”, pg. 32) and used to normalise mitochondrial function measures, as it is well-correlated with

mitochondrial density. Values of mitochondrial respiration are expressed as pmol O_2/s/U.CS, and values of mitochondrial H_2O_2 emission are expressed as fmol H_2O_2/s/U.CS.

Western Blots

Flash frozen muscle was homogenized in ice-cold RIPA buffer (150mM NaCl, 1% NP-40, 0.5% deoxycholate, 0.1% SDS, Tris-HCl (pH 7.5), 0.1% Na_3VO_4, 0.1% protease inhibitor cocktail (PIC Sigma-Aldrich P8340 1:1000)) using a bead mill homogeniser (Thermo Fisher Scientific, Rockford, IL, USA). Sample aliquots containing 20 µg of protein were suspended in a 1x Laemmli buffer solution (10% glycerol, 2% SDS, 0.25% bromophenol blue, 400 mM dithiothreitol (DTT), 0.5 M Tris-HCl (pH 6.8)), boiled at 95°C for 5 min., and subjected to separation with SDS-PAGE. Proteins were transferred to a 0.2 µM nitrocellulose membrane then incubated with blocking buffer (5% BSA in Tris buffered saline containing 0.1% Tween 20 (TBS-T)) for 1 hr. at RT. The membranes were then incubated overnight at 4°C with primary antibodies under gentle wavering. Samples were probed for fusion markers: MFN-1 (Abcam #ab126575 1:1000), MFN-2 (Abcam #ab57602 1:1000), and OPA-1 (Abcam #ab42364 1:1000); mitochondrial biogenesis markers: NRF-1 (Santa Cruz Biotechnologies #sc-33771 1:1000), NRF-2 (Santa Cruz Technology #sc-365949 1:1000) and PGC1α (Santa Cruz Biotechnologies #sc-13067 1:1000); mTOR pathway proteins: mTOR (Cell Signaling Technology # 2983 1:1000), p70 S6 kinase (Cell Signaling Technology #9202 1:1000), p-p70S6k (Thr389 Cell Signaling Technology #9205 1:1000), p-4E-BP1 (Cell Signaling Technology #2855 1:1000), S6RP (Cell Signalling Technology #2217S 1:1000), and p-S6RP (Ser240/Ser244 Cell Signalling Technology #2215S 1:1000); mitophagy/autophagy markers: LC3A/B (Cell Signalling Technology #12741S 1:1000), SQSTM1/p62 (Cell Signalling Technology #5114S 1:1000), p-ULK (Ser555 Abcam #ab5869 1:1000), parkin (Santa Cruz

Biotechnology #sc-32282 1:1000), PINK1 (Sigma Aldrich #SAB2500794 1:1000), BNIP3 (Santa Cruz Biotechnologies #sc-56167 1:1000). Secondary antibody anti-mouse (Promega #W402B 1:10000), anti-rabbit (Promega #W401B 1:10000), or anti-goat (Santa Cruz Biotechnologies #sc-2033 1:10000) was added for 1 hr. following primary antibodies. Loading controls used include α-tubulin (Abcam #ab15246 1:1000) and GAPDH (Santa Cruz Biotechnologies #sc-47724 1:10000). GAPDH is used for 15% gel membrane transfers due to lower molecular weight.

To determine autophagic flux *in vitro*, differentiated myotubes were treated with 50 μM chloroquine for 6 hr. Pelleted cells were lysed in ice-cold RIPA buffer using a 28-gauge needle and syringe and lysates were centrifuged for 10 min. at 14,000 g to remove cellular debris. Proteins were separated by SDS-PAGE, transferred to a 0.2 μM nitrocellulose membrane, and blocked for 1 hr. at RT. The membranes were probed for SQSTM1/p62 (Cell Signalling Technology #5114S 1:1000) and LC3A/B (Cell Signalling Technology #12741S 1:1000).

Statistics

Statistical analysis was performed in GraphPad Prism Software (GraphPad Software Inc., La Jolla, CA) using a two-way unpaired parametric Student's t-test. GraphPad Prism software was used to generate graphs, Seahorse cell mitochondrial stress profiles and bioenergetic boxplots were generated in Microsoft Excel. Data are presented as mean ± SEM, where a value of $p < 0.05$ was considered significant.

Results

Anthropometric and biochemistry data of follow-up biopsies

Individuals II: 1, II: 2, and II: 3 from family 1 (figure 9) and an age-, gender-, and weight-matched control for individual II: 3 R225W members were biopsied a second time in 2018 for additional analysis. The anthropometric and biochemistry data include a breakdown of body mass distribution and blood analyses for indicators of metabolic disease. There were no differences in anthropometric or plasma biochemistry markers between the control and R225W individuals (table 1).

Table 1. Characteristics of R225W and age-matched control subjects who underwent follow-up muscle biopsies in September 2018.

Measurements were conducted on individuals prior to undergoing muscle biopsies. Blood chemistry measurements were conducted following an overnight fast.

	R225W	Control
Age	62.2 ± 2	55.2 ± 2
BMI	30.25 ± 0.15	25.4 ± 3.2
Weight (lbs)	189.05 ± 8.95	159.26 ± 6.76
% Fat	35.4 ± 6.9	25.6 ± 10.7
Fat mass (lbs)	66.26 ± 9.75	41.5 ± 19
Fat free mass (lbs)	122.78 ± 18.74	117.5 ± 12.5
TBW	89.76 ± 13.75	86 ± 9
Diastolic BP	132 ± 15	122.5 ± 7.5
Systolic BP	86 ± 1	71 ± 6
Glucose Fasting (mmol/L)	5.35 ± 0.75	5.75 ± 0.45
HbA1c (%)	5.9 ± 0.8	6.1 ± 0
Creatinine	70 ± 2	79 ± 1
Insulin Fasting (pmol/L)	24 ± 10	67 ± 12
Cholesterol Fasting (mmol/L)	4.2 ± 1.2	3.55 ± 0.55
HDL Fasting (mmol/L)	1.67 ± 0.01	1 ± 0.12
Non-HDL Fasting (mmol/L)	2.5 ± 1.2	2.55 ± 0.65
LDL Fasting (mmol/L)	2.05 ± 0.85	1.95 ± 0.35
TGs Fasting (mmol/L)	1.11 ± 0.75	1.37 ± 0.74

Oxygen consumption and ATP production are increased in R225W myotubes

The Seahorse mitochondrial stress test assay is used to measure OCR and ECAR. The assay provides insight into mechanisms of mitochondrial OXPHOS function and glycolysis, allowing the investigation of metabolic differences between cell lines. An analysis tool is made publicly available by *Mookerjee et al.* to determine metabolic flexibility (Mookerjee et al., 2017). Under fuel-rich conditions, there were no differences in basal respiration (figure 10A, 10B). However, following the injection of oligomycin, to inhibit activity of the ATP synthase (complex V) (Seahorse XF Cell Mito Stress Test Kit | Agilent), we observed a 35.5% higher leak respiration in myotubes isolated from R225W individuals, as compared to matched controls ($p < 0.05$, figure 10A). Similarly, maximal oxygen consumption rate was on average trending to be 32.1% higher in the R225W myotubes than in their matched control myotubes ($p < 0.10$, figure 10A, 10B), and non-mitochondrial respiration was trending on average 85.8% higher in the affected individuals ($p < 0.10$, figure 10A, 10B). These values were derived from the chemical uncoupling agents FCCP and rotenone/antimycin A, respectively.

The ECAR measurement is a proxy measure for rate of glycolysis. Upon addition of monensin, which stimulates maximal glycolytic rate, we see a significantly higher maximal glycolysis rate in the control individuals by 28.5% as compared to the R225W affected individuals ($p < 0.05$, figure 10C, 10D). Using the Mookerjee method to assess bioenergetic capacity as a function of ATP production by glycolysis and ATP production by OXPHOS, the R225W myotubes had higher rate of ATP production from OXPHOS compared to matched control cells; this is evident in the areas of the rectangles for maximal respiration (figure 10F). However, glycolytic production of ATP is higher in control myotubes than in R225W myotubes in both maximal and basal respiration states (figure 10F). A difference in OXPHOS

ATP production basally is not discernible between R225W and control individuals in the bioenergetic boxplot (figure 10F).

Next, we sought to confirm our findings, by assessing cellular respiration in differentiated myotubes using the Oroboros O2K systems. Here, rather than assessing metabolic characteristics of adhered myotubes as in the Seahorse systems, oxygen consumption is measured in suspensions of permeabilized cells, using a Clarke type oxygen electrode. No differences in oxygen consumption were observed under any of the respiration conditions between R225W and control myotubes (figure 10E).

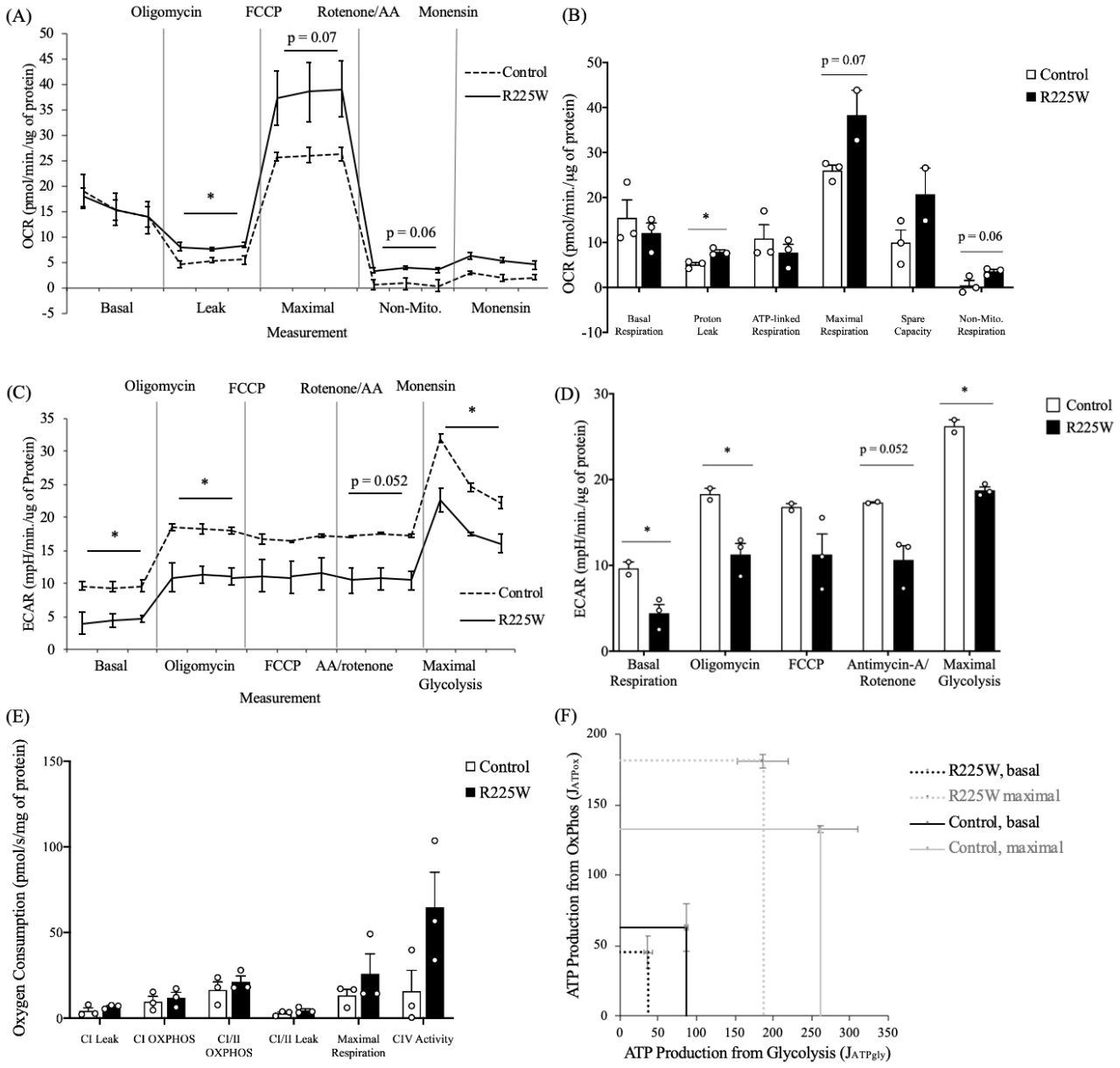

Figure 10. Leak respiration and bioenergetic capacity are increased in individuals with the R225W AMPK mutation.

Isolated primary human myoblasts were differentiated into myotubes for 7-10 days and underwent a mitochondrial stress test in an XFe96 Agilent Seahorse. Measurements 1-3 are basal respiration, 4-6 are leak respiration following oligomycin injection, 7-9 are maximal respiration following FCCP injection, 10-12 are non-mitochondrial respiration following antimycin A and rotenone injection, finally 13-15 are to measure maximal glycolysis following monensin injection. (A) Averaged raw OCR measurements between R225W and control myotubes. (B) Average OCR measurements in bar graph form in which basal respiration is raw basal minus non-mitochondrial respiration, ATP-linked respiration is raw basal minus leak respiration, and spare capacity is maximal minus raw basal respiration. (C) Averaged raw ECAR measurements between R225W and control myotubes. (D) Averaged ECAR

measurements in bar graph form. (E) Oxygen consumption of suspensions of permeabilized myotubes was measured simultaneously using high-resolution respirometry (OROBOROS ®). Oxygen consumption values are compared between affected and control myotubes for CI leak, CI OXPHOS, CI+CII OXPHOS, CI+CII leak, maximum respiration, and CIV activity respectively. (F) Bioenergetic capacity as a function of ATP production by glycolysis (J_{ATPgly}) and production by OXPHOS (J_{ATPox}). Data are mean±SEM (n = 3), *$p < 0.05$.

Acute AMPK inhibition leads to loss of difference in bioenergetic capacity, and increased glycogen content does not affect respiration

The Harper lab has previously demonstrated that there is a two-fold increase in glycogen content in skeletal muscle obtained from individuals with the R225W mutation in AMPK. These individuals also exhibit several gain-of-function phenotypes, including a remarkable increase in muscle fatigue-resistance *in vivo*. This same mutation in cardiac tissue causes a similar build-up of glycogen, and this is pathogenic, contributing to Wolff-Parkinson-White syndrome. Following this observation, we sought to determine whether the increased glycogen content contributed to the increased respiration in primary myotubes. We treated the myotubes with a chemical glycogen phosphorylase (GP) inhibitor (CP-316819), expecting to potentially observe a greater decrease in R225W respiration than control cell respiration characteristics in a mitochondrial stress test. However, in the presence of the GP inhibitor, CP-316819, no significant change between treated and untreated conditions was found ($p = 0.12$, figure 11A, 11B), indicating that the excess glycogen being stored in skeletal muscle is not being used at a different rate than in control individuals. OCR remained significantly different between R225W and control when treated which indicates that differences were maintained regardless of not having access to excess glycogen supply ($p < 0.05$, figure 11A, 11B). Changes were also not seen in ECAR with the addition of glycogen phosphorylase inhibitor (figure 11C, 11D).

Next, we sought to inhibit AMPK overall, in order to determine whether the active AMPK as a result of R225W was the direct cause for increased respiration, or whether this was an indirect result of increased mitochondrial content. Compound C (or dorsomorphin) is a non-specific AMPK inhibitor. When the R225W myotubes were treated with the inhibitor for 24 hours, the myotubes exhibited a marked change in difference between R225W and control myotubes in OCR (figure 11E, 11F) and ECAR (figure 11G, 11H) where previously significant changes became non-significant. It appears that control myotube maximal respiration markedly increases in the presence of Compound C, whilst R225W respiration remains the same (figure 11F). Interestingly, in the presence of Compound C, R225W myotube ECAR is elevated significantly and becomes similar to that of its control (figure 11H). This finding suggests that when the skeletal muscle isoform of AMPK was inhibited, R225W myotubes had increased glycolytic ATP production. This suggests that the mechanism driving increased bioenergetics capacity in the R225W myotubes may indeed be as a direct result of the mutation but is likely supported by additional pathways leading to chronic changes in mitochondrial capacity.

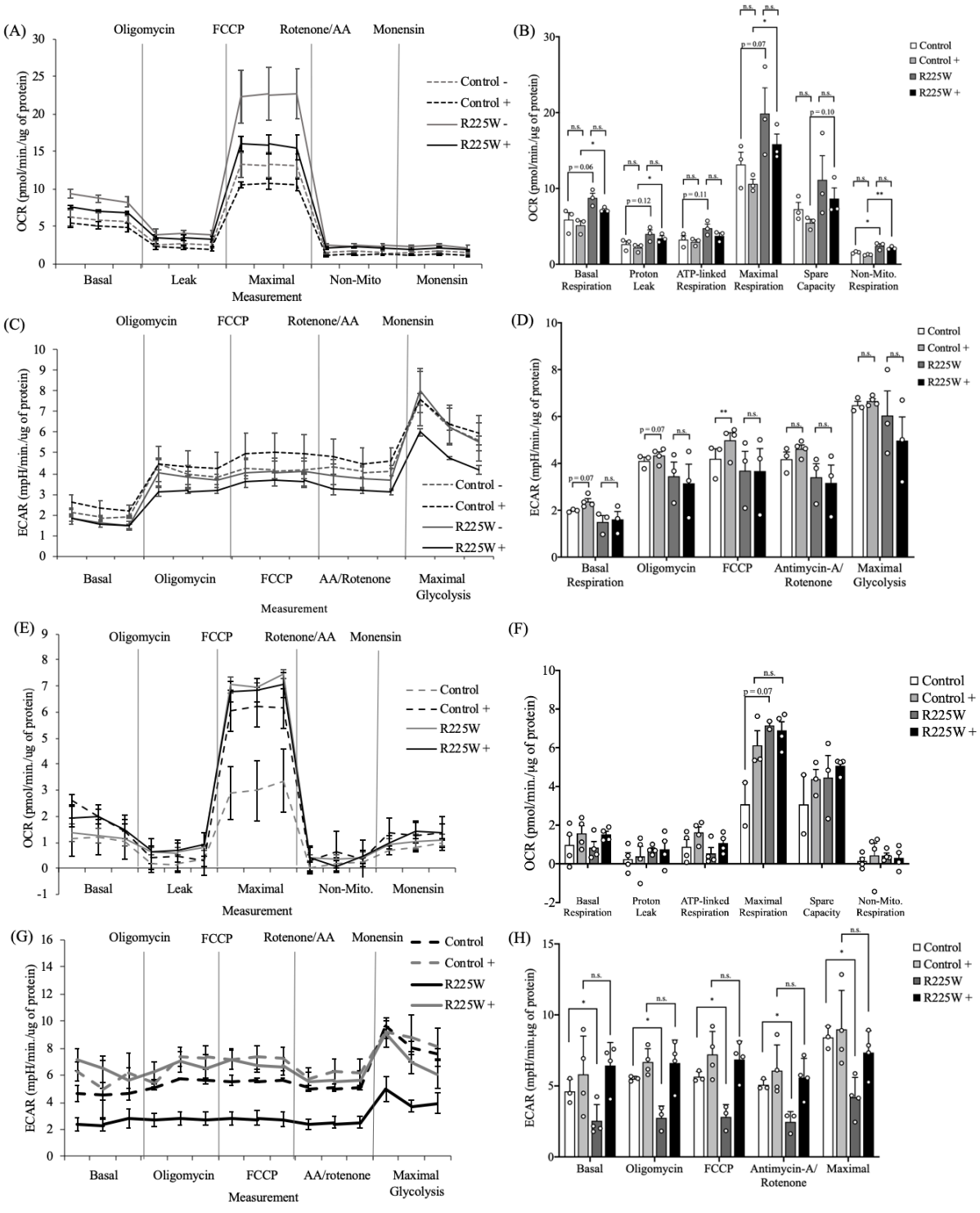

Figure 11. OCR and ECAR of R225W myotubes in presence of glycogen phosphorylase and compound C inhibitors.

Myotubes underwent a cell mitochondrial stress test in a XFe96 Agilent Seahorse. + refers to "in presence" of inhibitor, whilst – refers to "in absence" of inhibitor. (A) averaged raw OCR

measurements of myotubes in presence of GP inhibitor, (B) averaged OCR measurements in presence of GP inhibitor where basal respiration is raw basal minus non-mitochondrial respiration, ATP-linked respiration is basal minus leak respiration, and spare capacity is maximal minus basal respiration, (C) averaged raw ECAR measurements in presence of GP inhibitor, (D) ECAR measurements in bar graph format in presence of GP inhibitor, (E) averaged raw OCR measurements of myotubes in presence of Compound C inhibitor, (F) averaged OCR measurements in presence of Compound C inhibitor where basal respiration is raw basal minus non-mitochondrial respiration, ATP-linked respiration is basal minus leak respiration, and spare capacity is maximal minus basal respiration, (G) averaged raw ECAR measurements in presence of Compound C inhibitor, (H) ECAR measurements in bar graph format in presence of Compound C inhibitor. Data are mean±SEM (n = 3-4), *$p < 0.05$ and **$p < 0.01$.

R225W myotubes exhibit increased fatty acid oxidation

As AMPK activation is associated with increased FA import into mitochondria (Hardie and Pan, 2002), we next assessed respiration of the R225W myotubes when supplied with fatty acids using the Seahorse XFe96. Palmitate is a 16-carbon length fatty acid that must be imported into the mitochondria via the carnitine shuttle system in order to undergo β-oxidation. Longer-chain FFAs are relatively insoluble in the aqueous environment of *in vitro* work, to overcome this, palmitate is conjugated to BSA at a 1:6 palmitate:BSA ratio. Etomoxir is an irreversible CPT1 inhibitor, preventing palmitate:BSA from entering mitochondria for oxidation. A 55.8% decrease was seen from palmitate:BSA respiration to palmitate+etomoxir respiration in myotubes from R225W individuals ($p < 0.05$, figure 12A, 12B), as compared to no significant inhibition of respiration in myotubes from control individuals (figure 12C, 12D). There was also a significant 45.3% increase in basal respiration in myotubes from R225W individuals in presence of palmitate:BSA ($p < 0.05$, figure 12A, 12B), with no significant change in control myotubes (figure 12C, 12D). Raw values were analyzed as per Seahorse protocol. No change was observed in OCR due to uncoupling FFA which is determined by oligomycin palmitate:BSA rate minus oligomycin BSA rate (figure 12E). No change was observed in basal respiration due to exogenous FAs which is determined by basal

palmitate:BSA rate minus basal BSA rate minus OCR due to uncoupling by FFA. A 91.9% increase in R225W myotubes was observed at maximal respiration due to the addition of palmitate which is determined by maximal palmitate:BSA minus maximal BSA rate minus OCR due to uncoupling by FFA ($p < 0.05$, figure 12E). No change was observed in basal respiration due to endogenous FAs which is determined by basal BSA minus basal BSA+etomoxir rate. Finally, no change was observed in maximal respiration due to endogenous FAs which is determined by maximal BSA minus maximal BSA+etomoxir rate (figure 12E).

Next, we aimed to confirm and extend these findings through high resolution respirometry, in which FAO was assessed in digitonin permeabilized myotubes (figure 12F). We designed a unique protocol to assess FAO that is dependent on the activity of CPT1, or that bypasses CPT1 in the presence of palmitoylcarnitine and octanoylcarnitine. The CPT1-depedent leak respiration was 80.2% higher in R225W individuals, and CPT1-dependent CI+FAO OXPHOS was 77.8% higher ($p < 0.05$, figure 12F). The CPT1-independent respiration was trending to be increased following the addition of both palmitoylcarnitine and octanoylcarnitine ($p = 0.07$ and 0.06, respectively, figure 12F). Following the addition of FCCP, maximal respiration was 69.4% higher in myotubes from R225W individuals ($p < 0.05$, figure 12F). We additionally determined that in lysed primary myotubes, CPT1 specific activity was increased in R225W affected individuals by 30.8% (figure 12G). Since AMPK indirectly lowers malonyl-CoA content, a CPT1 inhibitor, these findings of increased CPT1 activity are consistent with our hypothesis. We expect that the increased ability of CPT1 to import FAs into the mitochondria also contributes to the increased FAO we observed in R225W myotubes.

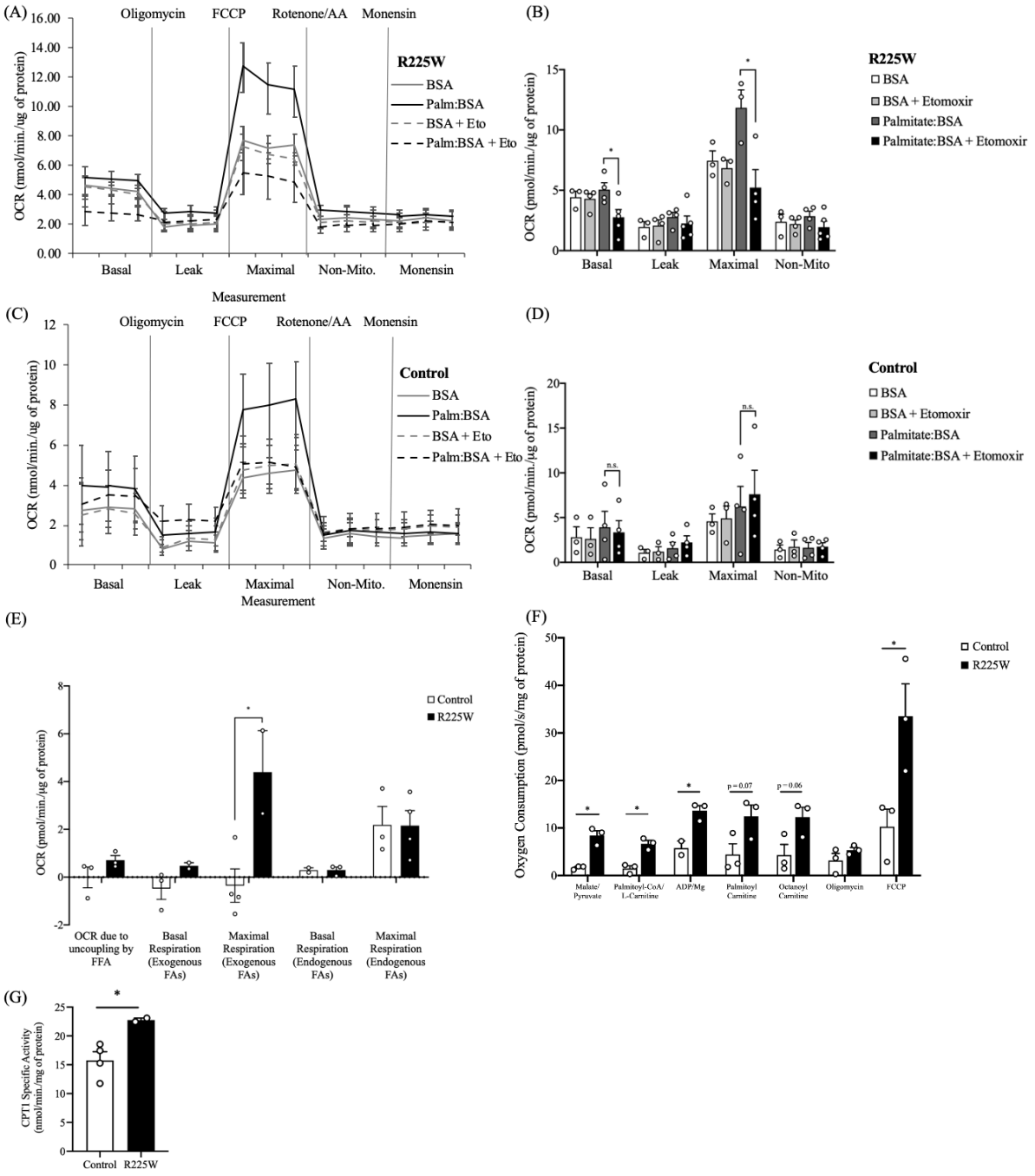

Figure 12. Increased FAO and increased CPT1 activity in myotubes from R225W individuals.

Isolated primary human myoblasts were differentiated into myotubes for 7-10 days and underwent a cell mitochondrial stress test in an XFe96 Agilent Seahorse Analyzer. Measurements 1-3 are basal respiration, 4-6 are leak respiration following oligomycin injection, 7-9 are maximal respiration following FCCP injection, 10-12 are non-mitochondrial respiration following antimycin A and rotenone injection. Myotubes were treated with palmitate:BSA and etomoxir. (A) averaged raw OCR measurements of R225W myotubes, (B) averaged OCR measurements of R225W myotubes in which basal respiration is raw basal

minus non-mitochondrial respiration, ATP-linked respiration is basal minus leak respiration, and spare capacity is maximal minus basal respiration, (C) averaged raw OCR measurements on control myotubes, (D) averaged OCR measurements of control myotubes in which basal respiration is raw basal minus non-mitochondrial respiration, ATP-linked respiration is basal minus leak respiration, and spare capacity is maximal minus basal respiration, (E) OCR measurements in which OCR due to uncoupling FFA is oligomycin palmitate:BSA-Eto rate minus oligomycin BSA-Eto rate, basal respiration (exogenous FAs) is basal palmitate:BSA-Eto rate minus basal BSA-Eto rate minus OCR due to uncoupling by FFA, maximal respiration (exogenous FAs) is maximal palmitate:BSA-Eto minus maximal BSA-Eto rate minus OCR due to uncoupling by FFA, basal respiration (endogenous FAs) is basal BSA-Eto minus basal BSA+Eto rate, and maximal respiration (endogenous FAs) is maximal BSA-Eto minus maximal BSA+Eto rate, (F) high resolution respirometry results following FAO protocol, and (G) CPT1 activity (nmol/min./mg of protein) measured on myotube homogenate. Data are mean±SEM (n = 3-4), *$p < 0.05$.

Activities of mitochondrial ETC complex proteins are increased in primary myotubes from R225W individuals

Mitochondrial ETC complex proteins harness the electrons from the oxidation of energy substrates for the synthesis of ATP through OXPHOS. We aimed to determine whether there were differences in the total maximal activities of specific ETC proteins using spectrophotometric assays of V_{max} activities. Activities were measured as total cellular activity in primary myotube lysate. There were significant increases in activities of complexes II, III, and IV, and a trending increase in CI-III and CII-III linked activities in cells of AMPK R225W individuals, as compared to controls, which is consistent with the observations of increased bioenergetic capacity (figure 13). However, there was no change in CI activity in the cells of R225W individuals as compared to the controls (figure 13A). CII activity is increased by 60.1% ($p < 0.05$, figure 13B), CIII activity is increased by 74.2% ($p < 0.05$, figure 13C), CIV activity is increased by 49.6% ($p < 0.01$, figure 13D), CI-II linked activity trends an increase by 34.6% ($p < 0.1$, figure 13E), and CII-CIII linked activity trends for an increase by 46.0% ($p < 0.1$, figure 13F) in the myotubes of R225W affected individuals as compared to their matched controls.

To assess whether increases in cellular respiration and activities of the ETC complex proteins activity were attributable to increased mitochondrial content of the myotubes, we next quantified the total cellular activity of citrate synthase (CS). Consistent with previous findings of increased mitochondrial content in the R225W individuals, here we found it to be 47.4% greater in myotubes R225W individuals than in the matched control cells ($p < 0.05$, figure 13G).

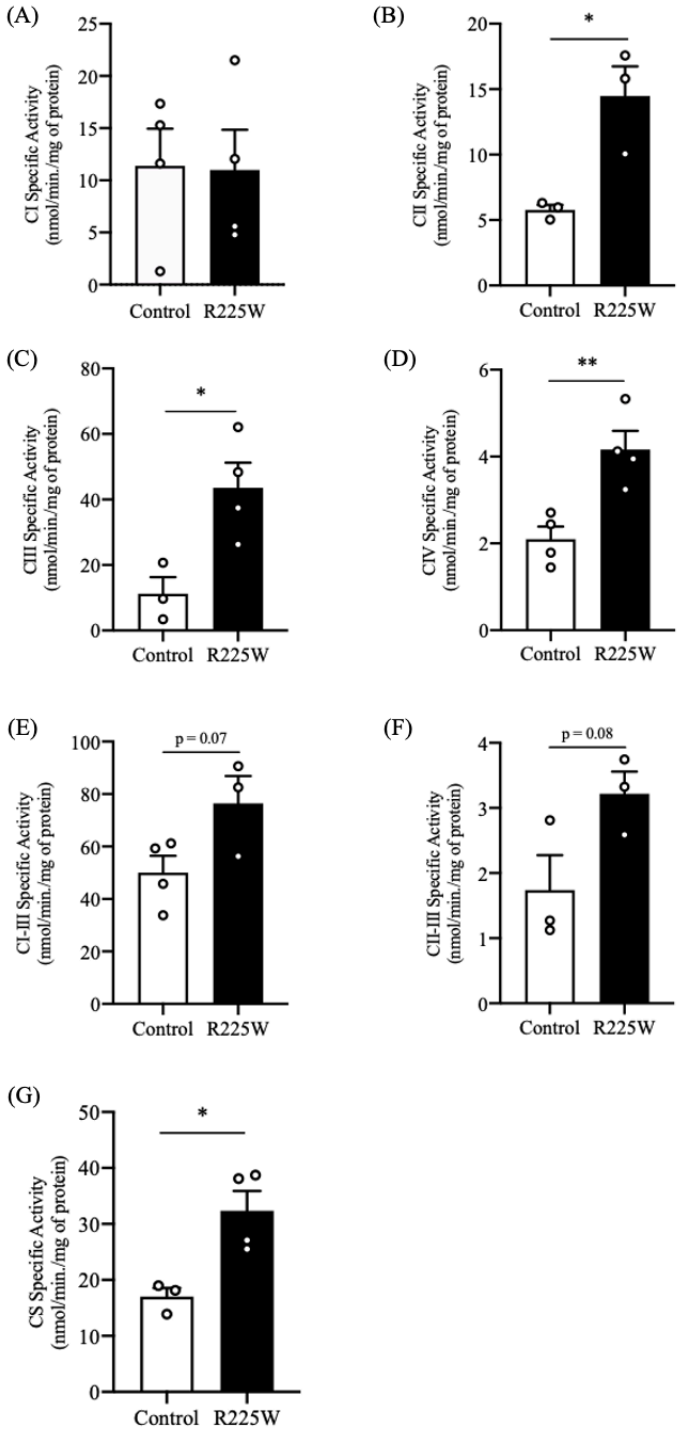

Figure 13. Increased activities of ETC proteins in myotubes of R225W affected individuals than in myotubes of matched controls.

Specific activities (nmol/min./mg of protein) of (A) complex I, (B) complex II, (C) complex III, (D) complex IV, (E) complex I-III linked, and (F) complex II-III linked activities were measured on R225W and control primary myotube lysates (G) CS activity measured on myotube homogenate. Data are mean±SEM (n = 3-4), *$p < 0.05$, **$p < 0.01$.

Respiration rates are lower in biopsied skeletal muscle of R225W individuals than in muscle of matched controls

To determine whether our findings of increased bioenergetic capacity in the primary muscle cells isolated from R225W individuals also translated to muscle tissue, we measured characteristics of oxygen consumption in freshly biopsied muscle using high resolution respirometry (figure 14A, 14B, 14C). We found that OXPHOS tends to be increased in muscle fibres of R225W individuals; as well as CIV activity (figure 14A). No firm conclusions can be drawn about FAO in muscle due to lower sample size ($n = 2$); the 3rd sample could not be run due to availability of muscle from biopsy (figure 14B). Lastly, ROS trends higher in R225W individuals overall between each individual and their matched control, but non-significantly due to large biological variability (figure 14C). Interestingly, CS activity in muscle homogenate appeared to have the opposite result to what we determined in myotubes (figure 11G, 14D). CS activity was significantly lower by 29.9% ($p < 0.05$, figure 14D) in muscle homogenate of R225W individuals. This is starkly different from the 47.4% higher CS activity seen in primary myotubes of R225W individuals ($p < 0.05$, figure 13G).

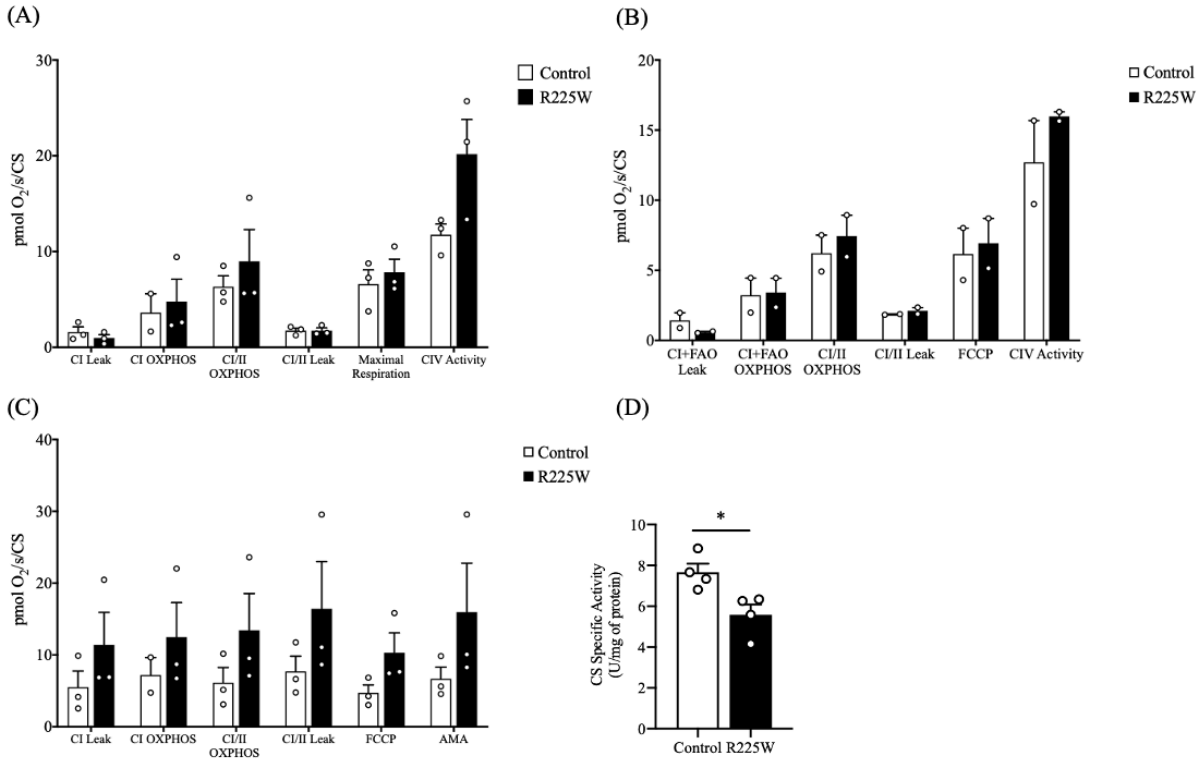

Figure 14. CS activity is decreased in R225W muscle homogenate, OXPHOS, FAO, and ROS production in biopsied muscle preparations did not change.

Biopsied muscle tissue was permeabilized, and used for determination of oxygen consumption, and FAO using high resolution respirometry. H_2O_2 emission was measured using fluorimetry Data were normalized to CS activity, a proxy measure of muscle mitochondrial content. (A) Characteristics of electron transport chain activity under various incubation conditions, (B) FAO measured by respirometry, where CI+FAO leak is measured with malate injection, then CI+FAO OXPHOS dependent on CPT1 is measured with L-carnitine and palmitoyl-CoA injection, (C) ROS emission measured by fluorimetry at all steady states with Amplex Ultra Red to measure H_2O_2 production in presence of SOD with peak excitation of 525 nm and emission at 615 nm. , and (D) CS activity in homogenized muscle (n = 4). Data are mean±SEM (n = 2-3), *$p < 0.05$.

Mitofusin protein levels are elevated in muscle from R225W individuals

Mitochondria exist as a functional network that adapts in size and function through fusion and fission processes to meet the metabolic demands of a cell. AMPK is thought to play a role in maintaining the balance of fusion and fission (Herzig and Shaw, 2018). Thus, we assessed the expression of key proteins involved in maintaining the balance of mitochondrial fusion and fission. Levels of the fusion proteins, MFN-1 and MFN-2, were found to be increased in the

biopsied muscle of R225W individuals compared to controls ($p < 0.05$, figure 15A, 15B, 15C). There was no significant change seen in the inner membrane fusion protein OPA-1 (figure 15A, 15D).

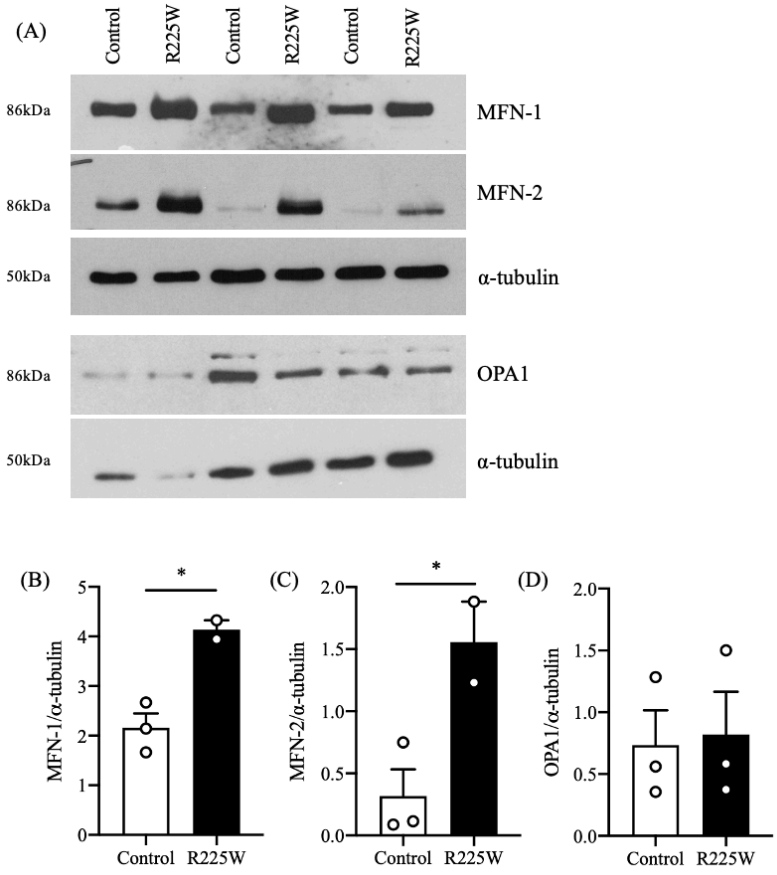

Figure 15. Fusion proteins MFN-1 and MFN-2 are increased in biopsied muscle of R225W individuals compared to controls.

Muscle was homogenized and prepared with DTT and Laemmli buffer. Samples were run on 6%-15% SDS-Tris gels at 120V and transferred to 0.2 μm nitrocellulose membranes. (A) blots of MFN-1, MFN-2, OPA-1, and loading controls, (B) quantified MFN-1 blot, (C) quantified MFN-2 blot, and (D) quantified OPA-1 blot. Data are mean±SEM (n = 3) *$p < 0.05$.

Markers of mitochondrial biogenesis in biopsied muscle are similar in R225W and control individuals

We hypothesized that mitochondrial biogenesis would be elevated in the muscle of R225W individuals, as AMPK can directly phosphorylate and activate PGC1α (Reznick and Shulman,

2006). Contrary to our hypothesis, we found no changes in the mitochondrial biogenesis markers NRF-1, NRF-2 and PGC1α (figure 16A, 16B, 16C, 16D).

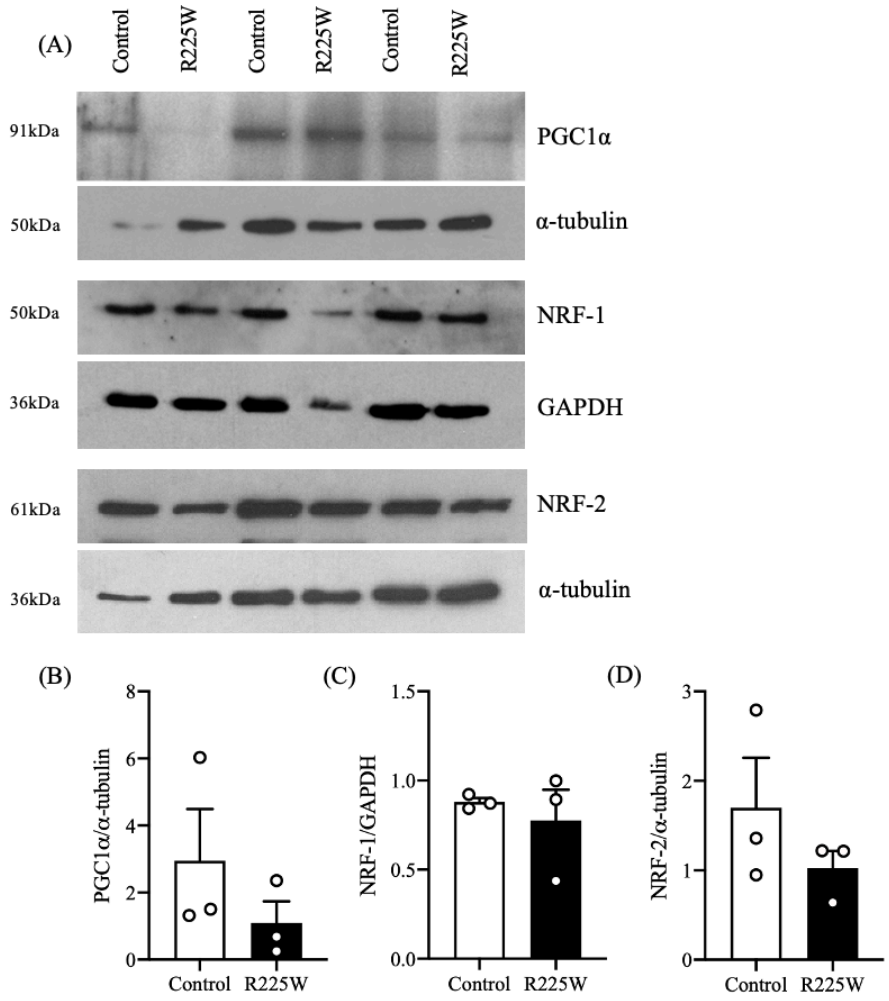

Figure 16. Levels of marker proteins of mitochondrial biogenesis are similar in biopsied muscle of R225W and control individuals.

Muscle was homogenized and prepared with DTT and Laemmli buffer. Samples were run on 6%-15% SDS-Tris gels at 120V and transferred to 0.2 µm nitrocellulose membranes. (A) blots of PGC1α, NRF-1, NRF2, and loading controls, (B) quantified PGC1α blot, (C) quantified NRF-1 blot, and (D) quantified NRF-2 blot. Data are mean±SEM (n = 3).

mTOR pathway is inhibited in R225W muscle homogenate

AMPK inhibits the mTOR pathway by supressing mTORC1 activity and phosphorylating the scaffold protein raptor (Herzig and Shaw, 2018). The inhibition of mTOR by AMPK leads to

suppression of cell proliferation and the induction of autophagy (Löffler et al., 2011). Here, we blotted for mTOR and downstream proteins to determine if the gain-of-function R225W mutation is associated with any changes in the mTOR pathway. We observed no significant change in the protein levels of total mTOR (figure 17A, 17B). Compared to muscle homogenate of control individuals, the level of p70S6K was trending to be decreased by 34.0% in R225W individuals ($p < 0.1$, figure 17A, 17C). The level of p-p70S6K was increased by 80.2% ($p < 0.05$, figure 17A, 17D). However, p-4EBP1 and S6RP levels were unchanged (figure 17A, 17E, 17F). The level of p-S6RP was decreased by 72.8% in R225W muscle homogenate (figure 17A, 17G).

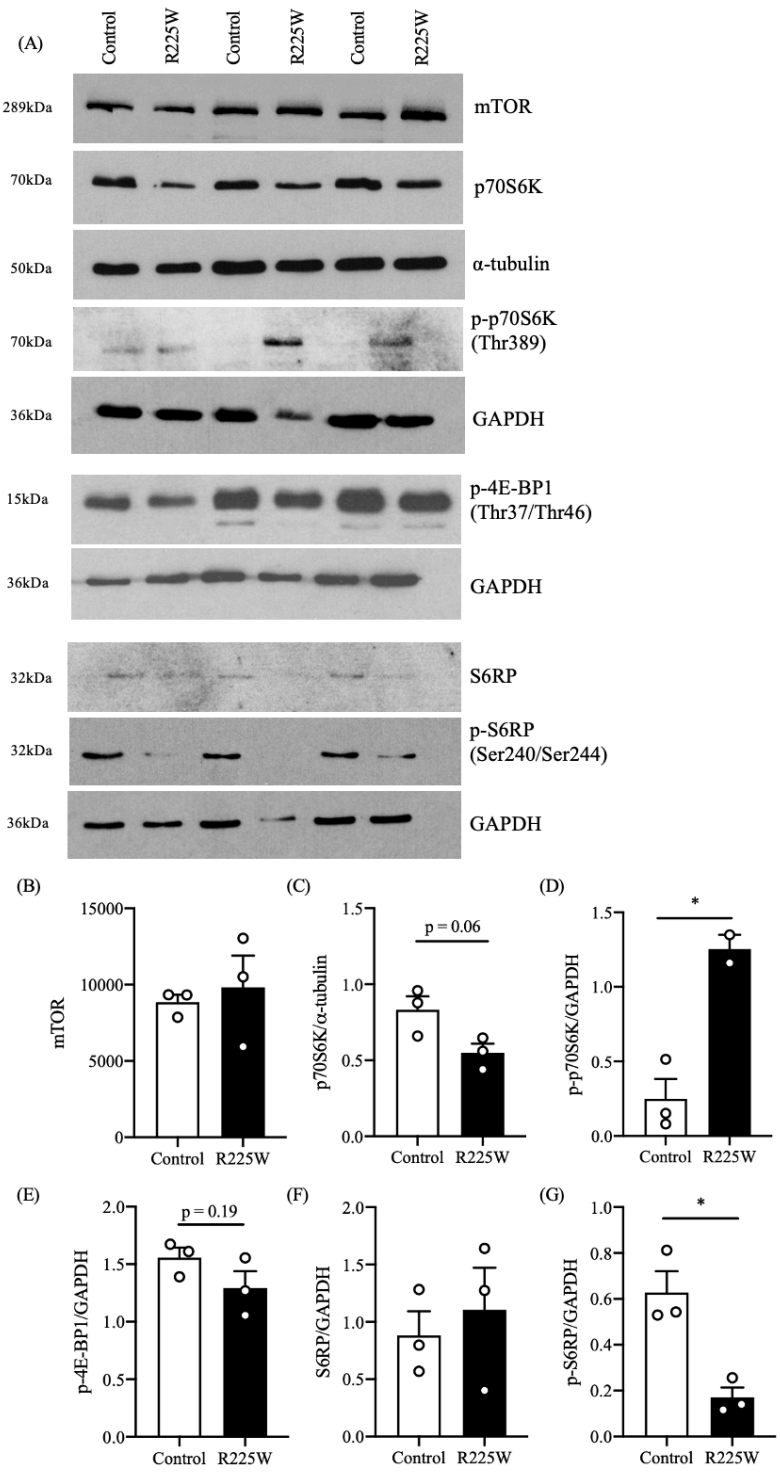

Figure 17. p70S6K, p-4E-BP1, and p-S6RP are decreased, and p-p70S6k is increased in biopsied muscle from R225W individuals as compared to controls.

Muscle was homogenized and prepared with DTT and Laemmli buffer. Samples were run on 6%-15% SDS-Tris gels at 120V and transferred to 0.2 µm nitrocellulose membranes. (A) blots of mTOR, p70S6K, p-p70s6K, p-4E-BP1, S6RP, p-S6RP, and loading controls, (B) quantified

mTOR blot, (C) quantified p70S6K blot, (D) quantified p-70S6K blot, (E) quantified 4E-BP1 blot, (F) quantified S6RP blot, and (G) quantified p-S6RP blot. Data are mean±SEM (n = 3) *p < 0.05.

The R225W mutation is associated with increased markers of autophagic flux capacity and mitophagy

As AMPK is a well-known inducer of autophagy, we sought to determine whether skeletal muscle from R225W individuals exhibited elevated autophagic flux. First, we assessed skeletal muscle homogenate for the expression of key autophagy proteins. We observed a significant decrease in p62 content by 72.6% ($p < 0.05$, figure 18A, 18B). However, we did not see differences in the levels of p-ULK, LC3A/B, and BNIP3 in R225W muscle homogenate (figure 18A, 18C, 18D, 18E). We saw no change in PINK1 (figure 18A, 18F), a marker of mitophagy, but saw a potential for an increase in parkin (n = 2, figure 18A, 18G). As the muscle samples were collected when participants were fasting, this may have led to an increase in basal autophagy in both R225W and control individuals (Bujak et al., 2015). We then tested characteristics of autophagic flux in primary myotubes in which flux mechanisms can be challenged *in vitro*. We treated the primary myotubes isolated from R225W and control individuals with chloroquine to assess capacity for autophagic flux. Chloroquine inhibits autophagic flux by decreasing autophagosome-lysosome fusion (Mauthe et al., 2018). Analyses revealed increased capacity for autophagic flux in R225W myotubes than in myotubes of matched controls as there was a significantly greater increase in build-up of LC3BII in myotubes of R225W than in control myotubes when autophagy was inhibited ($p < 0.05$, figure 19A, 19B, 19C, 19D). We saw no significant changes in p62 levels following chloroquine treatment (figure 19A, 19B, 19E, 19F).

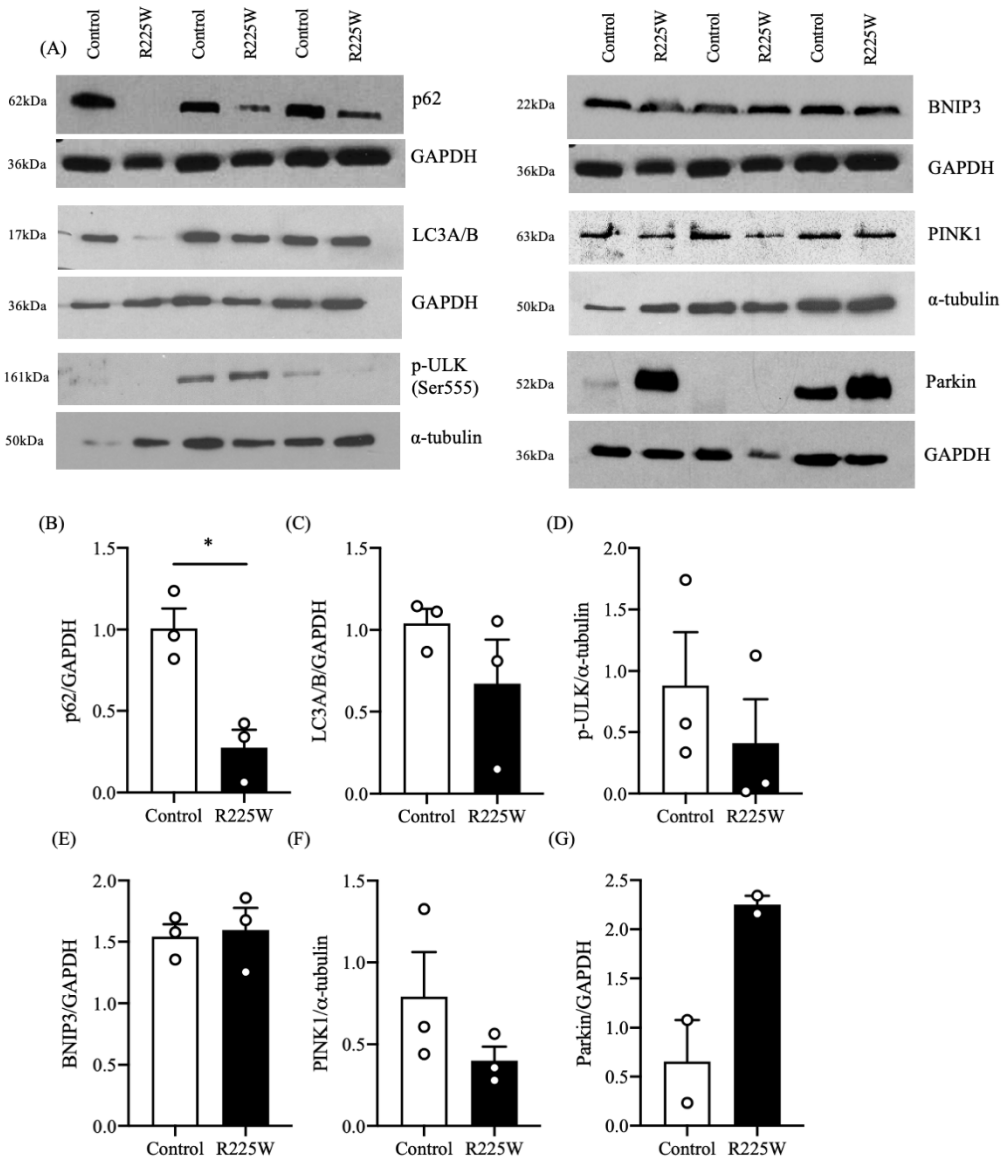

Figure 18. Protein levels of p62 are decreased in biopsied R225W compared to control muscle.

Muscle was homogenized and prepared with DTT and Laemmli buffer. Samples were run on 6%-15% SDS-Tris gels at 120V and transferred to 0.2 µm nitrocellulose membranes. (A) blots of p62, LC3A/B, p-ULK, BNIP3, PINK1, parkin and loading controls, (B) quantified p62 blot, (C) quantified LC3A/B blot, (D) quantified p-ULK blot, (E) quantified BNIP3 blot, (F) quantified PINK1 blot, and (G) quantified parkin blot. Data are mean±SEM (n = 3) *$p < 0.05$.

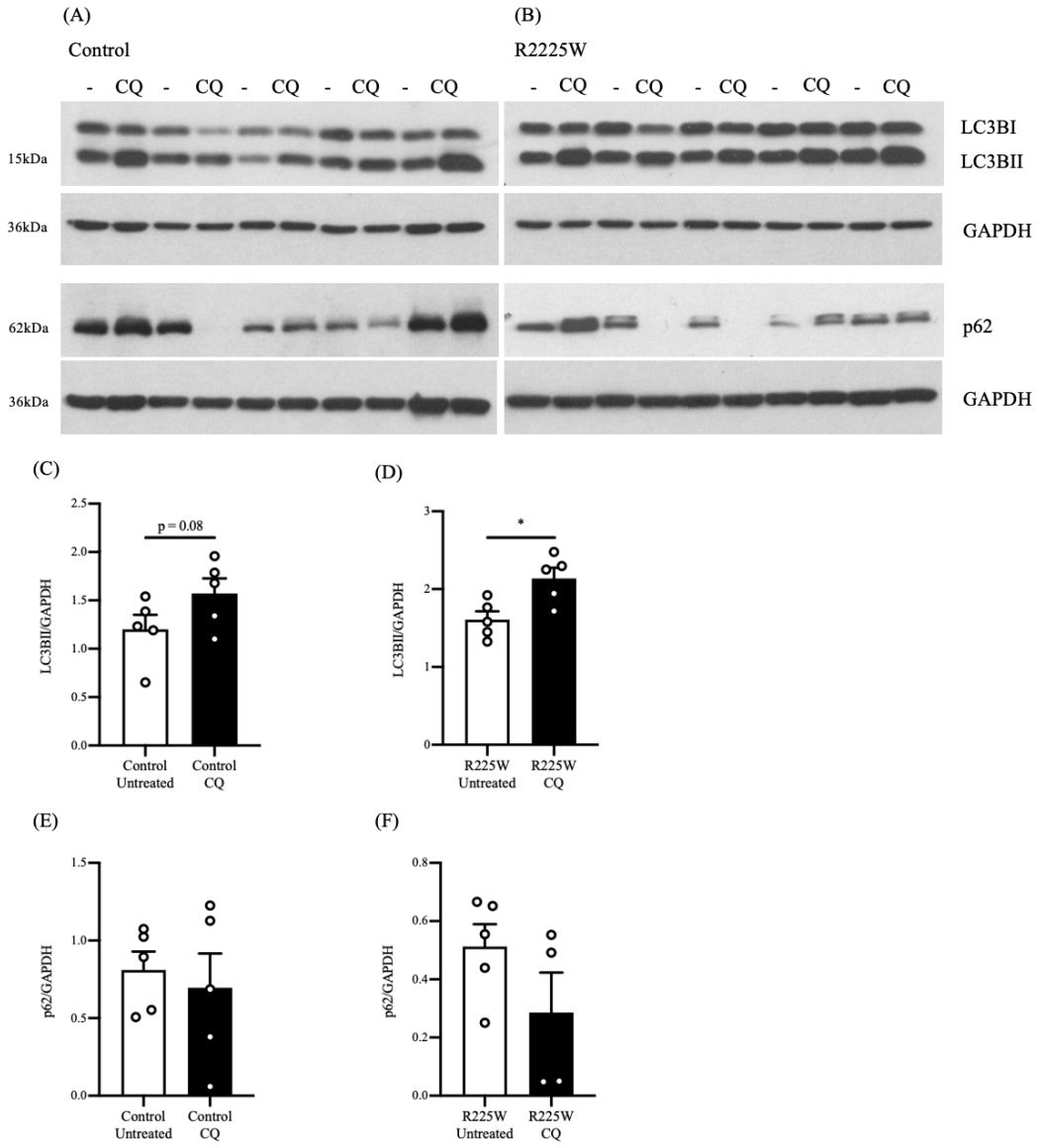

Figure 19. Increased level of LC3BII after chloroquine treatment in R225W compared to control myotubes.

Myotubes were differentiated for 7-10 days and treated with 50 μM chloroquine for 6 hours then harvested. Samples were run on 10-15% SDS-Tris gels a 120V and transferred to 0.2 μm nitrocellulose membranes. (A) control blots where – is untreated and CQ is chloroquine, (B) R225W blots where – is untreated and CQ is chloroquine, (C) quantified control LC3BII blot, (D) quantified R225W LC3BII blot, (E) quantified control p62 blot, and (F) quantified R225W p62 blot. Data are mean±SEM (n = 5) *$p < 0.05$.

Discussion

AMPK is considered a master regulator of cellular energy homeostasis due to its ability to sense and respond to changes in cellular energy levels (Garcia and Shaw, 2017). We have previously identified a rare gain-of function R225W mutation in the *PRKAG3* gene of the γ_3-subunit of AMPK which is highly selectively expressed in skeletal muscle. Individuals with this mutation demonstrate increased resistance to fatigue during exercise, which is complimented by additional changes in muscle such as an increased quantity of mitochondria and glycogen content compared with matched controls (Costford et al., 2007; Crawford et al., 2010). In the current study, we sought to extend our knowledge of the implications of the R225W mutation for muscle metabolism and cellular biology. Our findings demonstrate that R225W individuals exhibit greater bioenergetic capacity in OXPHOS, decreased glycolytic ATP production, and increased FAO, with evidence that these functional effects are as a direct result of the mutation and as a result of increased mitochondrial content. We also see evidence of increased fusion and autophagy/mitophagy in biopsied muscle from R225W individuals as compared to control muscle which elucidates the mechanism for more robust mitochondria.

Previous research has demonstrated that the chronic activation of AMPK results in various beneficial adaptions in mitochondrial oxidative capacity in skeletal muscle (DeFronzo and Tripathy, 2009). Consistent with our previous findings, and seminal studies using the pharmacological AMPK activator AICAR (Crawford et al., 2010; Costford et al., 2007) we demonstrate that R225W individuals exhibit increased proton leak and maximal respiration. The increased proton leak and maximal respiration are consistent with previous observations by *Crawford et al.* of increased respiration and mitochondrial yield from differentiated myotubes and CS activity on isolated mitochondria (Crawford et al., 2010). The increase in

OCR of myotubes is an expected phenotypic outcome of a mutation which causes a stark increase in mitochondrial content (Mookerjee and Brand, 2015). Furthermore, in order to examine whether the effects of the R225W mutation are a direct result of increased AMPK, or just mass effect associated with increased mitochondrial content, we examined myotube respiration following 24 hours of treatment with Compound C, a non-specific AMPK inhibitor. We observed that the difference in respiration between control and R225W myotube respiration was diminished, which indicates that AMPK may be partially driving increased myotube respiration. For example, given that myotubes were treated with inhibitor for 24 hours, it is possible that Compound C, which is non-specific and has many targets, exhibited off-target effects which resulted in the significant increase in control myotube respiration, although it had minimal impact on R225W respiration. Specifically, it is known that Compound C is capable of activating glucokinase, a rate-limiting step enzyme in glycolysis which may explain the observed increases in respiration (Liu et al., 2012). Furthermore, it is possible that the treatment with Compound C caused a cellular stress response which led to the increase in OCR. We also saw that ECAR of myotubes isolated from R225W individuals increased to the level of control myotubes after treatment with Compound C which indicates that glycolysis may have increased as a result of AMPK (or off-target) inhibition. More experiments are necessary to explore these and other possibilities.

Contrary to our hypothesis, the primary myotubes from the R225W carriers displayed a dramatic decrease in ECAR, a proxy measure of glycolysis (Mookerjee and Brand, 2015). We expected ECAR to increase as a result of AMPK because it is known that AMPK increases glucose uptake and glycolysis in cardiac muscle (Dyck and Lopaschuk, 2006). At the molecular level, AMPK can activate 6-phosphofructo-2-kinase/fructose-2, 6-bisphosphatase-

3 (PFKFB3) which in turn activates PFK1, a rate-limiting step in glycolysis (Herzig and Shaw, 2018; Rider et al., 2004). This unexpected finding may help to explain our previous observation of a remarkably increased resistance to fatigue during exercise (Crawford et al., 2010). Typically, substantial training is required to increase the threshold for exercising at maximal capacity prior to producing lactic acid; this concept is known as the lactate or anaerobic threshold (Ghosh, 2004). Lactic acid is a known contributor to feelings of muscle fatigue during exercise as an indicator to the body that it needs to rest, and as it begins to build-up, individuals may experience fatigue or soreness (Lindinger, 2007). A reduction in maximal anaerobic glycolysis is consistent with the possibility that a lower lactic acid production in muscle of the individuals with the R225W mutation may contribute to fatigue resistance. Furthermore, *Ljubicic et al.* notes that mitochondrial biogenesis as a result of AMPK activation by AICAR is followed by a hallmark increase in fatigue resistance (Ljubicic et al.). When considering the three-fold increase in skeletal muscle glycogen stores in the R225W carriers, we expected the readily available glycogen in skeletal muscle was being used at maximal respiration as the primary source of glucose via breakdown by glycogen phosphorylase. We hypothesized that maximal OCR respiration in R225W individuals in the presence of a glycogen phosphorylase inhibitor would be decreased. While skeletal muscle glycogen reserves are depleted only after liver reserves are used, previous studies have shown that use of skeletal muscle glycogen stores is critical in acute emergencies such as the "fight or flight" response (Jensen et al., 2011). FCCP elicits a similar mitochondrial response as the stress response does by uncoupling the mitochondrial membrane from the drive for ATP synthesis, and thus we anticipated that at maximal respiration these glycogen stores would be readily used (Demine et al., 2019; Brand and Nicholls, 2011). AMPK normally acts as a glycogen synthase inhibitor; however, its activation of glucose uptake and the glycolysis pathway can

override this action and thereby increase glycogen storage (Hunter et al., 2011). This may explain why we did not observe a decrease in respiration when we blocked access to glycogen storage. R225Q Hampshire pigs with the analogous phenotype (RN^-) were similarly found to deplete their glycogen stores at a normal rate when exercised (Andersson, 2003). Altogether, the excess storage is likely due to increased glucose uptake and a resulting increased ability to replenish glycogen stores (Hunter et al., 2011). This is consistent with the previous interpretation of data from *Crawford et al.* which demonstrated a two-fold increase in glycogen synthesis in myotubes isolated from R225W individuals than in control myotubes (Crawford et al., 2010). Further corroborating determinations are required to determine that glycogen is not used because the decrease in respiration in R225W myotubes was very close to showing a trend ($p = 0.12$).

Skeletal muscle is highly oxidative and has a dramatic fuel plasticity which allows ATP production to increase over 100-fold during maximal contraction (Porter and Wall, 2012). We found that CS activity is two-fold greater in the muscle of R225W individuals, but this does not reflect previous findings by *Crawford et al.* of a nine-fold increase (Crawford et al., 2010). This discrepancy can likely be explained due their use of a technique for isolating mitochondria which may be artificially selecting the healthiest mitochondria by removing damaged mitochondria, and thus elevating the reported CS activity (Frezza et al., 2007; Piper et al., 1985). CS activity is used to measure mitochondrial content of cells and tissue, and is also used to normalize data collected from cell and tissue preparations to levels of mitochondria (Porter and Wall, 2012). Many measures for mitochondrial content exist including cytochrome c oxidase activity and cardiolipin content, though the most robust method is considered quantitative morphometry of transmission electron microscopy (TEM) micrographs (Porter

and Wall, 2012). Interestingly, we found that the activities of a few of the respiratory chain complex proteins are increased by greater than two-fold in myotubes isolated from R225W individuals, suggesting that the intrinsic activities of ETC proteins may also elevated. This could occur through mechanisms including posttranslational modifications (PTMs), redox state, and cellular energy levels (Kramer et al., 2015; Berg et al., 2002; Hou et al., 2018). However, it is likely that the greatest contributor to increased activity is indeed increased mitochondrial content because the elevated complex activity becomes non-significant after CS normalization. Notably, CI activity did not change between R225W carrier myotubes and controls, which suggests that CI activity is lower per unit of mitochondrial content in myotubes of R225W individuals. Interestingly, metformin, the most commonly prescribed medication for T2DM, inhibits CI which leads to the indirect activation of AMPK (Abdelgadir et al., 2017). CI is the largest ETC complex, and the target of several PTMs which can modify its activity (Hou et al., 2018). It is possible that CI activity does not reflect the increased mitochondrial content in R225W cells due to PTM control of CI. Studies have shown specifically ROS-related PTMs leading to reduced activity of CI (Ryan et al., 2012; Vial et al., 2019). PTMs known to impact CI activity include carbonylation due to oxidative stress, and as well glutathionylation (Frohnert and Bernlohr, 2013; Marí et al., 2009). When there are decreases in glutathione (GSH), CI activity has also been shown to decrease which may be due to increased ROS causing a global shift of redox state to glutathione disulphide (GSSG) (Marí et al., 2009). Interestingly, metformin inhibition of CI also results in decreased ROS production; however, there is no indication that metformin directly introduces PTMs at CI (Vial et al., 2019). Intriguingly, the specific mechanism of action of metformin on CI is not well understood, but there is evidence that metformin suppresses the efficient coupling of redox and proton transfer domains in CI (Cameron et al., 2018; Fontaine, 2018). More

mechanistic studies are warranted to elucidate the possible PTM control of CI activity by AMPK in skeletal muscle.

Activation of AMPK in skeletal muscle leads to increased FAO and inhibition of FA synthesis by directly phosphorylating and inhibiting acetyl-CoA carboxylase (ACC), respectively. ACC catalyzes the conversion of acetyl-CoA to malonyl-CoA, a necessary substrate for FA biosynthesis (Galic et al., 2018; Berg et al., 2002). Therefore, AMPK inhibition of ACC promotes increased FAO and decreased FA synthesis. Consistent with our previous findings of increased FA uptake in R225W myotubes and lower IMTG in skeletal muscle of individuals with the R225W mutation (Crawford et al., 2010), FAO was increased in permeabilized myotubes isolated from R225W individuals. Importantly, malonyl-CoA inhibits CPT1 activity, which prevents longer-chain FAs from entering the mitochondrial matrix for β-oxidation (Hardie and Pan, 2002). Indeed, CPT1 activity is substantially increased in R225W myotubes, suggesting that the increase in FAO is attributable at least in part to the increased uptake of FAs. This functional effect may also be a result of increased mitochondrial content, allowing for a greater turnover of FAO. However, it is likely an interplay of mitochondrial content and constitutively active AMPK; with the mitochondria providing the infrastructure for an increased FAO, and AMPK acting to enhance fatty acid uptake through CPT1. Very early studies showed that AMPK activated by exercise resulted in malonyl-CoA depletion, ultimately leading to increased FAO (Winder and Hardie, 1996). *Smith et al.* showed that the same effect on FAO occurs with AICAR treatment, consistent with the notion that R225W similarly impacts FAO through increased AMPK activity (Smith et al., 2005). Similar effects are also observed in C2C12 muscle cells treated with metformin (Wang et al., 2014). In individuals with insulin resistance, hyperinsulinemia has several effects on muscle metabolism

including suppressing FAO and promoting lipid storage (Collier et al., 2006). Metformin is able to combat this by reversing the effects of insulin-induced changes in FA metabolism (Collier et al., 2006; Yu Wang et al., 2019). The mechanism through which metformin increases FAO remains unclear but it is speculated that it is due to an indirect activation of AMPK by depressed CI activity, or due to increased transcription of mtDNA (Collier et al., 2006; Lord et al., 2020). *Barnes et al.* determined an increase in p-ACC in transgenic mice with the analogous R225Q mutation, which suggests again that AMPK is directly involved in inhibiting ACC activity and promoting FAO (Barnes et al., 2005). Taken together, our results demonstrate that the R225W mutation indeed leads to increased FAO in skeletal muscle.

While research involving primary muscle cells allows the study of mechanistic aspects in muscle cells, the characteristics of primary muscle cells and biopsied muscle fibres can often portray different characteristics from each other (Eisner et al., 2014). For example, *Eisner et al.* demonstrated that human myotubes can exhibit up to 8 times more fusion events than the muscle fibres from the same donor (Eisner et al., 2014). Fusion/fission machinery and processes are more stable in muscle fibres than in myotubes, causing fusion/fission events to be less frequent (Eisner et al., 2014). We found that CS activity in muscle tissue biopsied from R225W carriers was lower than the matched controls, demonstrating the opposite effect seen on isolated myotubes and isolated mitochondria (Crawford et al., 2010). CS activity is a marker of mitochondrial density (Larsen et al., 2012), and thus it is possible that gross mitochondrial content could be impacted if mitochondrial turnover is dramatically different between myotubes and muscle fibres (Eisner et al., 2014). Increased fusion/fission events may lead to a higher CS activity because a more constant turnover rate – or more quality control – promotes

healthier and more robust mitochondria in myotubes (Eisner et al., 2014; Youle and Van Der Bliek, 2012).

Despite the lower CS activity, there is a consistent trend for increased CS-normalized oxygen consumption in permeabilized skeletal muscle fibres between each R225W individual and their matched control. While this did not reach significance due to low sample size, the trend for increased oxygen consumption supports increased intrinsic function of mitochondria. Metformin has similarly been shown to increase respiration by activating AMPK. Interestingly, we also observed a trend for increased H_2O_2 emission in the R225W permeabilized skeletal muscle fibres. Although not observed in muscle fibres, there is evidence that increased FAO can lead to elevated ROS production due to excessive electron flux in the ETC (Nobe& et al., 1990; Serra et al., 2013). Activation of AMPK does not directly lead to production of ROS, but with increased respiration, ROS is sometimes increased. AMPK activity has been previously associated with an increased amount of ROS production (Rabinovitch et al., 2017). In a feedback-loop type manner, ROS produced by mitochondria can also indirectly lead to an activation of AMPK by affecting the ATP:ADP ratio, which is assumed to occur via direct inhibition of the ETC by ROS (Hinchy et al., 2018; Akhova and Tkachenko, 2014). Furthermore, ROS may also activate AMPK by direct action on redox sensitive cysteine residues Cys299 and Cys304 (Hinchy et al., 2018). Overall further studies must be done to evaluate the impacts of constitutively active AMPK in R225W on ROS and vice versa.

Mitochondria are dynamic reticular structures that are continuously undergoing fusion and fission; the purposes of mitochondrial dynamics are not fully understood, but are thought to include quality control (Westermann, 2010). Consistent with our hypothesis of increased

mitochondrial dynamics, we detected higher protein expression of MFN-1 and MFN-2 in the muscle of R225W carriers, suggesting that R225W mitochondria undergo elevated fusion events in comparison to mitochondria in muscle of control individuals. *Kang et al.* showed that in hepatocytes, activation of AMPK by AICAR led to significantly increased expression of MFN-1 and OPA-1 which was associated with higher mitochondrial integrity (Kang et al., 2016). This apparent increase in fusion is not necessarily consistent with the idea of increased mitochondrial content seen in myotubes without an increase in mitochondrial biogenesis (Costford et al., 2007; Crawford et al., 2010), but it is consistent with how active the mitochondria are bioenergetically. Both mitochondrial fusion and fission are integral to optimizing bioenergetic capacity, especially in metabolically active cells; fusion allows for the exchange of metabolites and genes, whereas fission allows for the splitting off of damaged parts of the mitochondrial reticulum into smaller fragments for elimination through mitophagy (Westermann, 2012). Interestingly, the activation of AMPK by metformin in high-fat diet (HFD)-fed mouse hepatocytes led to decreased OPA-1 and increase in mitochondrial fission factor 1 (MFF1), suggesting that metformin promotes mitochondrial fission (Yu Wang et al., 2019). *Wang et al.* found that HFD-fed mice exhibited increased mitochondrial density when treated with metformin (Yu Wang et al., 2019). Overall, it is evident that mitochondrial dynamics are impacted by the R225W mutation and show some insight to the mechanism by which R225W myotubes exhibit increased mitochondrial robustness. Further markers for fission and fusion should be explored for more conclusive results, as well as visualizing characteristics of the mitochondrial reticulum using confocal microscopy, for example with translocase of the outer membrane 20 (TOM20) immunostaining.

Activation of AMPK leads to the induction of mitochondrial biogenesis through PGC1α and NRF-1 (Bergeron et al., 2001). NRF-2, however, plays important roles in monitoring cellular redox, regulating FAO, and ensuring the structural and functional integrity of mitochondria (Gureev et al., 2019; Dinkova-Kostova and Abramov, 2015). NRF-1 and PGC1α are strong inducers of mitochondrial biogenesis. NRF-1 promotes transcription of genes encoding the mitochondrial ETC complex proteins and has also been shown to be linked with mitochondrial transcription factor A (TFAM) (Marin et al., 2017). Interestingly, *Marin et al.* found that AMPK activated by AICAR promotes biogenesis by remodeling portions of the chromosome that encode biogenesis-related proteins (Marin et al., 2017). AMPK does this by reducing methylation, increasing acetylation, and subsequently loosening chromosome compaction in areas that PGC1α, NRF-1, NRF-2, and TFAM are located (Marin et al., 2017). However, we did not detect differences in the protein levels of NRF-1, NRF-2 nor PGC1α in muscle. Several epigenetic factors also regulate mitochondrial biogenesis such as DNA (cytosine-5)-methyltransferase 1 (DNMT1), retinoblastoma-binding protein 7 (RBBP7), and histone acetyltransferase 1 (HAT1) which are phosphorylated by AMPK and lead to increased mitochondrial biogenesis (Marin et al., 2017). Since the mechanisms of biogenesis are complex, it is possible that any one of these epigenetic markers are not being phosphorylated by AMPK in R225W muscle, which may be influencing the transcription of classic markers. Furthermore, without further probing of these or other potential factors, a definitive conclusion cannot be drawn regarding an effect of R225W on mitochondrial biogenesis.

AMPK is one of the key regulators of mTOR, protein synthesis and cell proliferation pathways (Herzig and Shaw, 2018). Contrary to our hypothesis that active AMPK will inhibit mTOR and its pathway, we observed a decrease in p70S6K and an increase in p-p70S6K, suggesting

that the mTOR pathway is not inhibited by constitutively active AMPK. However, studies have shown that other kinases such as 3-phosphoinositide-dependent protein kinase 1 (PDK1) are capable of directly phosphorylating and activating p-p70S6K (Williams et al., 2000; Pullen et al., 1998). Indeed, AMPK can activate the phosphoinositide 3-kinase (PI3K) pathway which leads to a downstream activation of PDK1 (Tao et al., 2010). Interestingly, p-S6RP and p-4E-BP1 were decreased in R225W muscle which is consistent with our hypothesis of decreased mTOR activity because these are commonly used markers of mTOR activity (Qin et al., 2016). Taken together, our data suggest that the mTOR pathway is inhibited as a result of the R225W mutation, but some further determinations are necessary.

The interplay between AMPK and mTOR activity has a great influence on autophagic flux, in which AMPK has an activating effect through ULK1, and mTOR regulates autophagic machinery (Jung et al., 2010). Studies have shown that mTOR inhibition by either rapamycin or starvation leads to a dephosphorylation of ULK1, suggesting that mTOR may have a direct effect on autophagic flux (Jung et al., 2010). ULK1 has an essential role in communicating nutrient levels and stress response to the cell which may regulate autophagy (Jung et al., 2010). However, we saw no change in p-ULK1, but did see a decrease in p62 in R225W muscle. *Declèves et al.* showed that AMPK activation in the presence of AICAR or metformin, p62 levels were normalized and LC3 levels were increased (Declèves et al., 2014). In muscle homogenate we were unable to detect LC3BII, which is highly expressed during autophagy, but localizes to the autophagosome membrane and rapidly degraded upon fusion with lysosomes making it difficult to detect under basal conditions (Tanida et al., 2008). However, when myotubes were treated with chloroquine, an inhibitor of autophagosome-lysosome fusion (Mauthe et al., 2018), myotubes of R225W individuals demonstrated increased LC3BII

build-up compared to their matched controls. Thus, our results are consistent with constitutively active AMPK enhancing autophagic flux capacity. Furthermore, we anticipated that mitophagy would be increased in muscle of R225W individuals, which could be attributed to increased mitochondrial content, and maintenance of mitochondrial health. While parkin appears to be increased in muscle of R225W individuals we did not see a significant change in PINK1; a greater sample size would be required to test this possibility. *Kang et al.* documented a 120% increase in parkin following AICAR treatment, which led to increased mitophagy (Kang et al., 2016). While, metformin has been shown to promote mitophagy in a PINK1-parkin mediated manner (Song et al., 2016), recent research demonstrates that AMPK can promote mitophagy in a PINK1-parkin-independent manner by activating TANK binding kinase 1 (TBK1) (Seabright et al., 2020). The findings of *Seabright et al.* also suggest that TBK1 activation is mediated by AMPK (Seabright et al., 2020). Taken together, an increase in parkin expression is not necessarily sufficient to confirm increased mitophagy. Additional research including measurements of induced mitophagy such as visualizing increased colocalization of mitochondria and lysosomes are required for confirmation of elevated mitophagy due to the R225W mutation.

Conclusion

The R225W mutation which leads to elevated AMPK activity primarily shows phenotypic effects as a result of an interplay between direct AMPK action and increased mitochondrial content. Functional effects include increased ATP flux due to OXPHOS, increased FAO, increased activities of several ETC proteins, and increased ROS production. We suggest that the enhanced muscle cell bioenergetics may be mechanistically attributed to increased fusion cycles and that the quality of mitochondria is also potentially improved due to increased

mitophagy and autophagy. Altogether, the R225W mutation includes many phenotypic characteristics that are similar to those induced by the chemical activation of AMPK (e.g. by AICAR) or through metformin treatment. Thus, the R225W mutation provides a uniquely useful model to study the functions of AMPK in skeletal muscle. In a broader sense, it also advances our understanding of potential mechanisms through which AMPK activation may be useful in the treatment of metabolic diseases.

Bibliography

Abdelgadir, E., R. Ali, F. Rashid, and A. Bashier. 2017. Effect of Metformin on Different Non-Diabetes Related Conditions, a Special Focus on Malignant Conditions: Review of Literature. *J. Clin. Med. Res.* 9:388–395. doi:10.14740/jocmr2922e.

Akhova, A. V., and A.G. Tkachenko. 2014. ATP/ADP alteration as a sign of the oxidative stress development in *Escherichia coli* cells under antibiotic treatment. *FEMS Microbiol. Lett.* 353:69–76. doi:10.1111/1574-6968.12405.

Ali, O. 2013. Genetics of type 2 diabetes. *World J. Diabetes*. 4:114. doi:10.4239/wjd.v4.i4.114.

Andersson, L. 2003. Identification and characterization of AMPK γ3 mutations in the pig. *In* Biochemical Society Transactions. Portland Press Ltd. 232–235.

Antoun, G., F. McMurray, A.B. Thrush, D.A. Patten, A.C. Peixoto, R.S. Slack, R. McPherson, R. Dent, and M.E. Harper. 2015. Impaired mitochondrial oxidative phosphorylation and supercomplex assembly in rectus abdominis muscle of diabetic obese individuals. *Diabetologia*. 58:2861–2866. doi:10.1007/s00125-015-3772-8.

Barnes, B.R., C.L. Yun, T.L. Steiler, Y. Leng, D. Galuska, J.F.P. Wojtaszewski, L. Andersson, and J.R. Zierath. 2005. Changes in exercise-induced gene expression in 5′-AMP-activated protein kinase γ3-null and γ3 R225Q transgenic mice. *Diabetes*. 54:3484–3489. doi:10.2337/diabetes.54.12.3484.

Berg, J.M., J.L. Tymoczko, and L. Stryer. 2002. The Regulation of Cellular Respiration Is Governed Primarily by the Need for ATP.

Bergeron, R., J.M. Ren, K.S. Cadman, I.K. Moore, P. Perret, M. Pypaert, L.H. Young, C.F. Semenkovich, and G.I. Shulman. 2001. Chronic activation of AMP kinase results in NRF-1 activation and mitochondrial biogenesis. *Am. J. Physiol. - Endocrinol. Metab.* 281. doi:10.1152/ajpendo.2001.281.6.e1340.

Birk, J.B., and J.F. Wojtaszewski. Predominant alpha2/beta2/gamma3 AMPK activation during exercise in human skeletal muscle. *J.Physiol*. 577:1021–1032.

Bonora, M., S. Patergnani, A. Rimessi, E. de Marchi, J.M. Suski, A. Bononi, C. Giorgi, S. Marchi, S. Missiroli, F. Poletti, M.R. Wieckowski, and P. Pinton. 2012. ATP synthesis and storage. *Purinergic Signal.* 8:343–357. doi:10.1007/s11302-012-9305-8.

Brand, M.D., and D.G. Nicholls. 2011. Assessing mitochondrial dysfunction in cells. *Biochem. J.* 435:297–312. doi:10.1042/BJ20110162.

Bujak, A.L., J.D. Crane, J.S. Lally, R.J. Ford, S.J. Kang, I.A. Rebalka, A.E. Green, B.E. Kemp, T.J. Hawke, J.D. Schertzer, and G.R. Steinberg. 2015. AMPK activation of muscle autophagy prevents fasting-induced hypoglycemia and myopathy during aging. *Cell Metab.* 21:883–890. doi:10.1016/j.cmet.2015.05.016.

Cameron, A.R., L. Logie, K. Patel, S. Erhardt, S. Bacon, P. Middleton, J. Harthill, C. Forteath, J.T. Coats, C. Kerr, H. Curry, D. Stewart, K. Sakamoto, P. Repiščák, M.J. Paterson, I. Hassinen, G. McDougall, and G. Rena. 2018. Metformin selectively targets redox control of complex I energy transduction. *Redox Biol.* 14:187–197. doi:10.1016/j.redox.2017.08.018.

Chen, L., B. Tuo, and H. Dong. 2016. Regulation of intestinal glucose absorption by ion channels and transporters. *Nutrients*. 8. doi:10.3390/nu8010043.

Cholewski, M., M. Tomczykowa, and M. Tomczyk. 2018. A comprehensive review of chemistry, sources and bioavailability of omega-3 fatty acids. *Nutrients*. 10.

doi:10.3390/nu10111662.
Clausius, R. 1850. Ueber die bewegende Kraft der Wärme und die Gesetze, welche sich daraus für die Wärmelehre selbst ableiten lassen. *Ann. der Phys. und Chemie*. 155:368–397. doi:10.1002/andp.18501550306.
Collier, C.A., C.R. Bruce, A.C. Smith, G. Lopaschuk, and D.J. Dyck. 2006. Metformin counters the insulin-induced suppression of fatty acid oxidation and stimulation of triacylglycerol storage in rodent skeletal muscle. *Am. J. Physiol. Metab.* 291:E182–E189. doi:10.1152/ajpendo.00272.2005.
Costford, S.R., N. Kavaslar, N. Ahituv, S.N. Chaudhry, W.S. Schackwitz, R. Dent, L.A. Pennacchio, R. McPherson, and M.E. Harper. 2007. Gain-of-function R225W mutation in human AMPKγ3 causing increased glycogen and decreased triglyceride in skeletal muscle. *PLoS One*. 2:e903. doi:10.1371/journal.pone.0000903.
Crawford, S.A., S.R. Costford, C. Aguer, S.C. Thomas, R.A. Dekemp, J.N. Dasilva, D. Lafontaine, M. Kendall, R. Dent, R.S.B. Beanlands, R. McPherson, and M.E. Harper. 2010. Naturally occurring R225W mutation of the gene encoding AMP-activated protein kinase (AMPK)γ3 results in increased oxidative capacity and glucose uptake in human primary myotubes. *Diabetologia*. 53:1986–1997. doi:10.1007/s00125-010-1788-7.
Davidson, B.C., and R.C. Cantrill. 1985. Fatty acid nomenclature. A short review. *South African Med. J.* 633–634.
Declèves, A.-E., K. Sharma, and J. Satriano. 2014. Beneficial Effects of AMP-Activated Protein Kinase Agonists in Kidney Ischemia-Reperfusion: Autophagy and Cellular Stress Markers. *Nephron Exp. Nephrol.* 128:98–110. doi:10.1159/000368932.
DeFronzo, R.A., E. Ferrannini, L. Groop, R.R. Henry, W.H. Herman, J.J. Holst, F.B. Hu, C.R. Kahn, I. Raz, G.I. Shulman, D.C. Simonson, M.A. Testa, and R. Weiss. 2015. Type 2 diabetes mellitus. *Nat. Rev. Dis. Prim.* 1:1–22. doi:10.1038/nrdp.2015.19.
DeFronzo, R.A., and D. Tripathy. 2009. Skeletal muscle insulin resistance is the primary defect in type 2 diabetes. *Diabetes Care*. 32 Suppl 2. doi:10.2337/dc09-s302.
Demine, S., P. Renard, and T. Arnould. 2019. Mitochondrial Uncoupling: A Key Controller of Biological Processes in Physiology and Diseases. *Cells*. 8. doi:10.3390/cells8080795.
Diabetes Canada. What is diabetes? - Diabetes Canada.
Dinkova-Kostova, A.T., and A.Y. Abramov. 2015. The emerging role of Nrf2 in mitochondrial function. *Free Radic. Biol. Med.* 88:179–188. doi:10.1016/j.freeradbiomed.2015.04.036.
Divakaruni, A.S., A. Paradyse, D.A. Ferrick, A.N. Murphy, and M. Jastroch. 2014. Analysis and interpretation of microplate-based oxygen consumption and pH data. *In* Methods in Enzymology. Academic Press Inc. 309–354.
Doevendans, P.A., and H.J. Wellens. 2001. Wolff-Parkinson-White Syndrome: A Genetic Disease? *Circulation*. 104:3014–3016.
Du, W. 2004. Rendement Napole Gene and Pork Quality. *Ontario Minist. Agric.*
Duchen, M.R. 2000. Mitochondria and calcium: From cell signalling to cell death. *J. Physiol.* 529:57–68. doi:10.1111/j.1469-7793.2000.00057.x.
Dudkina, N. V., R. Kouřil, K. Peters, H.P. Braun, and E.J. Boekema. 2010. Structure and function of mitochondrial supercomplexes. *Biochim. Biophys. Acta - Bioenerg.* 1797:664–670. doi:10.1016/j.bbabio.2009.12.013.
Dyck, J.R.B., and G.D. Lopaschuk. 2006. AMPK alterations in cardiac physiology and pathology: Enemy or ally? *J. Physiol.* 574:95–112. doi:10.1113/jphysiol.2006.109389.

Eisner, V., G. Lenaers, and G. Hajnóczky. 2014. Mitochondrial fusion is frequent in skeletal muscle and supports excitation-contraction coupling. *J. Cell Biol.* 205:179–195. doi:10.1083/jcb.201312066.
Engelking, L.R. 2015. Introduction to Glycolysis (The Embden-Meyerhoff Pathway (EMP)). *In* Textbook of Veterinary Physiological Chemistry. Elsevier. 153–158.
Fontaine, E. 2018. Metformin-Induced Mitochondrial Complex I Inhibition: Facts, Uncertainties, and Consequences. *Front. Endocrinol. (Lausanne).* 9:753. doi:10.3389/fendo.2018.00753.
Frezza, C., S. Cipolat, and L. Scorrano. 2007. Organelle isolation: Functional mitochondria from mouse liver, muscle and cultured filroblasts. *Nat. Protoc.* 2:287–295. doi:10.1038/nprot.2006.478.
Friedman, J.R., and J. Nunnari. 2014. Mitochondrial form and function. *Nature*. 505:335–343. doi:10.1038/nature12985.
Frohnert, B.I., and D.A. Bernlohr. 2013. Protein Carbonylation, Mitochondrial Dysfunction, and Insulin Resistance. *Adv. Nutr.* 4:157–163. doi:10.3945/an.112.003319.
Galic, S., K. Loh, L. Murray-Segal, G.R. Steinberg, Z.B. Andrews, and B.E. Kemp. 2018. AMPK signaling to acetyl-CoA carboxylase is required for fasting-and cold-induced appetite but not thermogenesis. *Elife*. 7. doi:10.7554/eLife.32656.
Garcia, D., and R.J. Shaw. 2017. Molecular Cell AMPK: Mechanisms of Cellular Energy Sensing and Restoration of Metabolic Balance. *Mol. Cell*. 66:789–800. doi:10.1016/j.molcel.2017.05.032.
Ghosh, A.K. 2004. Anaerobic threshold: Its concept and role in endurance sport. *Malaysian J. Med. Sci.* 11:24–36.
Gonzalez-Franquesa, A., and M.E. Patti. 2017. Insulin resistance and mitochondrial dysfunction. *In* Advances in Experimental Medicine and Biology. Springer New York LLC. 465–520.
Gu, X., Y. Yan, S.J. Novick, A. Kovach, D. Goswami, J. Ke, M.H.E. Tan, L. Wang, X. Li, P.W. De Waal, M.R. Webb, P.R. Griffin, H.E. Xu, and K. Melcher. 2017. Deconvoluting AMP-activated protein kinase (AMPK) adenine nucleotide binding and sensing. *J. Biol. Chem.* 292:12653–12666. doi:10.1074/jbc.M117.793018.
Gureev, A.P., E.A. Shaforostova, and V.N. Popov. 2019. Regulation of mitochondrial biogenesis as a way for active longevity: Interaction between the Nrf2 and PGC-1α signaling pathways. *Front. Genet.* 10:435. doi:10.3389/fgene.2019.00435.
Hardie, D.G. 2011. AMPK and autophagy get connected. *EMBO J.* 30:634–635. doi:10.1038/emboj.2011.12.
Hardie, D.G., and D.A. Pan. 2002. Regulation of fatty acid synthesis and oxidation by the AMP-activated protein kinase. *In* Biochemical Society Transactions. 1064–1070.
Hatting, M., C.D.J. Tavares, K. Sharabi, A.K. Rines, and P. Puigserver. 2018. Insulin regulation of gluconeogenesis. *Ann. N. Y. Acad. Sci.* 1411:21–35. doi:10.1111/nyas.13435.
Herzig, S., and R.J. Shaw. 2018. AMPK: Guardian of metabolism and mitochondrial homeostasis. *Nat. Rev. Mol. Cell Biol.* 19:121–135. doi:10.1038/nrm.2017.95.
Hinchy, E.C., A. V. Gruszczyk, R. Willows, N. Navaratnam, A.R. Hall, G. Bates, T.P. Bright, T. Krieg, D. Carling, and M.P. Murphy. 2018. Mitochondria-derived ROS activate AMP-activated protein kinase (AMPK) indirectly. *J. Biol. Chem.* 293:17208–17217. doi:10.1074/jbc.RA118.002579.
Honka, M.J., A. Latva-Rasku, M. Bucci, K.A. Virtanen, J.C. Hannukainen, K.K.

Kalliokoski, and P. Nuutila. 2018. Insulin-stimulated glucose uptake in skeletal muscle, adipose tissue and liver: A positron emission tomography study. *Eur. J. Endocrinol.* 178:523–531. doi:10.1530/EJE-17-0882.

Hou, W.L., J. Yin, M. Alimujiang, X.Y. Yu, L.G. Ai, Y.Q. Bao, F. Liu, and W.P. Jia. 2018. Inhibition of mitochondrial complex I improves glucose metabolism independently of AMPK activation. *J. Cell. Mol. Med.* 22:1316–1328. doi:10.1111/jcmm.13432.

Houten, S.M., S. Violante, F. V Ventura, and R.J.A. Wanders. 2016. The Biochemistry and Physiology of Mitochondrial Fatty Acid β-Oxidation and Its Genetic Disorders. *Annu. Rev. Physiol. is online*. 78:23–44. doi:10.1146/annurev-physiol-021115-105045.

Huang, W.-C., and I.-C. Tang. 2007. Bacterial and Yeast Cultures – Process Characteristics, Products, and Applications. *New Technol. Appl.* 185–223. doi:10.1016/B978-044452114-9/50009-8.

Hunter, R.W., J.T. Treebak, J.F.P. Wojtaszewski, and K. Sakamoto. 2011. Molecular mechanism by which AMP-activated protein kinase activation promotes glycogen accumulation in muscle. *Diabetes*. 60:766–774. doi:10.2337/db10-1148.

Jensen, J., P.I. Rustad, A.J. Kolnes, and Y.-C. Lai. 2011. The Role of Skeletal Muscle Glycogen Breakdown for Regulation of Insulin Sensitivity by Exercise. *Front. Physiol.* 2:112. doi:10.3389/fphys.2011.00112.

Jeon, S.M. 2016. Regulation and function of AMPK in physiology and diseases. *Exp. Mol. Med.* 48:e245. doi:10.1038/emm.2016.81.

Jin, S.M., and R.J. Youle. 2012. PINK1-and Parkin-mediated mitophagy at a glance. *J. Cell Sci.* 125:795–799. doi:10.1242/jcs.093849.

Jung, C.H., S.H. Ro, J. Cao, N.M. Otto, and D.H. Kim. 2010. MTOR regulation of autophagy. *FEBS Lett.* 584:1287–1295. doi:10.1016/j.febslet.2010.01.017.

Kang, S.W.S., G. Haydar, C. Taniane, G. Farrell, I.M. Arias, J. Lippincott-Schwartz, and D. Fu. 2016. AMPK Activation prevents and reverses drug-induced mitochondrial and hepatocyte injury by promoting mitochondrial fusion and function. *PLoS One*. 11. doi:10.1371/journal.pone.0165638.

Katsarou, A., S. Gudbjörnsdottir, A. Rawshani, D. Dabelea, E. Bonifacio, B.J. Anderson, L.M. Jacobsen, D.A. Schatz, and A. Lernmark. 2017. Type 1 diabetes mellitus. *Nat. Rev. Dis. Prim.* 3:1–17. doi:10.1038/nrdp.2017.16.

Kerr, D., J. Knott, and D. Cavan. 2007. The changing shape of type 2 diabetes. *Pract. Diabetes Int.* 24:13–14. doi:10.1002/pdi.1038.

Khandia, R., M. Dadar, A. Munjal, K. Dhama, K. Karthik, R. Tiwari, M.I. Yatoo, H.M.N. Iqbal, K.P. Singh, S.K. Joshi, and W. Chaicumpa. 2019. A Comprehensive Review of Autophagy and Its Various Roles in Infectious, Non-Infectious, and Lifestyle Diseases: Current Knowledge and Prospects for Disease Prevention, Novel Drug Design, and Therapy. *Cells*. 8:674. doi:10.3390/cells8070674.

Komatsu, M., and Y. Ichimura. 2010. Physiological significance of selective degradation of p62 by autophagy. *FEBS Lett.* 584:1374–1378. doi:10.1016/j.febslet.2010.02.017.

Kramer, P.A., J. Duan, W.J. Qian, and D.J. Marcinek. 2015. The measurement of reversible redox dependent post-translational modifications and their regulation of mitochondrial and skeletal muscle function. *Front. Physiol.* 6:347. doi:10.3389/fphys.2015.00347.

Larsen, S., J. Nielsen, C.N. Hansen, L.B. Nielsen, F. Wibrand, N. Stride, H.D. Schroder, R. Boushel, J.W. Helge, F. Dela, and M. Hey-Mogensen. 2012. Biomarkers of mitochondrial content in skeletal muscle of healthy young human subjects. *J. Physiol.* 590:3349–3360. doi:10.1113/jphysiol.2012.230185.

Li, C., and H.-M. Zhou. 2011. The Role of Manganese Superoxide Dismutase in Inflammation Defense. *Enzyme Res.* 2011:1–6. doi:10.4061/2011/387176.

Li, S., Y. Kong, L. Si, Z. Chi, C. Cui, X. Sheng, and J. Guo. 2014. Phosphorylation of mTOR and S6RP predicts the efficacy of everolimus in patients with metastatic renal cell carcinoma. *BMC Cancer*. 14:376. doi:10.1186/1471-2407-14-376.

Li, Y.J., Y.L. Cao, J.X. Feng, Y. Qi, S. Meng, J.F. Yang, Y.T. Zhong, S. Kang, X. Chen, L. Lan, L. Luo, B. Yu, S. Chen, D.C. Chan, J. Hu, and S. Gao. 2019. Structural insights of human mitofusin-2 into mitochondrial fusion and CMT2A onset. *Nat. Commun.* 10. doi:10.1038/s41467-019-12912-0.

Lindinger, M.I. 2007. Combating muscle fatigue: Extracellular lactic acidosis and catecholamines. *J. Physiol.* 581:419. doi:10.1113/jphysiol.2007.132209.

Liu, S., M.J. Ammirati, X. Song, J.D. Knafels, J. Zhang, S.E. Greasley, J.A. Pfefferkorn, and X. Qiu. 2012. Insights into mechanism of glucokinase activation: Observation of multiple distinct protein conformations. *J. Biol. Chem.* 287:13598–13610. doi:10.1074/jbc.M111.274126.

Liu, W.J., L. Ye, W.F. Huang, L.J. Guo, Z.G. Xu, H.L. Wu, C. Yang, and H.F. Liu. 2016. p62 links the autophagy pathway and the ubiqutin-proteasome system upon ubiquitinated protein degradation. *Cell. Mol. Biol. Lett.* 21. doi:10.1186/s11658-016-0031-z.

Ljubicic, V., P. Miura, M. Burt, L. Boudreault, S. Khogali, J.A. Lunde, J.-M. Renaud, and B.J. Jasmin. Chronic AMPK activation evokes the slow, oxidative myogenic program and triggers beneficial adaptations in mdx mouse skeletal muscle. doi:10.1093/hmg/ddr265.

Löffler, A.S., S. Alers, A.M. Dieterle, H. Keppeler, M. Franz-Wachtel, M. Kundu, D.G. Campbell, S. Wesselborg, D.R. Alessi, and B. Stork. 2011. Ulk1-mediated phosphorylation of AMPK constitutes a negative regulatory feedback loop. *Autophagy*. 7:696–706. doi:10.4161/auto.7.7.15451.

Lord, S.R., J.M. Collins, W.C. Cheng, S. Haider, S. Wigfield, E. Gaude, B.A. Fielding, K.E. Pinnick, U. Harjes, A. Segaran, P. Jha, G. Hoefler, M.N. Pollak, A.M. Thompson, P.G. Roy, R. English, R.F. Adams, C. Frezza, F.M. Buffa, F. Karpe, and A.L. Harris. 2020. Transcriptomic analysis of human primary breast cancer identifies fatty acid oxidation as a target for metformin. *Br. J. Cancer*. 122:258–265. doi:10.1038/s41416-019-0665-5.

Lunt, S.Y., and M.G. Vander Heiden. 2011. Aerobic Glycolysis: Meeting the Metabolic Requirements of Cell Proliferation. *Annu. Rev. Cell Dev. Biol.* 27:441–464. doi:10.1146/annurev-cellbio-092910-154237.

Mahlapuu, M., C. Johansson, K. Lindgren, G. Hjälm, B.R. Barnes, A. Krook, J.R. Zierath, L. Andersson, and S. Marklund. 2004. Expression profiling of the γ-subunit isoforms of AMP-activated protein kinase suggests a major role for γ3 in white skeletal muscle. *Am. J. Physiol. - Endocrinol. Metab.* 286:E194-200. doi:10.1152/ajpendo.00147.2003.

Makrecka-Kuka, M., G. Krumschnabel, and E. Gnaiger. 2015. High-resolution respirometry for simultaneous measurement of oxygen and hydrogen peroxide fluxes in permeabilized cells, tissue homogenate and isolated mitochondria. *Biomolecules*. 5:1319–1338. doi:10.3390/biom5031319.

Marí, M., A. Morales, A. Colell, C. García-Ruiz, and J.C. Fernández-Checa. 2009. Mitochondrial glutathione, a key survival antioxidant. *Antioxidants Redox Signal.* 11:2685–2700. doi:10.1089/ars.2009.2695.

Marin, T.L., B. Gongol, F. Zhang, M. Martin, D.A. Johnson, H. Xiao, Y. Wang, S.

Subramaniam, S. Chien, and J.Y.J. Shyy. 2017. AMPK promotes mitochondrial biogenesis and function by phosphorylating the epigenetic factors DNMT1, RBBP7, and HAT1. *Sci. Signal.* 10. doi:10.1126/scisignal.aaf7478.

Martínez-Reyes, I., and N.S. Chandel. 2020. Mitochondrial TCA cycle metabolites control physiology and disease. *Nat. Commun.* 11:1–11. doi:10.1038/s41467-019-13668-3.

Marusich, M.F., B.H. Robinson, J.W. Taanman, S.J. Kim, R. Schillace, J.L. Smith, and R.A. Capaldi. 1997. Expression of mtDNA and nDNA encoded respiratory chain proteins in chemically and genetically-derived Rho0 human fibroblasts: A comparison of subunit proteins in normal fibroblasts treated with ethidium bromide and fibroblasts from a patient with mtDNA depletion syndrome. *Biochim. Biophys. Acta - Mol. Basis Dis.* 1362:145–159. doi:10.1016/S0925-4439(97)00061-6.

Mauthe, M., I. Orhon, C. Rocchi, X. Zhou, M. Luhr, K.J. Hijlkema, R.P. Coppes, N. Engedal, M. Mari, and F. Reggiori. 2018. Chloroquine inhibits autophagic flux by decreasing autophagosome-lysosome fusion. *Autophagy*. 14:1435–1455. doi:10.1080/15548627.2018.1474314.

Merrill, A.L.. W.B.K. 1973. Energy Value of Foods Basis and Derivation. *Agric. Handb.* 74:1–105.

Merrill, R.A., and S. Strack. 2014. Mitochondria: A kinase anchoring protein 1, a signaling platform for mitochondrial form and function. *Int. J. Biochem. Cell Biol.* 48:92–96. doi:10.1016/j.biocel.2013.12.012.

Misra, P., and R. Chakrabarti. 2007. The role of AMP kinase in diabetes. *Indian J. Med. Res.* 125:389–398.

Mittler, R. 2017. ROS Are Good. *Trends Plant Sci.* 22:11–19. doi:10.1016/j.tplants.2016.08.002.

Mookerjee, S.A., and M.D. Brand. 2015. Measurement and analysis of extracellular acid production to determine glycolytic rate. *J. Vis. Exp.* 2015. doi:10.3791/53464.

Mookerjee, S.A., A.A. Gerencser, D.G. Nicholls, and M.D. Brand. 2017. Quantifying intracellular rates of glycolytic and oxidative ATP production and consumption using extracellular flux measurements. *J. Biol. Chem.* 292:7189–7207. doi:10.1074/jbc.M116.774471.

Musa, J., M.F. Orth, M. Dallmayer, M. Baldauf, C. Pardo, B. Rotblat, T. Kirchner, G. Leprivier, and T.G.P. Grünewald. 2016. Eukaryotic initiation factor 4E-binding protein 1 (4E-BP1): A master regulator of mRNA translation involved in tumorigenesis. *Oncogene*. 35:4675–4688. doi:10.1038/onc.2015.515.

Musi, N., and L.J. Goodyear. 2003. AMP-activated protein kinase and muscle glucose uptake. *In* Acta Physiologica Scandinavica. 337–345.

Nilsson, E.C., C.L. Yun, S. Martinsson, S. Glund, P. Garcia-Roves, L.T. Svensson, L. Andersson, J.R. Zierath, and M. Mahlapuu. 2006. Opposite transcriptional regulation in skeletal muscle of AMP-activated protein kinase γ3 R225Q transgenic Versus knock-out mice. *J. Biol. Chem.* 281:7244–7252. doi:10.1074/jbc.M510461200.

Nobe&, C.D., W.W. Hay, and M.D. Brand. 1990. The Mechanism of Stimulation of Respiration by Fatty Acids in Isolated Hepatocytes". 265. 12910–12915 pp.

De Palma, C., F. Morisi, S. Pambianco, E. Assi, T. Touvier, S. Russo, C. Perrotta, V. Romanello, S. Carnio, V. Cappello, P. Pellegrino, C. Moscheni, M.T. Bassi, M. Sandri, D. Cervia, and E. Clementi. 2014. Deficient nitric oxide signalling impairs skeletal muscle growth and performance: involvement of mitochondrial dysregulation. *Skelet. Muscle*. 4:22. doi:10.1186/s13395-014-0022-6.

Peterson, R.T., B.N. Desai, J.S. Hardwick, and S.L. Schreiber. 1999. Protein phosphatase 2A interacts with the 70-kDa S6 kinase and is activated by inhibition of FKBP12-rapamycin-associated protein. *Proc. Natl. Acad. Sci. U. S. A.* 96:4438–4442. doi:10.1073/pnas.96.8.4438.

Piper, H.M., O. Sezer, M. Schleyer, P. Schwartz, J.F. Hütter, and P.G. Spieckermann. 1985. Development of ischemia-induced damage in defined mitochondrial subpopulations. *J. Mol. Cell. Cardiol.* 17:885–896. doi:10.1016/S0022-2828(85)80102-4.

Polianskyte-Prause, Z., T.A. Tolvanen, S. Lindfors, V. Dumont, M. Van, H. Wang, S.N. Dash, M. Berg, J.B. Naams, L.C. Hautala, H. Nisen, T. Mirtti, P.H. Groop, K. Wähälä, J. Tienari, and S. Lehtonen. 2019. Metformin increases glucose uptake and acts renoprotectively by reducing SHIP2 activity. *FASEB J.* 33:2858–2869. doi:10.1096/fj.201800529RR.

Porter, C., and B.T. Wall. 2012. Skeletal muscle mitochondrial function: Is it quality or quantity that makes the difference in insulin resistance? *J. Physiol.* 590:5935–5936. doi:10.1113/jphysiol.2012.241083.

Del Prato, S., P. Marchetti, and R.C. Bonadonna. 2002. Phasic insulin release and metabolic regulation in type 2 diabetes. *In* Diabetes. American Diabetes Association. S109–S116.

Pullen, N., P.B. Dennis, M. Andjelkovic, A. Dufner, S.C. Kozma, B.A. Hemmings, and G. Thomas. 1998. Phosphorylation and activation of p70(s6k) by PDK1. *Science (80-.).* 279:707–710. doi:10.1126/science.279.5351.707.

Qin, X., B. Jiang, and Y. Zhang. 2016. 4E-BP1, a multifactor regulated multifunctional protein. *Cell Cycle*. 15:781–786. doi:10.1080/15384101.2016.1151581.

Rabinovitch, R.C., B. Samborska, B. Faubert, E.H. Ma, S.P. Gravel, S. Andrzejewski, T.C. Raissi, A. Pause, J. St.-Pierre, and R.G. Jones. 2017. AMPK Maintains Cellular Metabolic Homeostasis through Regulation of Mitochondrial Reactive Oxygen Species. *Cell Rep.* 21:1–9. doi:10.1016/j.celrep.2017.09.026.

Reddy, J.K., and T. Hashimoto. 2001. Peroxisomal B-Oxidation and Peroxisome Proliferator-Activated Receptor a: An Adaptive Metabolic System. *Annu. Rev. Nutr.* 21:193–230. doi:10.1146/annurev.nutr.21.1.193.

Reznick, R.M., and G.I. Shulman. 2006. The role of AMP-activated protein kinase in mitochondrial biogenesis. *J. Physiol.* 574:33–39. doi:10.1113/jphysiol.2006.109512.

Rider, M.H., L. Bertrand, D. Vertommen, P.A. Michels, G.G. Rousseau, and L. Hue. 2004. 6-Phosphofructo-2-kinase/fructose-2,6-bisphosphatase: Head-to-head with a bifunctional enzyme that controls glycolysis. *Biochem. J.* 381:561–579. doi:10.1042/BJ20040752.

Ruderman, N.B., A.K. Saha, D. Vavvas, and L.A. Witters. 1999. Malonyl-CoA, fuel sensing, and insulin resistance. *Am. J. Physiol. - Endocrinol. Metab.* 276. doi:10.1152/ajpendo.1999.276.1.e1.

Ryan, K., D.S. Backos, P. Reigan, and M. Patel. 2012. Post-translational oxidative modification and inactivation of mitochondrial complex I in epileptogenesis. *J. Neurosci.* 32:11250–11258. doi:10.1523/JNEUROSCI.0907-12.2012.

Sanz, P. 2008. AMP-Activated Protein Kinase: Structure and Regulation. *Curr. Protein Pept. Sci.* 9:478–492. doi:10.2174/138920308785915254.

Saxton, R.A., and D.M. Sabatini. 2017. mTOR Signaling in Growth, Metabolism, and Disease. *Cell*. 168:960–976. doi:10.1016/j.cell.2017.02.004.

Schieber, M., and N.S. Chandel. 2014. ROS function in redox signaling and oxidative stress. *Curr. Biol.* 24:R453. doi:10.1016/j.cub.2014.03.034.

Schönfeld, P., and L. Wojtczak. 2016. Short- and medium-chain fatty acids in energy metabolism: The cellular perspective. *J. Lipid Res.* 57:943–954. doi:10.1194/jlr.R067629.

Seabright, A.P., N.H.F. Fine, J.P. Barlow, S.O. Lord, I. Musa, A. Gray, J.A. Bryant, M. Banzhaf, G.G. Lavery, D.G. Hardie, D.J. Hodson, A. Philp, and Y. Lai. 2020. AMPK activation induces mitophagy and promotes mitochondrial fission while activating TBK1 in a PINK1-Parkin independent manner. *FASEB J.* 34:6284–6301. doi:10.1096/fj.201903051R.

Seahorse Bioscience. Preparation of Bovine Serum Albumin-Palmitate conjugate for XF24 FAO Assays.

Seahorse XF Cell Mito Stress Test Kit | Agilent.

Sergi, D., N. Naumovski, L.K. Heilbronn, M. Abeywardena, N. O'Callaghan, L. Lionetti, and N. Luscombe-Marsh. 2019. Mitochondrial (dys)function and insulin resistance: From pathophysiological molecular mechanisms to the impact of diet. *Front. Physiol.* 10:532. doi:10.3389/fphys.2019.00532.

Serra, D., P. Mera, M.I. Malandrino, J.F. Mir, and L. Herrero. 2013. Mitochondrial fatty acid oxidation in obesity. *Antioxidants Redox Signal.* 19:269–284. doi:10.1089/ars.2012.4875.

Shriver, L.P., and M. Manchester. 2011. Inhibition of fatty acid metabolism ameliorates disease activity in an animal model of multiple sclerosis. *Sci. Rep.* 1. doi:10.1038/srep00079.

Smith, A.C., C.R. Bruce, and D.J. Dyck. 2005. AMP kinase activation with AICAR further increases fatty acid oxidation and blunts triacylglycerol hydrolysis in contracting rat soleus muscle. *J. Physiol.* 565:547–553. doi:10.1113/jphysiol.2004.081687.

Smith, M.E., and D.G. Morton. 2010. The stomach: basic functions. *In* The Digestive System. Churchill Livingstone. 39–50.

Song, Y.M., W.K. Lee, Y.H. Lee, E.S. Kang, B.S. Cha, and B.W. Lee. 2016. Metformin restores parkin-mediated mitophagy, suppressed by cytosolic p53. *Int. J. Mol. Sci.* 17. doi:10.3390/ijms17010122.

Spinazzi, M., A. Casarin, V. Pertegato, L. Salviati, and C. Angelini. 2012. Assessment of mitochondrial respiratory chain enzymatic activities on tissues and cultured cells. *Nat. Protoc.* 7:1235–1246. doi:10.1038/nprot.2012.058.

Srivastava, R.A.K., S.L. Pinkosky, S. Filippov, J.C. Hanselman, C.T. Cramer, and R.S. Newton. 2012. AMP-activated protein kinase: An emerging drug target to regulate imbalances in lipid and carbohydrate metabolism to treat cardio-metabolic diseases. *J. Lipid Res.* 53:2490–2514. doi:10.1194/jlr.R025882.

Tanida, I., T. Ueno, and E. Kominami. 2008. LC3 and autophagy - Methods in Molecular Biology. *Methods Mol. Biol.* 445:77–88. doi:10.1007/978-1-59745-157-4-4.

Tao, R., J. Gong, X. Luo, M. Zang, W. Guo, R. Wen, and Z. Luo. 2010. AMPK exerts dual regulatory effects on the PI3K pathway. *J. Mol. Signal.* 5:1. doi:10.1186/1750-2187-5-1.

Thornton, C. 2017. AMPK: keeping the (power)house in order? *Neuronal Signal.* 1. doi:10.1042/ns20160020.

Vial, G., D. Detaille, and B. Guigas. 2019. Role of Mitochondria in the Mechanism(s) of Action of Metformin. *Front. Endocrinol. (Lausanne).* 10:294. doi:10.3389/fendo.2019.00294.

Viollet, B., S. Horman, J. Leclerc, L. Lantier, M. Foretz, M. Billaud, S. Giri, and F.

Andreelli. 2010. AMPK inhibition in health and disease. *Crit. Rev. Biochem. Mol. Biol.* 45:276–295. doi:10.3109/10409238.2010.488215.

Wang, C., F. Liu, Y. Yuan, J. Wu, H. Wang, L. Zhang, P. Hu, Z. Li, Q. Li, and J. Ye. 2014. Metformin suppresses lipid accumulation in skeletal muscle by promoting fatty acid oxidation. *Clin. Lab.* 60:887–896. doi:10.7754/Clin.Lab.2013.130531.

Wang, Y., A.W. Mohsen, S.J. Mihalik, E.S. Goetzman, and J. Vockley. 2010. Evidence for physical association of mitochondrial fatty acid oxidation and oxidative phosphorylation complexes. *J. Biol. Chem.* 285:29834–29841. doi:10.1074/jbc.M110.139493.

Westermann, B. 2010. Mitochondrial fusion and fission in cell life and death. *Nat. Rev. Mol. Cell Biol.* 11:872–884. doi:10.1038/nrm3013.

Westermann, B. 2012. Bioenergetic role of mitochondrial fusion and fission. *In* Biochimica et Biophysica Acta - Bioenergetics. Elsevier. 1833–1838.

Williams, M.R., J.S.C. Arthur, A. Balendran, J. Van der Kaay, V. Poli, P. Cohen, and D.R. Alessi. 2000. The role of 3-phosphoinositide-dependent protein kinase 1 in activating AGC kinases defined in embryonic stem cells. *Curr. Biol.* 10:439–448. doi:10.1016/S0960-9822(00)00441-3.

Willows, R., M.J. Sanders, B. Xiao, B.R. Patel, S.R. Martin, J. Read, J.R. Wilson, J. Hubbard, S.J. Gamblin, and D. Carling. 2017. Phosphorylation of AMPK by upstream kinases is required for activity in mammalian cells. *Biochem. J.* 474:3059–3073. doi:10.1042/BCJ20170458.

Winder, W.W., and D.G. Hardie. 1996. Inactivation of acetyl-CoA carboxylase and activation of AMP-activated protein kinase in muscle during exercise. *Am. J. Physiol. - Endocrinol. Metab.* 270. doi:10.1152/ajpendo.1996.270.2.e299.

Youle, R.J., and A.M. Van Der Bliek. 2012. Mitochondrial fission, fusion, and stress. *Science (80-.).* 337:1062–1065. doi:10.1126/science.1219855.

Yu Wang, A., H. An, T. Liu, and F.E. Wondisford. 2019. Metformin Improves Mitochondrial Respiratory Activity through Activation of AMPK. *CellReports*. 29:1511-1523.e5. doi:10.1016/j.celrep.2019.09.070.

Zachari, M., and I.G. Ganley. 2017. The mammalian ULK1 complex and autophagy initiation. *Essays Biochem.* 61:585–596. doi:10.1042/EBC20170021.

Zhang, J., Y. Wang, X. Liu, R.K. Dagda, and Y. Zhang. 2017. How AMPK and PKA Interplay to Regulate Mitochondrial Function and Survival in Models of Ischemia and Diabetes. doi:10.1155/2017/4353510.

Zhang, X., Y. Song, M. Feng, X. Zhou, Y. Lu, L. Gao, C. Yu, X. Jiang, and J. Zhao. 2015. Thyroid-stimulating hormone decreases HMG-CoA reductase phosphorylation via AMP-activated protein kinase in the liver. *J. Lipid Res.* 56:963–971. doi:10.1194/jlr.M047654.

Zhao, J.X., X. Yan, J.F. Tong, W.J. Means, R.J. McCormick, M.J. Zhu, and M. Du. 2009. Mouse AMPK{gamma}3 R225Q mutation affecting its growth performance when fed a high energy diet. *J Anim Sci*.

Zhao, R.Z., S. Jiang, L. Zhang, and Z. Bin Yu. 2019. Mitochondrial electron transport chain, ROS generation and uncoupling (Review). *Int. J. Mol. Med.* 44:3–15. doi:10.3892/ijmm.2019.4188.

Contributions of Collaborators

Thank you to Dr. Robert Dent (M.D.), and Dr. Ruth McPherson (M.D., Ph.D.) for their time spent recruiting human subjects and for conducting the *vastus lateralis* biopsies of all AMPK R225W individuals and their controls at the University of Ottawa Heart Institute. I would also like to thank Heather Doelle (Research Coordinator at UOHI) for coordinating the logistics of each biopsy for my project.

Thank you to Dr. Chantal Pileggi (Ph.D.) for her expertise and assistance in all training, and specifically aid in performing and analyzing high resolution respirometry experiments on myotubes and muscle fibres.

Curriculum Vitae

Section A: University Educational Background

University of Ottawa – May 2019 – July 2020

- Master of Science in Biochemistry (Dr. Mary-Ellen Harper Laboratory)

University of Ottawa – September 2015 – April 2019

- Honours Bachelor of Science in Biochemistry and Minor in Mathematics (conferred May 23rd, 2019)

Section B: Research-specific Honours, Scholarships and Awards during University

$15,000 Ontario Graduate Scholarship (OGS) – May 2019 – April 2020

- The Ontario Graduate Scholarship was awarded for my 2019-2020 year of Master's in Biochemistry based on academic merit in my last 2 years of undergraduate studies and a written research proposal. A minimum GPA of A- (8.0/10.0) is required to be considered, however a much higher GPA is required to be considered competitive for the award. The OGS scholarship was founded in order to encourage excellence in graduate studies.

$10,000 Excellence Scholarship – May 2019 – April 2020

- The Excellence Scholarship was awarded for my 2019-2020 year of Master's in Biochemistry because I was also the recipient of a major external award (OGS). In order to receive a major external award, academic merit and written research proposals are considered, and GPA required is A- (8.0/10.0) for the final 2 years of undergraduate, however a much higher GPA is considered competitive. In order to receive the Excellence Scholarship, I first had to successfully receive an OGS award.

$5,000 NSERC CREATE MATRIX Scholarship – May 2019 – April 2020

- The MATRIX (Metabolomics Advanced Training and International Exchange Program) Scholarship is a scholarship that was awarded for my 2019-2020 year of Master's in Biochemistry to allow me to get advanced training in cutting-edge metabolomics. This scholarship is open to graduate students at the Faculty of Medicine in the University of Ottawa and in my case was awarded to supplement the OGS award.

$1,000 Undergraduate Research Opportunity Program – November 2017 – April 2018

- Awarded on the basis of academic excellence to experience research at the University of Ottawa, to write an abstract, and present a research poster. Minimum GPA to apply

is 7.5/10.0, however priority is given to those who have excellent academic standing. Application requires a letter of intent submit jointly by the professor and student.

Section C: Other Honours, Scholarships and Awards during University

$500 Alexandre Sabourin Award for Arts and the Community – September 2018 – April 2019

- This award was granted to me for my 4th year of undergraduate studies. The criteria to receive this award was to have excellent artistic endeavours, and to apply these artistic endeavours to aiding the community. As someone who had spent a lot of my childhood learning piano and ballet, I have also spent a lot of my time during my studies giving back to my community with the skills that I learned by primarily running the Heart of the City Piano Program for financially unstable families.

$4,000 x 4 Renewable Admission Scholarship – September 2015 – April 2019

- This scholarship was awarded for my Bachelor of Science in Biochemistry (Minor in Math) based on academic merit in secondary school. With an admission average of above 95%, I fell into the highest bracket of the scholarship, receiving $4000 per year, and this could be maintained if the CGPA did not drop below 8.5. A high enough average was maintained, so the total amount granted for all 4 years was $16,000.

Section D: Research Experience

Time frame: May 2018 – July 2020
Supervisor: Dr. Mary-Ellen Harper
Position: MSc. Candidate, H.B.Sc. Student
Project Title: Bioenergetic implications of the AMPKγ_3 R225W mutation in human muscle

In this project I was the primary individual conducting assays. I completed all the experiments, and analyses for the project. Characterizing the mutation involved running several experiments using Agilent Seahorse cell mitochondrial stress test technology, Western blots, microscopy, HPLC, high resolution respirometry and fluorimetry, and specific enzymatic activity assays.

Time frame: November 2017 – April 2018
Supervisor: Dr. Douglas Gray (OHRI)
Position: UROP Scholarship Student
Project Title: The effects of lithium on subcellular localization of USP4 in HeLa cells

In this position, I was responsible for doing the fundamental determinations to determine whether the inhibition of GSK-3 β by lithium would affect the subcellular localization of USP4, a deubiquinating enzyme. USP4 is a known contributor to the development of brain metastases from primary lung cancer cells. By inhibiting the kinase with lithium, we were determining whether the kinase could be a potential target for inhibiting USP4, and thus terminating the metastatic pathway.

Section E: Employment

Yamaha Music School – September 2016 – June 2020
- Piano teacher, preparation of students for Royal Conservatory of Music examinations and concerts
- Ages 5-50

Total Hours: 950

Private Tutor – September 2013 – Present
- Tutoring students in subjects including biology, chemistry, physics, and mathematics from Grade 11 to 2nd year university level.

Science Preparatory Workshop Mentor – August 2018
- Giving a series of presentations to 300 students over the course of 1 week
- Teaching assistant for biology and chemistry laboratories over the course of 1 week

Total Hours: 34

Student Mentor Physics, Chemistry University of Ottawa – August 2017 – April 2019
- Weekly mentoring of a group of students in the CHM1311/1321 courses (2018-2019)
- Weekly mentoring of a group of students in the PHY1331/1321/1322 courses (2017-2018)

Total Hours: 350

Government of Canada, Health Canada (CO-OP) – May 2017 – August 2017
- Compliance and Enforcement Division, Healthy Environments and Consumer Safety Branch
- Full Time Junior Regulatory Compliance and Enforcement Advisor

Total Hours: 640

Section F: Non-Academic Activities

Heart of the City Piano Program Hospital Program Founder – May 2019 – Present
- Expansion of the original Canada-wide program which targets financial accessibility issues with music education to allow for music education across health barriers

Total Hours: 30

Indigo Girls Group – Director of Operations – February 2020 – Present
- Partook as Ottawa Branch Leader November 2019 – May 2020
- Partook as Finance and Fundraising Leader September 2018 – November 2019
- Creating programming for empowering young girls to have confidence in themselves

Total Hours: 200

Pulsar Collective Director of Volunteer and Human Resources – May 2018 – Present
- A new organization spearheaded by Cassidy Swanston and funded by NSERC
- Promoting gender equality in STEM to girls in high schools

Total Hours: 150

Ontario Science Games – Head Coordinator – October 2019 – July 2020

- President of planning committee for an interdisciplinary weekend of competition from several universities in Ontario
- Responsibilities included: chairing meetings, planning/scheduling games, recruiting ambassadors and volunteers, staying on top of planning committee's work

Total Hours: 200

University of Ottawa Healthcare Conference – Social Chair – May 2019 – January 2020

- Organized venue and food for conference
- Worked alongside other executives to bring exciting speakers on interdisciplinary healthcare including Dr. Jane Philpott

Total Hours: 150

University of Ottawa Relay for Life – Social Chair – June 2019 – May 2020

- Organized events throughout the evening and scheduling of ceremonies
- Worked alongside other executives to promote and successfully raise $29,000 for the Canadian Cancer Society

Total Hours: 150

Science Students' Association Vice-President of Social Activities – May 2018 – April 2019

- Planning orientation week for 700 students and coordinating 200 guides
- Organizing events throughout the school year such as Trivia Nights, Festive Days, Self-Care Services
- Chairing committee meetings to plan events such as Formal and Grad Ball
- Attend biweekly executive meetings, monthly general council meetings, and weekly Social Round Tables
- A part of: Formal, Grad Ball, Elections, Scholarships/Grants, SSA 2020, Constitution, and Scholastic Events Committees

Total Hours: 970

Heart of the City Piano Program Ottawa Chapter Executive Co-Director – January 2016 – August 2020

- Volunteered at Vincent Massey Public School to teach piano
- Teaching children piano who would otherwise not be able to learn piano
- Coordinating an executive team of 13 in order to provide lessons at 5 elementary schools across Ottawa

Total Hours: 200

Science Students' Association Biochemistry Representative – October 2017 – April 2018

- Organizing a program information session, and a social event for the Biochemistry students
- Attending monthly Biochemistry Curriculum Review meetings with members of the Department of Biochemistry to share the student perspective on curriculum changes
- Attend Faculty Council once a semester with the heads of departments in the Faculty of Science

Total Hours: 40

Section G: Other

Personal Endeavour in Piano Playing – January 2001 – Present

- Grade 10 RCM Piano Performance and Corequisites completed with First Class Honours (August 2016)
- Playing piano at ARCT diploma level (estimated completion: August 2020)
- Competing in Kiwanis Music Festival (2nd place in Grade 10 List D May 2014, 1st place in ARCT List B April 2018, 3rd place ARCT List C April 2018)
- Composing recreationally

Total Hours: 2000

Personal Endeavour in Dance – September 2003 – Present

- Advanced 1 RAD Ballet Vocational Syllabus completed (November 2013)
- Training and performing primarily ballet and modern
- Other forms of dance include contemporary, lyrical, jazz, tap, character, and Serbian folklore at an advanced level
- Participated in uOttawa Dance Club as Modern choreographer and as dancer for several dance forms

Total Hours: 1500